INSTYTUT BIOCYBERNETYKI I INŻYNIERII BIOMEDYCZNEJ IM. MACIEJA NAŁĘCZA

POLSKIEJ AKADEMII NAUK

Ph.D. Thesis

Discipline of science – Biomedical Engineering

Field of science – Engineering and Technology

Label-free methods of lactoferrin determination using new selective DNA-based bioreceptor

Bezznacznikowe metody oznaczania laktoferyny
z wykorzystaniem nowego selektywnego bioreceptora
opartego na DNA

Agnieszka Paziewska-Nowak, M.Sc. Eng.

Supervisor: Prof. Dorota G. Pijanowska, Ph.D., D.Sc.

Auxiliary supervisor: Marcin Urbanowicz, Ph.D., Eng.

WARSAW 2024

Table of content

5

Label-free methods of lactoferrin determination using new selective DNA-based bioreceptor

Abstract

Lactoferrin (Lf) is an endogenous multipotent glycoprotein of immunomodulatory nature. Lf is considered an essential element of host defense because it can respond to physiological changes. Its structural features provide functionalities such as maintaining Fe^{3+} homeostasis, antimicrobial activity against various bacteria and viruses, and anti-inflammatory and anticancer effects. It also plays a protective and repairing role over the human genome. It is able to bind to DNA and, under certain conditions, acts as a deoxyribonuclease (DNase), activating transcription and regulating the cell cycle. Yet, there is insufficient experimental confirmation in the literature on the mechanisms of such interaction, while the possibility of utilizing the DNA as the putative lactoferrin bioreceptor has not been challenged. Therefore, this doctoral dissertation is devoted to developing a new DNA-type bioreceptor for selective detection of lactoferrin in real samples by utilizing label-free, bioreceptor non-destructive techniques such as surface plasmon resonance and electrochemical impedance spectroscopy. The work thus is divided into two main parts: indicating the DNA sequence of the highest affinity towards the target protein and utilizing it to develop a new impedimetric biosensor to quantify lactoferrin in human saliva.

In the first part of the doctoral thesis, the results of developing an innovative DNA oligonucleotide-based bioreceptor with a high affinity and selectivity for lactoferrin using the surface plasmon resonance method were presented and discussed. The aim was to investigate the affinity of various designed oligonucleotides for the target protein. Further investigations were carried out on the 5'[TAGAGGATCAAAAAA]₄TAGAGGATCAAA3' hybridized sequence, which was 72 base pairs long and had the highest affinity for lactoferrin. The detailed analysis of the interaction between lactoferrin and the selected DNA sequence provided rate and equilibrium constants. The kinetic analysis revealed ono-to-one binding with kinetic constants $k_a = (2.49 \pm 0.03) \cdot 10^4 \ M^{-1} \cdot s^{-1}$ and $k_d = (1.89 \pm 0.02) \cdot 10^3 \ s^{-1}$ – association and dissociation rate constants, respectively, and $K_A = (0.13 \pm 0.05) \cdot 10^8 \ M^{-1}$ and $K_D = (7.61 \pm 0.18) \cdot 10^{-8} \ M$ – association and dissociation equilibrium constants, respectively. The thermodynamic studies were conducted in the 291.15 – 305.15 K temperature range to determine the ΔH^o, ΔS^o, and ΔG^o for van't Hoff characteristic. The complex formation was found to be endothermic and entropically driven, and the interaction was of a hydrophobic

nature. The selectivity of the chosen DNA sequence towards lactoferrin was confirmed with interferents' response constituting less than 3% of the reference lactoferrin signal.

The dsDNA oligonucleotide of unique sequence H_2N-$(CH_2)_6$-5'[TAGAGGATCAAA-AAA]$_4$TAGAGGATCAAA3' was utilized as a biorecognition element for developing a lactoferrin impedimetric biosensor. The spatial orientation of the bioreceptor layer was established by immobilizing the oligonucleotide via the H_2N- group at the 5' end. The developed biosensor was characterized by impedance spectroscopy using both faradaic and non-faradaic models, and the analysis of experimental data allowed the proposal of the Randles-based electrical equivalent circuit. The equivalent circuit charge transfer resistance parameter R_{3f} of the faradaic model was revealed to be quantitatively dependent on the lactoferrin concentration. The biosensor characteristic is a dependence between the ratio of resistance R_{3f} before/after bioreceptor-analyte interaction and the analyte concentration. The developed impedimetric biosensor demonstrated a linear response for laboratory samples in the lactoferrin concentration range up to 625 nM, with a limit of detection of 1.25 nM and a limit of quantification of 2.5 nM. The subsequent study established the application of this biosensor for quantitative lactoferrin detection in human saliva samples. The results were consistent with the surface plasmon resonance, utilizing the same DNA-type bioreceptor and with colorimetric immunoassay. The proposed impedimetric DNA-based biosensor for lactoferrin addresses the growing need for rapid, simple, and effective analytical methods for detecting immunomodulators with potential applications in clinical diagnosis.

The work fits into the paradigm of biomedical engineering by proposing a new approach to developing the DNA-based bioreceptor and next utilizing it to establish a label-free sensitive impedimetric biosensor for clinically important analyte lactoferrin. The research provided a new bioreceptor design and development methodology by selecting surface plasmon resonance as a leading technique for real-time binding analyses. The SPR results were analyzed in depth, resulting in the identification of a DNA oligonucleotide as the primary and specific lactoferrin bioreceptor, confirmed by a selectivity study with interferents as well as for determination of lactoferrin in biological fluids, such as saliva. Moreover, a short overview of the results showed the advantage of the developed DNA-based recognition element over antibody-based and biomimetic ones. The research implementation provides a new approach to the design of specific bioreceptors for label-free sensing. It can be used to

further work on biorecognition layer development for clinically significant large molecules, especially proteins.

Bezznacznikowe metody oznaczania laktoferyny z wykorzystaniem nowego selektywnego bioreceptora opartego na DNA

Streszczenie

Laktoferyna jest wielofunkcyjnym białkiem endogennym o właściwościach immunomodulujących. Jest uważana za kluczowy element system obronnego ze względu na zdolność do odpowiadania na zmiany fizjologiczne w organizmie gospodarza. Jej cechy strukturalne warunkują właściwości takie jak utrzymywanie homeostazy jonów Fe^{3+}, aktywność antymikrobiologiczna przeciwko różnorodnym bakteriom i wirusom, oraz efekty przeciwzapalny i antynowotworowy. Laktoferyna odgrywa również rolę ochronną i naprawczą w stosunku do ludzkiego genomu. Białko to jest zdolne do wiązania się z DNA i w określonych warunkach działania jak deoksyrybonukleaza (DNaza), aktywując transkrypcję i regulując cykl komórkowy. Mimo to, w literaturze nie ma wystarczająco wyczerpujących danych eksperymentalnych opisujących mechanizm tejże interakcji, natomiast możliwość wykorzystania DNA jako potencjalnego bioreceptora laktoferyny nie została dotychczas podjęta w badaniach naukowych. Niniejsza rozprawa doktorska poświęcona jest opracowaniu nowego bioreceptora typu DNA do selektywnego oznaczania laktoferyny w próbkach rzeczywistych za pomocą bezznacznikowych, nieniszczących dla bioreceptora technik, takich jak powierzchniowy rezonans plazmonów i elektrochemiczna spektroskopia impedancyjna. Praca składa się z dwóch głównych części: określenia sekwencji DNA o najwyższym powinowactwie do białka docelowego oraz wykorzystania jej do opracowania nowego bioczujnika impedancyjnego do ilościowych oznaczeń laktoferyny w próbkach śliny ludzkiej.

W pierwszej części pracy doktorskiej, zaprezentowano i omówiono wyniki badań wykorzystujących metodę powierzchniowego rezonansu plazmonów do opracowania nowego bioreceptora typu DNA wykazującego wysokie powinowactwo i selektywność względem laktoferyny. Celem było zbadanie powinowactwa różnych typów oligonukleotydów do białka docelowego. Dalsze badania prowadzono z użyciem zhybrydyzowanej sekwencji 5'[TAGAGGATCAAA-AAA]$_4$TAGAGGATCAAA3' o długości 72 par zasad azotowych, która wykazywała największe powinowactwo do laktoferyny. Szczegółowa analiza interakcji laktoferyny z wybraną sekwencją DNA dostarczyła informacji dotyczących stałych szybkości i stałych równowagi interakcji. Analiza kinetyki oddziaływania pozwoliła na ustalenie stechiometrii oddziaływania

wskazując na typ jeden-do-jednego z wartościami stałych kinetycznych, w tym odpowiednio stałych szybkości asocjacji i dysocjacji $k_a = (2.49 \pm 0.03) \cdot 10^4$ M^{-1}·s^{-1} i $k_d = (1.89 \pm 0.02) \cdot 10^3$ s^{-1}, oraz stałych równowagi asocjacji i dysocjacji – K_A $(0.13 \pm 0.05) \cdot 10^8$ M^{-1} i $K_D = (7.61 \pm 0.18) \cdot 10^{-8}$ M. W zakresie temperatur od 291,15 do 305,15 K przeprowadzono badania termodynamiczne w celu wyznaczenia ΔH^o, ΔS^o, and ΔG^o do charakterystyki van't Hoffa. Ustalono, że tworzenie kompleksu laktoferyna-DNA ma charakter endotermiczny, napędzany zamianą entropi, natomiast interakcja ma naturę hydrofobową. Selektywność wybranej sekwencji DNA względem laktoferyny została potwierdzona wobec interferentów, dla których odpowiedź stanowiła mniej niż 3% referencyjnego sygnału pochodzącego od laktoferyny.

Oligonukleotyd dsDNA o unikalnej sekwencji H$_2$N-(CH$_2$)$_6$-5'[TAGAGGATCAAA-AAA]$_4$TAGAGGATCAAA3' został użyty jako bioreceptor do opracowania impedancyjnego bioczujnika laktoferyny. Orientację przestrzenną warstwy bioreceptorowej uzyskano unieruchamiając oligonukleotyd za pomocą grupy H$_2$N- na końcu 5'. Opracowany bioczujnik został scharakteryzowany metodą spekroskopii impedancyjnej z użyciem modelu faradajowskiego i niefaradajowskiego, zaś analiza danych eksperymentalnych umożliwiła zaproponowanie elektrycznego modelu zastępczego opartego na modelu Randlesa. Wartość elementu zastępczego opisującego rezystancję transferu elektronów R_{3f} modelu faradajowskiego okazała się być zależną od stężenia laktoferyny. Charakterystykę bioczujnika określono jako zależność między stosunkiem rezystancji R_{3f} przed/po interakcji bioreceptor-analit i stężeniem analitu. Opracowany bioczujnik impedancyjny wykazał liniową odpowiedź dla próbek laboratoryjnych w zakresie stężeń laktoferyny do 625 nM, z granicą wykrywalności 1,25 nM i granicą oznaczalności 2,5 nM, przy czułości dla zakresu liniowego na poziomie . W kolejnych badaniach zastosowano opracowany bioczujnik do ilościowego oznaczania laktoferyny w próbkach śliny ludzkiej. Wyniki badań były zgodne z wynikami uzyskanymi metodą powierzchniowego rezonansu plazmonów z wykorzystaniem tego samego receptora typu DNA oraz kolorymetrycznego testu immunologicznego. Zaproponowany impedancyjny bioczujnik laktoferyny z opracowanym bioreceptorem typu DNA odpowiada na narastające zapotrzebowanie na szybkie, proste i skuteczne metody analityczne do wykrywania immunomodulatorów o potencjalnym zastosowaniu w diagnostyce klinicznej.

Praca wpisuje się w paradygmat inżynierii biomedycznej poprzez zaproponowanie nowatorskiej metody opracowania bioreceptora opartego na DNA, a następnie jego wykorzystania do wytworzenia czułego, bezznacznikowego impedancyjnego bioczujnika laktoferyny, która jest analitem o znaczeniu klinicznym. Badania dostarczyły nowej metodyki projektowania i opracowywania bioreceptorów z wykorzystaniem powierzchniowego rezonansu plazmonów jako głównej techniki pozwalającej na analizę oddziaływań międzycząsteczkowych w czasie rzeczywistym. Szeroko omówiono ograniczenia i zalety badań metodą SPR, wynikiem których był wybór jednego oligonukleotydu DNA o określonej sekwencji, jako najbardziej obiecującego i specyficznego bioreceptora laktoferyny, co potwierdzono w badaniu selektywności z udziałem interferentów. Ponadto porównanie wyników własnych wykazało przewagę opracowanego elementu bioreceptorowego opartego na DNA nad elementami opartymi na przeciwciałach i biomimetycznymi. Realizacja badań zapewnia nowe podejście do projektowania specyficznych bioreceptorów dla potrzeb metod bezznacznikowych i może zostać wykorzystana w dalszych pracach nad rozwojem warstw bioczujnikowych dla dużych cząsteczek istotnych klinicznie, w szczególności białek.

Słowa kluczowe: bioreceptor typu oligonukleotyd DNA, bezznacznikowe oznaczanie oparte na powinowactwie molekularnym, laktoferyna, bioczujnik impedancyjny, powierzchniowy rezonans plazmonów;

Graphical abstract
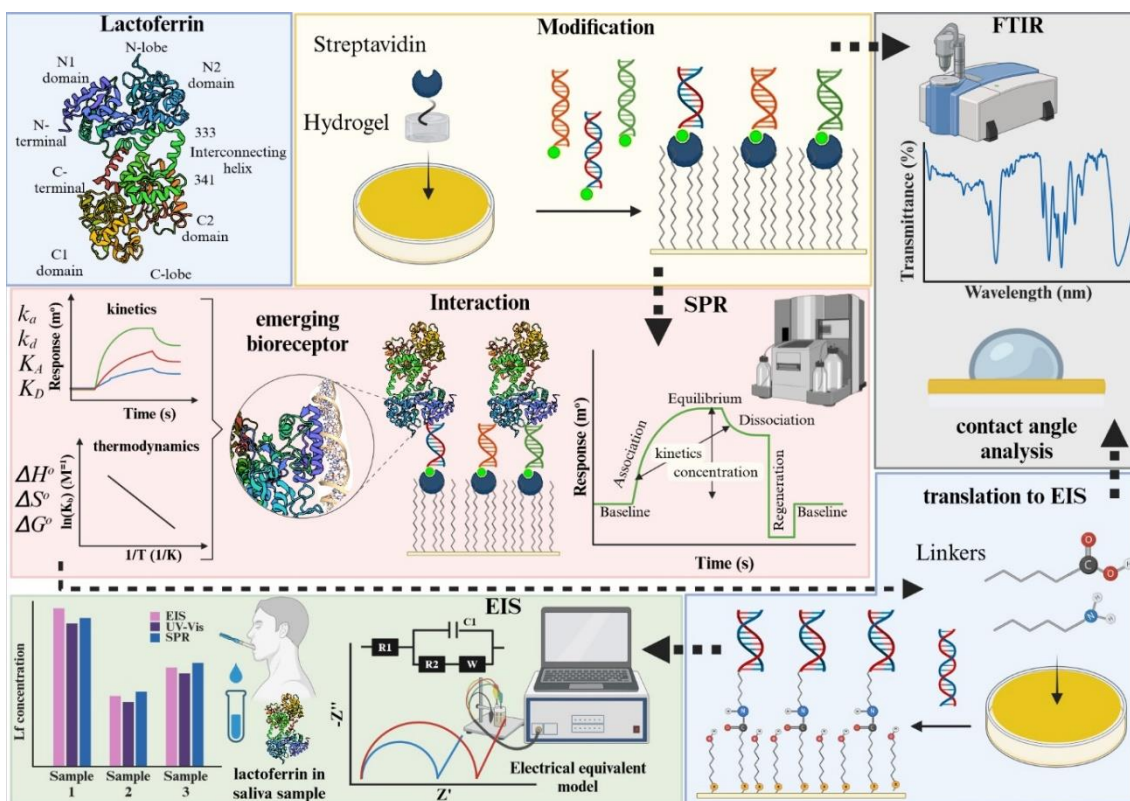
List of abbreviations

Ab – antibody

AC – alternating current

BLI – biolayer interferometry

bp – base pairs

BS3 – suberic acid bis(3-sulfo-*N*-hydroxysuccinimide ester) sodium salt

BSA – bovine serum albumin

BS(PEG)9 – PEGylated bis(sulfosuccinimidyl)suberate

CA – contact angle

CV – cyclic voltammetry

DA – dopamine hydrochloride

DAD – dynamic array diode

DC – direct current

DNA – deoxyribonucleic acid

DPV – differential pulse voltammetry

*ds*DNA – double-stranded DNA

EDC – *N*-(3-dimethylaminopropyl)-*N*′-ethylcarbodiimide hydrochloride

EIS – electrochemical impedance spectroscopy

ELISA – enzyme-linked immunosorbent assay

EMSA – electrophoretic mobility shift assay

FRET – fluorescence resonance energy transfer

FTIR – Fourier transform infrared spectroscopy

G4 – G-quadruplex

GA – glutaraldehyde

GluOx – glutamate oxidase

GOx – glucose oxidase

HPLC – high-performance liquid chromatography

HRP – horseradish peroxidase

IL-1β – interleukin 1β

IL-18 – interleukin 18

ITC – isothermal titration calorimetry

IUPAC – International Union of Pure and Applied Chemistry

LA – human lactalbumin

LAK – lymphokine-activated killer cells

LOD – limit of detection

LOQ – limit of quantification

LPS – lipopolysaccharide

MAP – mitogen-activated protein

MCH – 6-mercapto-1-hexanol

MUA – 11-mercaptoundecanoic acid

MW – molecular weight

NA – nucleic acid

nb – nucleobase

NF-κB – nuclear factor kappa B

NK – natural killer cells

OCP – open circuit potentiometry

PAMAM – poly(amidoamine) dendrimer

PDA – polydopamine

pI – isoelectric point

SAD – streptavidin derivatized carboxymethyl dextran hydrogel

SAHC – streptavidin derivatized linear polycarboxylate hydrogel

SFIA – stopped-flow immunoassay

SPR – surface plasmon resonance

*ss*DNA – single-stranded DNA

sulfo-NHS – *N*-hydroxysulfosuccinimide sodium salt

TNF-α – tumor necrosis factor alpha

UV – ultraviolet light

Vis – visual light

List of symbols

R – gas constant

K_D – dissociation equilibrium constant

K_A – association equilibrium constant

W_{hybr} – hybridization efficiency

T – temperature

k_a – association rate constant

k_d – dissociation rate constant

ΔS^0 – binding entropy change

ΔH^0 – binding enthalpy change

ΔG^0 – Gibbs free energy change

K_b – binding constant

m – mass immobilized

δ – loading density of ligand

τ – time constant

R_s – solution resistance

R_{ct} – charge transfer resistance

C_{dl} – double layer capacitance

Q – constant phase element

W – Warburg element

R_p – polarization resistance

Z_W – Warburg impedance

Z_F – faradaic impedance

I_C – coulombic current

I_F – faradaic current

N_A – Avogadro number

N_δ – number of molecules bound

C_{Lf} – lactoferrin concentration

Introduction

Lactoferrin (Lf) is a remarkable protein that defends the host against infections and tissue injuries in vertebrates. It is highly versatile and can interact with various host and microbial targets, providing antimicrobial properties while regulating innate and adaptive immune responses. Lactoferrin has been found to modulate immune cell activation, migration, and growth, either upregulating or downregulating them as required. Numerous studies have highlighted lactoferrin's immunomodulatory effects, which are evident in lactoferrin-knockout, lactoferrin-overexpressing transgenic models, and dietary lactoferrin. Although the mechanisms behind these properties are not fully understood, recent *in vitro* studies have proposed various theories. Lactoferrin has been shown to target negatively charged molecules, such as pro-inflammatory microbial molecules and host components, including DNA, proteoglycan, glycosaminoglycan chains, and surface cell receptors. By signaling through these receptors, lactoferrin influences immune cells and cytokine-balance-controlling cell activity, which is considered a primary way lactoferrin affects the complex immune machinery. Numerous reports show lactoferrin's clinical significance in inflammatory diseases, especially those of autoimmune background, such as Leśniowski-Crohn's disease [1–3], as well as neurodegenerative diseases, for instance, Alzheimer's disease [4–6]. Understanding lactoferrin's multiple ways of influencing the immune machinery and the known and potential mechanisms that may explain its properties is an emerging research topic. Lactoferrin, similarly to other proteins in clinical diagnostics, if at all, is mainly determined with immunoassays – commercial enzyme-linked immunosorbent assay (ELISA) kits that require qualified staff and advanced instrumentation. Despite the high sensitivity and selectivity of antibody-based assays, they display some major drawbacks: the necessity of labeling, invalidity under excess concentrations of analyte, depuration from the bound label, or variability between batches. Except for antibodies, other proteins such as nucleolin – a multifunctional protein localized primarily in the nucleolus, also found in the nucleoplasm, cytoplasm, and cell membrane, lipopolysaccharide, or CD14 – a pathogen recognition receptor present in two forms cell membrane protein (mCD14) and soluble (sCD14) were already reported to interact with Lf, however, none of these interactions are selective enough to serve as bioreceptors. For the above reasons, Lf is not yet included in routine testing despite being considered a marker of at least two life-threatening diseases. The potential solution to the lack of lactoferrin routine diagnostics in real samples is the development of a cheap, feasible, selective, and sensitive method for its

17

detection based on other molecules that exhibit the potential of interacting specifically with this protein, for instance, deoxyribonucleic acid (DNA). Interestingly, Lf is capable of interacting with some specific DNA sequences, and the details of such interaction, as well as its potential in biosensing application, have not yet been explored, hence becoming the topic of interest. Recent progress in the development of nucleic acids synthesis has brought fast, simple, and affordable methods that allows to introduce them in many fields, including biosensing, in a much broader manner than ever before. Large analytes, such as proteins of molecular weight (MW) above several kDa, are often challenging to be specifically determined due to the negative effects of their size on the spatial and conformal conditions of biorecognition layer-target molecule setup. The steric hindrance is a challenge that efficiently limits the utility of bulky receptors like antibodies, while recently trending nanobodies – single-domain antibody (sdAb), are still in their infancy and expensive. On the contrary, DNA structures offer alterable sequences and sizes, and in the case of aptamers – shape, they are easier to immobilize and label compared to antibodies. Still, in order to obtain a highly specific and sensitive DNA-based biorecognition element, it is crucial to understand the supramolecular interactions between the DNA receptor and target molecule. Label-free, real-time method of surface plasmon resonance offers the possibility of studying kinetics and thermodynamic aspects of intermolecular complex formation at the supramolecular level. It is extremely useful in designing and developing new bioreceptors, with the advantage of resembling the biosensing approach by immobilizing one of the interacting molecules (receptor or target). In contrast, structural studies via nucleic magnetic resonance spectroscopy are performed in a liquid state, where both receptor and target are not immobilized. Another label-free technique is electrochemical impedance spectroscopy. As non-destructive, it is a method of choice for verification of interaction, as well as for quantitative analysis. When combined with electrochemical impedance spectroscopy, surface plasmon resonance allows for insightful analysis of strength, dynamics, and binding forces that drive receptor-target complex formation. As such, it gives the opportunity to develop fast, efficient, and affordable methods for receiving specific new bioreceptors that can be further introduced in biosensing applications.

Purpose and theses

The subject of the doctoral dissertation is the development of a DNA-based bioreceptor selective to endogenous immunomodulator lactoferrin and its utilization in the biosensing of this protein in human saliva. The presence of lactoferrin in saliva is associated with host defense against oral pathogens and control of the oral microbiome. The research conducted in the frame of this work covers the following research problems and issues:

o the influence of DNA sequence (oligonucleotides differ in sequence, size, single-stranded or double-stranded), as well as immobilization conditions having an impact on spatial orientation and interaction – resulted in the establishing of biofunctionalization procedure of gold surface plasmon resonance sensors with the use of various DNA oligonucleotides and identification of the DNA sequence with the highest affinity (highest output signal) towards lactoferrin,

    o the influence of analyte concentration and temperature on the interaction between DNA of the selected sequence – Lf bioreceptor, and lactoferrin – target molecule using surface plasmon resonance – resulted in obtaining affinity, kinetic, and thermodynamic constants,

o the influence of modification conditions such as linker-to-blocker concentration ratio on the immobilization level and the effect of measurement conditions such as utilization of redox probe, frequency range, and applied potential on the impedimetric response to receptor-analyte interaction – resulted in transferring the modification method to impedimetric technique and establishing metrological parameters of the developed DNA-based biosensor,

o the application potential of the developed impedimetric biosensor in measurements of lactoferrin levels in human saliva – resulted in obtaining experimental data consistent with reference methods, confirming the usefulness of the constructed biosensor.

The research aimed to develop a new bioreceptor selective towards lactoferrin by adapting a feasible and straightforward approach to designing the specific DNA probe based on sequences reported in the literature that interact with lactoferrin. The utilization of surface plasmon resonance allowed to perform the affinity screening of various proposed DNA oligonucleotides that differed in sequence (content and order of nucleobases in the strand),

length, and form – hybridized and unhybridized (double- and single-stranded), which led to establishing the DNA oligonucleotide of highest affinity to the target protein. Next, the steady-state and dynamic analyses (kinetic and thermodynamic) were carried out in order to obtain detailed information on the interaction mechanism and driving forces and calculate equilibrium and rate constants to eventually evaluate if the selected DNA meets the criteria for affinity-based bioreceptor (affinity constant $> 10^{-6}$ M refers to specific interaction). The identified bioreceptor was, at this stage, employed to the impedimetric biosensor, and the metrological parameters were assessed for lactoferrin laboratory samples under physiological pH. Ultimately, the developed biosensor with DNA biorecognition layer was applied to quantitative measurements of lactoferrin concentration in human saliva samples of healthy volunteers, and its utility was evaluated by comparing the results with two reference methods.

Within the discussed subject, the theses were proposed:

T1. The DNA molecule of the defined sequence exhibits a high affinity towards endogenous immunomodulator lactoferrin and can serve as a selective bioreceptor for label-free biosensors.

T2. Affinity screening using surface plasmon resonance enables the identification of the designed DNA oligonucleotide that selectively interacts with a target protein.

T3. Impedimetric detection of lactoferrin with the identified bioreceptor enables the assessment of analyte concentration in biological samples under physiological pH conditions.

Scope

Developing new biosensing layers based on DNA to detect large protein targets is challenging due to the complex nature of such interactions. This research aimed to develop a selective and stable new bioreceptor for lactoferrin. Since Lf, as an endogenous immunomodulator, is capable of interacting with DNA, the investigation has focused on a DNA-type bioreceptor.

The research tackles the following aspects: (i) proposition of new methodology based on SPR supported affinity screening for development of selective lactoferrin DNA-type bioreceptor simple approach, finalized with identification of particular DNA sequence selective towards target protein, (ii) a description of interaction of selected bioreceptor with lactoferrin using label-free method of surface plasmon resonance, including kinetic and thermodynamic aspects of complex formation, (iii) estimation of rate and equilibrium constants as well as thermodynamic constants by fitting mathematic models of interaction (kinetic and thermodynamic) to experimental data, (iv) establishing methodology of transferring the surface modification procedure using DNA-type bioreceptor from surface plasmon resonance to electrochemical technique, (v) development of impedimetric label-free biosensor equipped with DNA-based biorecognition layer and determination of its metrological parameters, and (vi) implementation of developed impedimetric biosensor to lactoferrin measurements in human saliva samples.

The doctoral thesis scope consists of three major parts. The first – the literature review, is divided into four chapters. Chapter 1 describes the analyte of choice and highlights its clinical significance. Chapter 2 introduces the characteristics of molecular recognition systems in biosensing applications by showing the recent trends in their development. A comparison of different biorecognition elements is provided. The chapter puts a particular emphasis on surface plasmon resonance as a method for the development of new (bio)receptors, especially DNA-type. Chapter 3 presents detailed information on lactoferrin determination methods with the division according to the readout type. The section is finished with the motivation for the undertaken research, in which the drawbacks of existing methods and challenges related to developing novel lactoferrin bioreceptor are pointed out.

The second part of the dissertation focuses on details of the experimental work. It starts with the list of the materials and instrumentation in chapter 5, followed by the description of the developed methodology in chapter 6, which is divided into thirteen subsections. These subsections relate closely to the chronological course of the research, as follows: justification

for the DNA sequences selection, preparation of the surface plasmon resonance sensors, affinity and dynamic analyses, selectivity of the bioreceptor in the presence of interferents, preliminary lactoferrin quantification onto hydrogel-based sensors, transfer of the modification method toward impedimetric-type sensors with linearly linked bioreceptor, verification of the surface modifications, supporting electrochemical measurements, leading impedimetric measurements methodology and reference tests. The chapter is complemented by the description of utilized biological samples and their preparation, as well as the methodology of alternative biorecognition systems based on immunosensing and biomimetic sensing that were examined within the doctoral research.

The third major part of the dissertation collects the results of the investigations, which corresponds to the methodology subsections of the previous chapter. In chapter 7, different aspects of the interaction between lactoferrin and the developed DNA bioreceptor are arranged in six subsections. The immobilization and interaction results under various experimental conditions are followed by the affinity analysis. Then, the results of dynamic analyses, kinetic and thermodynamic, are shown, as well as the selectivity of the developed bioreceptor vs. interferents. Lastly, the quantitative analysis with the surface plasmon resonance onto hydrogel-based sensors is demonstrated. The results devoted to the transfer of the modification method toward biosensing surfaces suitable for electrochemical analyses and the characterization of new impedimetric biosensors are included in chapter 8. It also contains the outcome of quantitative concentration analysis and estimation of biosensor shelf-life. The results of measurements in real samples constitute a separate chapter 9, while in chapter 10, the results obtained for alternatively investigated bioreceptors (antibodies and molecularly imprinted polymers) are collected. The research outcome is discussed in chapter 11, in which the results were confronted with the current state of knowledge regarding the interaction of proteins with DNA and the determination of lactoferrin.

Eventually, the dissertation is closed with a summary and conclusions, including prospects for the research.

The primary outcome of the research discussed and summarized in this dissertation is presented in two publications. The first article, "DNA-based molecular recognition system for lactoferrin biosensing", *Int. J. Biol. Macromol.* 253 (2023) 126747 refers to the development of a selective DNA-type bioreceptor for lactoferrin and a description of the interaction mechanism, whereas the second work entitled "Label-free impedimetric biosensor based on a novel DNA-type receptor for selective determination of lactoferrin in

human saliva", *Sens. Actuators B Chem.* 405 (2024) 135377 is focused on designing and developing a label-free impedimetric DNA-based biosensor for lactoferrin and application to measurements in real samples.

Literature review

1. Lactoferrin and its significance

Lactoferrin is a non-heme glycoprotein belonging to the transferrin group, meaning it is capable of binding iron ions. Contrary to transferrin, which transports iron within the organism, lactoferrin is rather sequestrating iron from the environment, with an extremely high binding constant of around 10^{22} M [7,8]. It was first isolated from cow's milk in 1939, whereas in 1960, independent laboratories confirmed that Lf is the main iron-binding protein in human milk. Lactoferrin is a multipotent protein with immunomodulatory properties, meaning it can recognize the immune status and take appropriate action by either up or down-regulating the immune response through various mechanisms [9,10]. The most important functions of Lf within an organism include antibacterial, antiviral, antioxidant, anticancer, and anti-inflammatory activities [11]. Lf concentration increases locally at the infection site, being secreted from secondary granules (neutrophils). Hence, it is considered a marker of activity for inflammatory diseases of immune background: Leśniowski-Crohn's disease and inflammatory bowel disease [12,13]. Lf is present in almost any body fluid, including plasma, urine, or saliva; however, it is most abundant in milk, especially colostrum. Recent research on neurodegenerative diseases, including Alzheimer's disease, indicated salivary lactoferrin as a possible marker of early cognitive decline [5,6] and correlated its level with cortical amyloid-beta load, cortical integrity, and memory in aging [14,15]. Hence, lactoferrin is considered a salivary biomarker used to diagnose Alzheimer´s disease [16]. The antimicrobial activity of Lf was proven in oral infections by *Streptococcus mutans* [17]. The clinical significance of this protein arises since the newest research focuses on its utility as a tool in the fight against SARS-CoV-2 [18,19]. Despite its increasing relevance, lactoferrin is not included in diagnostic routines since there is a lack of detection methods that are cheap, feasible, and sensitive enough to gain the attention of clinicians. To introduce details of lactoferrin, the structural characteristics and biological properties will be discussed in the following subsections, with particular emphasis on its role in the host defense system – Lf as guardian of the human genome [20].

1.1. Characteristics and biological properties

Lactoferrin is a bulky glycoprotein with MW approximately 80 kDa and 703 amino acid residues. The Lf spatial structure presents two spherical lobes: the N lobe containing 1-333 amino acid residues, the C lobe with 345-691 amino acid residues, and a helical-shaped

bridge with residues from 334 to 344 that connects the lobes. Each lobe of Lf has a MW of approximately 40 kDa. The homologous lobes show approximately 37% similarity (125 identical residues in the corresponding protein sections). Each lobe has two parts, the so-called α and β domains, called N1, N2 and C1, respectively, C2. Overall, Lf has two lobes and four domains [7,9]. Each lobe has one cavity where iron is bonded. The structure and Fe^{3+} binding sites are presented in Fig. 1. The affinity of lactoferrin for iron is approximately two times greater than that of transferrin, which may be partly due to cooperative interactions between the two lobes of lactoferrin – lobes stabilize each other under physiological conditions, while under an acidic environment, the helix bridge unfolds. Then, the structure relaxes, losing the complexed iron ions. The complexation constant of iron ions is very high ($K\sim10^{22}$ M) [7]. Due to the presence of two iron-binding sites, there are three known metallated forms for all Lfs, which differ in their iron-loading: apo- (without iron), a monoferric form (one iron per protein), and a diferric or saturated holo- form (two irons per protein) [21]. Typically, two forms of lactoferrin can be found *in vivo*: free – apolactoferrin and iron-saturated – hololactoferrin. The third form of lactoferrin constitutes a small percentage of total Lfs. Apo- and holo-lactoferrin differ in their tertiary structure [7]. During binding with Fe^{3+} ions, the structure of the protein changes significantly (movement of the domains around the iron molecule and interactions between the lobes) – the process of closure around the iron molecule with the simultaneous attachment of two bicarbonate anions. Fe^{3+} in binding sites of each lobe is bound by four amino acid residues (2 Tyr, 1 Asp, 1 His), and it is strong but reversible binding. As mentioned before, iron release occurs due to lower pH (probable role of bicarbonate ions). Occupied binding sites provide three negative charges to balance the tri-positive iron ions, while the N-terminal helix, together with the arginine (Arg) side chain, having a positive charge, balances the negatively charged bicarbonate anions. The process of binding and releasing iron occurs due to the flexibility of the unbound form (apoLf) and the corresponding stiffness of the bound form (holoLf) [21]. Lf can also bind other trivalent ions, e.g. Ga^{3+}, Al^{3+}, Co^{3+}, Mn^{3+}, divalent ions, e.g. Cu^{2+}, Zn^{2+}, V^{2+} and trivalent lanthanides An^{3+}, Ln^{3+} [22]. The binding of ions other than iron probably results from the participation of Lf in their metabolism within the organism. Lf has a strong cationic character, with an isoelectric point (pI) equal to 8.7, which results in a high affinity for binding to receptors of various types of cells and anions. However, the distribution of positive charge on the Lf surface is highly uneven with three characteristic areas where the most positive charge is accumulated: at the end of the N lobe (residues 1 to

7), along the outer line of the first turn of the helix connecting the lobes (residues 13 to 30), and in the area inside the N lobe in the vicinity of the binding helix. Due to the concentration of positive charge at the N-terminus and the adjacent C-terminus (residues 27-30), this area has been proposed as a binding site for DNA, heparin, lipopolysaccharides (LPS), and glycosaminoglycans (most likely species-specific) [23,24].
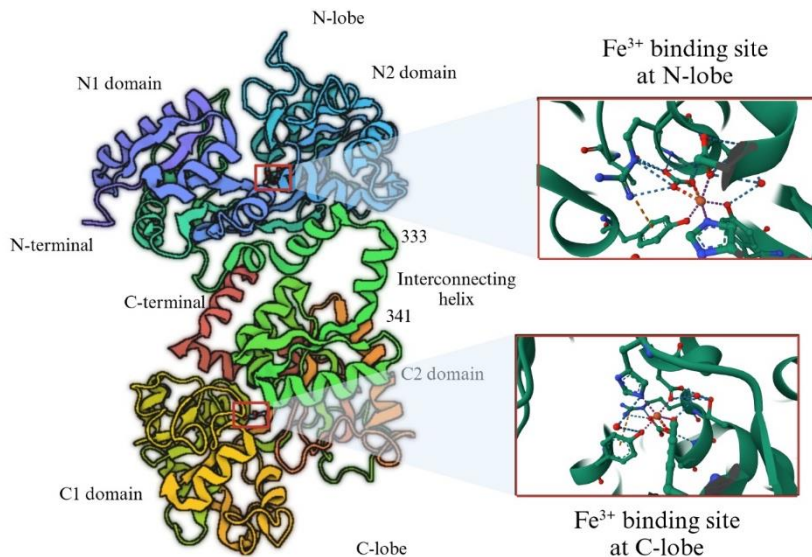
Fig. 1. Lactoferrin structure and the iron ion binding sites. Based on PDB DOI: 10.2210/pdb1B0L/pdb.

1.2.   Clinical significance of lactoferrin

Lactoferrin is secreted by secretory epithelial cells, included in the exocrine (pancreatic secretory) system, and stored in secondary and tertiary granules of neutrophils [25]. It occurs in all human body fluids: milk, blood, saliva, tears, semen, mucous secretions of the respiratory tract, secretions from the gastrointestinal tract, cerebrospinal fluid, neutrophils, neutrophils, feces, and others, produced in its final and free form, without precursors. The concentration of lactoferrin in healthy humans in plasma is the lowest at around 1 $\mu g \cdot mL^{-1}$, 5 $\mu g \cdot mL^{-1}$ in cerebrospinal fluid, 0.07 $mg \cdot mL^{-1}$ in saliva, up to 5 $mg \cdot mL^{-1}$ in milk [26]. This protein is resistant to the action of proteolytic enzymes, such as trypsin and its derivatives [9]. Release of lactoferrin follows the degranulation, which occurs under the influence of interleukin 8 (IL-8) – chemoattracting cytokine activating neutrophils in inflammatory regions, and the binding of some surface immunoglobulins – therefore, the concentration of lactoferrin in the plasma increases in inflammatory conditions, iron overdose, and infectious

diseases [27]. Lactoferrin is a protein known for its antibacterial and bacteriostatic properties [27,28]. It works by depriving bacteria of the iron they need to grow. At the same time, iron ions are essential for producing hydroxyl radicals, which participate in oxidative stress, indicating the antioxidant role of Lf protein. Lactoferrin also has anti-inflammatory properties, as it is involved in the mitogen-activated protein (MAP) kinase pathway and the nuclear factor kappa B (NF-κB) pathway. This protein can directly suppress the production of inflammatory cytokines by inhibiting the binding of NF-κB to cytokine growth promoters. Lactoferrin is a protein produced in excess during inflammation of the respiratory system's mucous membranes [29,30]. Elevated levels of lactoferrin are observed in non-infectious inflammatory conditions such as neurodegenerative diseases [31,32], colitis [33], and allergies [34]. In sepsis, the Lf levels can increase from 0.4-2.0 $\mu g \cdot mL^{-1}$ to 200 $\mu g \cdot mL^{-1}$ in the blood [35,36]. Lactoferrin can inhibit the production of several cytokines, including tumor necrosis factor-alpha (TNF-α) and interleukin 1β (IL-1β), which are key mediators of the inflammatory response [37]. Additionally, lactoferrin can bind and sequester both bacterial LPS and soluble CD14 glycoprotein, which is a cytokine whose production is induced by LPS [38–40]. This action prevents further development of the inflammatory pathway promoted by CD14 (part of the innate immune system) and contributes to the protein's anti-inflammatory activity. Regulatory function over immune system under inflammation results from Lf ability to interact with many cells, including most leukocytes. Lf has a pleiotropic immunomodulatory effect on immune cells: lymphocytes, macrophages, and Langerhans cells [41,42]. It influences the proliferation and differentiation of immune system cells – lymphocytes B and T and promotes preferential maturation of CD4-CD8 T cells into the CD4+ helper line. Lactoferrin can suppress or induce the process of myelopoiesis (bone marrow production), most likely due to modifying the production of a factor stimulating the production of interleukin-1β and granulocyto-macrophages. The antiviral effect of Lf was reported toward viruses such as Hepatitis C virus (HCV), Herpes Simplex Virus-1 (HSV-1), Zika virus, Chikungunya virus, Human Immunodeficiency Virus (HIV)-1, and Human Coronaviruses (HCoVs) [30,43–45]. Lf can bind to dendritic cells, which also affects bone cells, such as osteoblasts. Another interesting function of Lf is its enzymatic activity – in milk, Lf is the protein with the highest activity of amylase, DNase, RNase, and ATPase [46–48]. It is believed that the anticancer activity of Lf results from its ability to induce the secretion of interleukin 18 (IL-18) in the gastrointestinal tract, subsequent systemic activation of natural killer (NK) and lymphokine-activated killer (LAK)

cells, and increased numbers of CD8 T lymphocytes (CD8 – antigen present on the surface of T lymphocytes) [42]. Lf is considered a marker of intestinal inflammation [49,50], able to bind with intestinal epithelial cells through intelectin-1 protein [3,12], and therapeutic response in Leśniowski-Crohn's disease [33,51–53], both of autoimmune origin. Furthermore, it has been proposed as a marker of inflammatory neurodegenerative diseases, e.g. Alzheimer's disease and dry eye disease. Lf has a protective function of the body against skin and pulmonary allergies [34,54] – it is overproduced in patients with allergies, which involves the activation of mast cells (cells of connective tissue and mucous membranes) and basophils and the migration of cells presenting antibodies caused by the activity of pro-inflammatory factors (IL -1β and TNF-α). Lf can bind polymorphic protein - apolipoprotein E-low density lipoprotein receptor (ApoE/LDL, also known as LDL cholesterol), i.e., LRP-1 (LDL Receptor Related Protein) – functions as a signaling receptor on the surface of osteoblasts, fibroblasts and hepatocytes [55]. Recently, lactoferrin gained extensive attention due to its putative role in blocking SARS-CoV-2 attachment through binding with the spike protein of the virus [19,56]. It has been discovered that lactoferrin (Lf) can directly bind to DNA and acts as DNase under certain conditions [57,58]. This activates transcription and regulates the cell cycle [20]. Such findings have been further supported by studies that show that the DNA-Lf complex has protective and repairing roles in different types of cells, such as during inflammation or wound healing [59,60]. While several research articles have been on Lf's interaction with DNA, only three short sequences have been identified as specifically interacting with Lf. These sequences are (1) GGCACTT(G/A)C, (2) TAGA(A/G)GATCAAA, and (3) ACTACAGTCTACA [61]. Other authors have reported that Lf has a preference for binding with double-stranded (*ds*) DNA over single-stranded (*ss*) DNA [62]. They also observed that the interaction with holo-Lf was slightly stronger than with apo-Lf, which differs in tertiary structure. The putative Lf region that can interact with DNA is indicated in Fig. 2, and it involves amino acids 20 to 24, according to crystallographic studies [63,64]. The amino acids Phe-Gln-Trp-Gln-Arg are part of the α-helix outer region of the N-terminus of lactoferrin, which is well exposed and plausibly accessible for DNA structure.
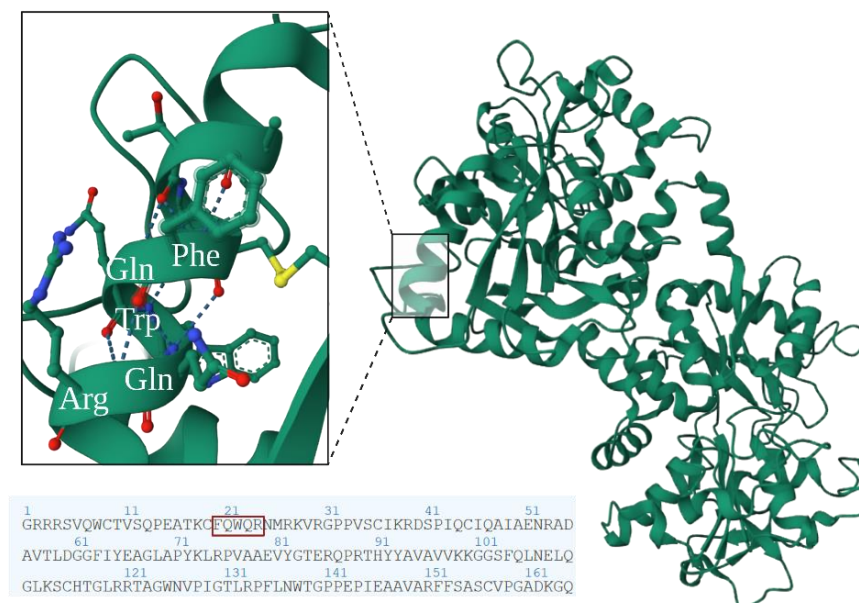
Fig. 2. The lactoferrin region consists of 5 amino acid Phe-Gln-Trp-Gln-Arg sequence (FQWQR) contributing to direct interaction with DNA (PDB DOI: 10.2210/pdb1B0L/pdb) [65].

2. Molecular recognition in (bio)sensors

The term molecular recognition refers to the specific interaction resulting in non-covalent binding between two or more molecules and is usually described by supramolecular chemistry tools. This interaction may include hydrogen bonding, electrostatic forces, hydrophobic forces, van der Waals forces, metal coordination, π-π stacking interactions, and appear between host and guest as a result of their molecular complementarity [66]. Molecular recognition may be divided into biological and artificial systems – due to an understanding of the interactions that occur at the supramolecular level in living organisms, it is possible to create synthetic systems mimicking nature. From the perspective of (bio)sensing application, there are two major approaches for biorecognition: catalytic enzyme-based and affinity-based (Fig. 3). The latter involves biorecognition based on immune system mechanisms (antibodies) or nucleic acids [67]. Antibodies are typically used to recognize antigens – large analyte molecules such as proteins and their fragments, peptides, polysaccharides, lipids, etc. [68]. In the case of enzymes, the recognition of substrate molecules is determined by the protein structure surrounding the active site. Enzymatic layers play a catalytic role in the substrate reaction and are used to indirectly detect target analyte (substrate), usually small molecules. A separate broad group of recognition elements in (bio)sensing applications is called biomimetic sensing, in which the
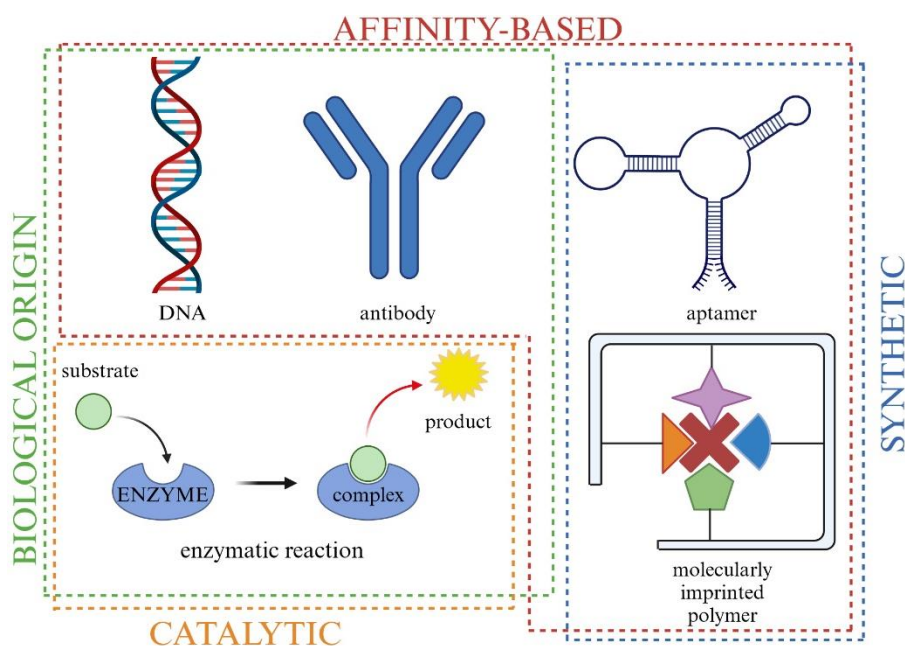
29

Fig. 3. Schematic representation of major molecular recognition systems, affinity-based and catalytic.

biorecognition role is realized by a specifically designed molecular cavity capable of capturing the target molecule. Briefly, biomimetic sensing is based on the mutual affinity of molecular target and synthetic receptor, which mimics the behavior of biological system [69]. The biologically active molecules that may display bioreceptor properties (affinity-based approach) are nucleic acids [70], which include DNA and RNA molecules of various sequences and lengths, among others aptamers [71], which are synthetic, typically single-stranded DNA or RNA tertiary structures of alterable sequence, size, and shape. They are obtained through combinatorial procedures *in vitro*. Unlike enzymes and antibodies, nucleic acid molecules with a characteristic sequence can be used as a recognition element for both small targets, such as mercury ions [72–74] or low-molecular-weight drugs [75–79], and large molecules exceeding tens of kDa, such as proteins [80–82]. On the other hand, enzymatic sensors are attractive due to their versatility in possible catalytic reaction products, such as ions, electrons, heat, or light, allowing various detection methods to be applied. In the case of affinity-based biosensors, the receptor-target molecule bonds are weak physical bonds, covalent bonds are not encountered, and the product of the interaction is complex. The type of interaction between receptor and target analyte is crucial to the sensitivity and selectivity of DNA-based biosensors [83]. As such, the development process of a bioreceptor for biosensing purposes must consider two aspects of ligand-analyte binding: the mechanism of interaction and the resulting specificity.

2.1. Surface plasmon resonance for the development of new (bio)receptors

One technique for studying receptor-target molecule interaction, enabling real-time monitoring of complex formation, is surface plasmon resonance (SPR). The surface plasmon phenomenon occurs when a polarized light beam excites a dielectric/metallic layer interface under total internal reflection conditions (Fig. 4).
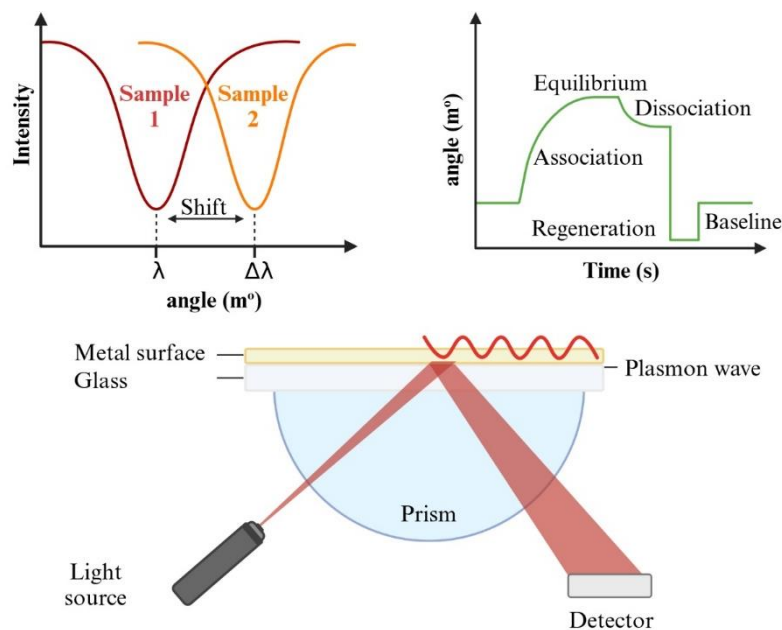
Fig. 4. The principle of SPR under total internal reflection, incident light photons are absorbed in the metal surface, and their field energy is transferred to electrons (free electrons constellations on the metal surface), which convert into surface plasmons.

An electromagnetic surface wave, which is a collective oscillation of the free electron gas density on the surface of noble metals, known as a surface plasmon, can couple to the evanescent field at the metal/liquid interface [84]. This coupling takes place at a specific angle of incidence, where the intensity of the reflected light reaches the minimum and is called the surface plasmon resonance angle. The plasmons resonate at the same light frequency, leading to light absorption at that angle. As a result, a dark line is created in the reflected beam, which contains a lot of information. The minima shift reflects changes in the refractive index due to molecular binding events or conformational changes in the molecules bound. By monitoring this shift over time, it is possible to study the binding kinetics and molecular binding events. To utilize the SPR technique for analytical purposes, specific ligands or bio-receptors are fixed to the metal layer surface [85]. When exposed to the sample, analyte molecules interact with the immobilized ligands, resulting in observable

31

changes in the refractive index in the vicinity of the metal surface. The SPR angle position depends on various factors, including the optical properties of the prism, the metal, the liquid medium, the metal film thickness, and the wavelength of the light source used. The penetration depth is determined by the wavelength of the incident light and the refractive indexes of the dielectric substrate and ambient, which are considered a dielectric medium. Depending on the system configuration, the depth of penetration can vary. However, an SPR biosensor typically cannot detect events beyond 600 nm from the sensor chip surface, with a range of 200 nm up to 300 nm being more common.

To study large macromolecules and their complexes, such as a protein-DNA complex, researchers usually use Nuclear Magnetic Resonance (NMR) spectroscopy. This technique helps collect structural restraints for further structural calculations [86–88]. However, it is important to note that NMR studies are performed in a liquid state. Other techniques used in DNA-protein interaction studies include Chromatin Immuno Precipitation (ChIP), DNA footprinting (investigating the sequence specificity of DNA-binding proteins *in vitro*), electrophoretic mobility shift assay (EMSA), and systematic evolution of ligands by exponential enrichment (SELEX) procedure, which are reviewed by Ferraz et al. [83]. Regarding binding kinetics and affinities, it was concluded that the filter binding assay and EMSA are useful and easy methods. However, advanced optical methods such as surface plasmon resonance and spectroscopy techniques are more sensitive. As all the techniques as mentioned earlier have their limitations, the SPR method was used to perform kinetic and thermodynamic analyses that can provide a deeper insight into the specificity and stability of DNA-protein complex formation. The SPR method is highly sensitive and allows for kinetic and thermodynamic analyses to be performed under immobilized ligand conditions, reflecting the sensor's surface conditions. This makes it a valuable tool for future sensor technology applications, particularly label-free methods [89–91]. The use of the SPR method is proposed for the study, as it allows for direct, real-time, and label-free measurements, as well as kinetic and thermodynamic analyses. This provides a basis for identifying the target recognition molecule and developing specific biorecognition layers, with ligand immobilized on the sensor's surface [89,92]. In SPR, the binding of the ligand with the target molecule (analyte) and any other molecules – both selective and non-specific interactions can be directly observed [93,94]. Thus, it was successfully used to develop various biosensing and biomimetic surfaces [95] or to discover new biomarkers [96].

2.2. Characteristics and comparison of recognition elements in (bio)sensing

It is essential to understand the advantages and disadvantages of each type of biorecognition element to develop new biosensors for diagnostics successfully. This chapter will compare the characteristics of different kinds of molecular recognition systems in the context of biosensing applications. These recognition systems can be divided into several groups based on the type of recognition element responsible for selectively capturing the analyte from the sample. One of the groups frequently used in clinical diagnostics is immunosensors. These are defined as a combination of a transducer and an immunocomplex that produces a recognition episode, which can later be transformed into a measurable signal. The immunoreaction is what allows for the selective detection of molecules, as it has high binding constants (usually greater than 10^{-6} M) [97]. Clinical diagnostics often employ immunoassays like the enzyme-linked immunosorbent assay (ELISA), which requires specialized equipment and trained personnel and therefore consumes time and resources. In comparison, point-of-care (POC) devices like immunosensors are more convenient. A simple in-use, low-cost, and rapid technology for POC-type portable immunodetection devices is lateral flow assays (LFAs) [98]. The very first POC system was a glucose test, which diabetic patients can easily perform at home without visiting a medical facility. The commercial glucose test is a type of catalytic biosensor that uses enzymes to catalyze a reaction and detect the product through measurable means [99]. Enzymatic biosensors have the advantage of various products of enzymatic reactions, including protons, electrons, light, heat, and color products, allowing for a wide range of detection techniques [100]. However, these biosensors might be limited by sensitivity drop due to fouling that reduces the signal and the presence of interferents, such as reactive oxygen species and radicals, in the sample matrix. Unlike other biosensors, preventing non-specific interactions is more challenging when using a classical enzymatic biosensing approach with specific biological matrices. Additionally, the majority of enzymes are susceptible to changes in temperature, pH, and concentration, which can lead to substrate or product inhibition and loss of receptor activity. Therefore, the development of biosensors is focused on providing the most optimal conditions to maintain enzymatic activity. Nucleic acids (NAs) such as DNA and RNA are often used as biorecognition molecules, particularly as probes to detect complementary strands through the hybridization process. DNA's unique structure enables interactions with a plethora of molecules, including some proteins (e.g. histones), pharmaceuticals (such as anticancer drugs), toxins, dyes, etc. [101]. The main advantage of DNA probes is

demonstrated by their ability to amplify the target sequence through polymerase chain reaction (PCR) and to enhance the signal generated by the biosensor. In recent years, there have been numerous works on the usage of DNA walkers – a class of NA nanomachines in which the NA walker moves along the nucleic acid track – in the biosensing field (Fig. 5). Advanced platforms using DNA walkers have been employed to detect e.g. antibiotics, enzymes and bacteria [102], nonetheless, significantly increasing cost and complexity of biosensor, almost disqualifying their applicatory potential in commercial testing. Aptamers are synthetic structures of single-stranded DNA or RNA or peptide, which undergo changes in sequence, 3D structure, and folding pattern changes upon binding with a target molecule. Typically, they are designed and produced through a process called SELEX, which involves *in vitro* combinatorial selection supported by different techniques such as sequencing [103].
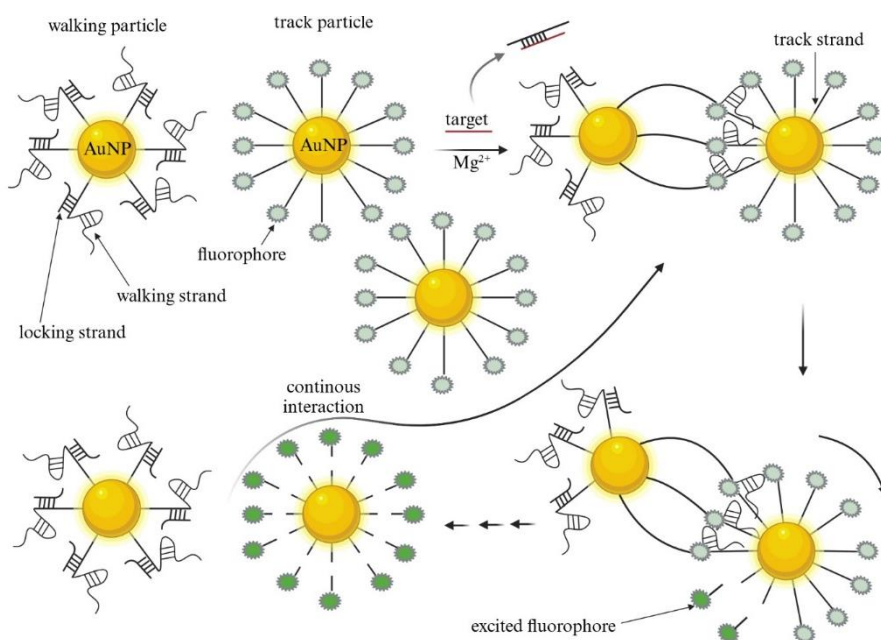
Fig. 5. Schematic illustration of the interparticle motional DNA walker triggered by the target. Based on Zhang *et al*. [104].

The undoubted advantage of aptamers is the freedom of design, including size, shape, and sequence, giving the possibility to develop specific receptors for any target. In practice, the tertiary structure of aptamers strongly depends on solution conditions, hence losing their properties in most real samples, e.g., blood. Compared to immunoreaction, the affinity of aptamer-target interaction is similar or even higher; while having a much smaller recognition element, it is easier to avoid steric hindrance during biosensor development. Steric hindrance is a phenomenon occurring due to steric effects such as steric bulk. It results in limiting the

interaction pace within or between molecules. While it can be used to the advantage of selectivity by limiting the unwanted side reactions, typically, it affects the intermolecular interactions negatively, especially by decreasing the activity of ligands that are immobilized. In biosensing applications, such lowered ligand activity leads to a dramatic drop in sensitivity.

Another synthetic receptor for protein detection is a biomimetic cavity produced in the process of molecular imprinting in polymer (MIP) [105]. It differs significantly from other systems as it overcomes issues like poor chemical and thermal stability, rapid wear of the biorecognition layer, and low reproducibility in biosensors with biological recognition elements. Various types of polymers, including naturally occurring matrices, conductive polymers, etc., were employed for manufacturing biomimetic layers, which mimic the behavior of biological receptors. Imprinting can be accomplished with two primary strategies: bulk imprinting, which involves using the whole target as a template molecule, and epitope imprinting, primarily used for large targets such as proteins. In epitope imprinting, only a selected fragment of the molecule, such as a peptide, is used as a template since templating the whole molecule in this case is not feasible. It poses a significant challenge for molecularly imprinted polymers, namely achieving selectivity. The size, shape, and surface functional groups determine the final molecular compatibility of biomimetic cavities toward specific molecules. Other types of molecular recognition systems in biosensing applications concern supramolecular complexes of host-guest, such as ionophore-ion, in which non-covalent interactions through weak forces are fully reversible under precise conditions [106]. The following subsections will demonstrate the main features of the aforementioned biorecognition elements of the affinity-based approach in biosensing.

2.2.1. Immunosensors

Antibodies (Abs) are glycoproteins involved in a defense mechanism of the immune system. Abs can be divided into five subclasses (IgG, IgM, IgA, IgD, IgE), depending on their heavy chain constant region sequences. However, the basic structure is a large Y-shaped molecule of around 150 kDa, made of four peptide chains joined by disulfide bonds. The building blocks of Abs are constant fragment (Fc) and antigen-binding fragment (Fab). The different Abs classes are depicted schematically in Fig. 6. These types of proteins react to foreign substances called antigens (Ag) through the binding site of their Fab region [107]. Ag-Ab

binding occurs through non-covalent interactions, forming the Ag-Ab complex that exhibits high selectivity and sensitivity. Immunoassays are analytical tools developed using Ag-Ab complexes. The principle of immunoassays relies on detecting a specific macromolecule, known as an antigen, using an antibody of high affinity toward the target. Notably, there are two types of antibodies: monoclonal, in which one particular Ab is able to interact with one target molecule, and polyclonal, which can capture multiple target molecules per one Ab. Interestingly, the development of the recombination method allowed the production of functional Ab fragments in a variety of systems, including mammalian, insect, yeast, and plant, which contributed greatly to their widespread use in biosensors [108].

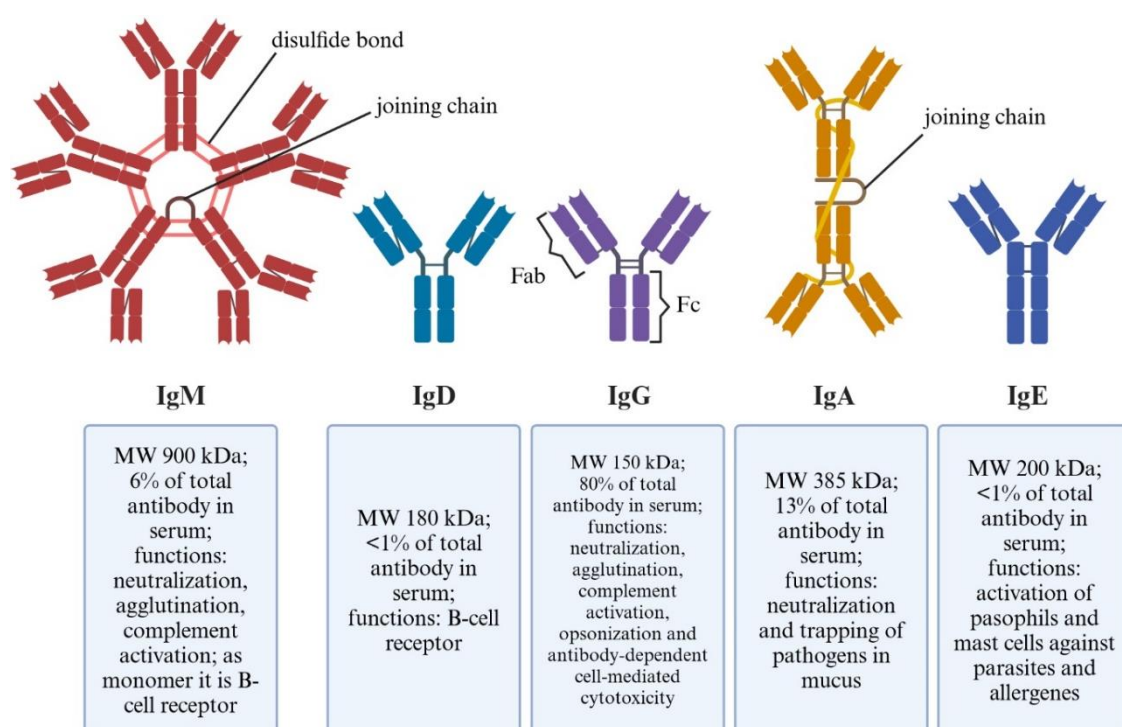| IgM	IgD	IgG	IgA	IgE
MW 900 kDa; 6% of total antibody in serum; functions: neutralization, agglutination, complement activation; as monomer it is B-cell receptor	MW 180 kDa; <1% of total antibody in serum; functions: B-cell receptor	MW 150 kDa; 80% of total antibody in serum; functions: neutralization, agglutination, complement activation, opsonization and antibody-dependent cell-mediated cytotoxicity	MW 385 kDa; 13% of total antibody in serum; functions: neutralization and trapping of pathogens in mucus	MW 200 kDa; <1% of total antibody in serum; functions: activation of pasophils and mast cells against parasites and allergenes

Fig. 6. Types of antibodies and their different characteristics, including structure, MW, abundance in serum, and biological functions.

They are powerful tools commercially available in various formats for detecting very low levels of hormones, enzymes, viruses, toxins, tumor antigens, and bacterial antigens, typically around 10^{-12}-10^{-9} mol·L^{-1}. Since Ab-Ag complexes do not exhibit any specific optical features nor are electrochemically active, labeling is a must to be able to generate a signal adequate for the used transducer in biosensor applications [109]. Hence, labels such as enzymes, radioisotopes, chemiluminescent probes, fluorophores, redox probes, etc., are used, depending on the transducer technology. The enzyme-linked immunosorbent assay

(ELISA) is one of the most widely used types of tests in biomedical research, both scientific and diagnostic, which uses the labeling of antibodies with an enzyme in order to obtain an analytical signal proportional to the concentration of a target molecule (Fig. 7).
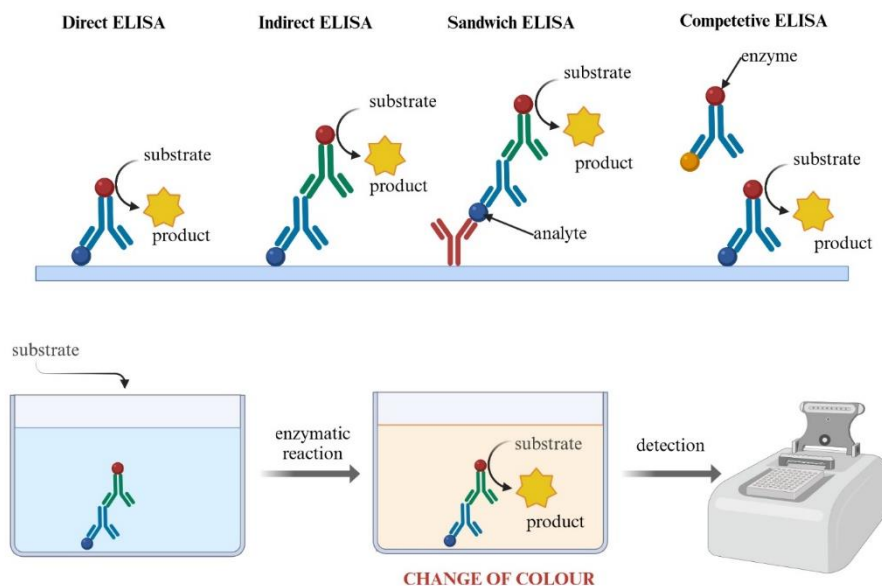

Fig. 7. Variants of ELISA and the basic principle of ELISA operation: indirect detection using the colored product of enzymatic reaction, where the enzyme serves as a label.

Such necessity of labeling is the main drawback of immunoassays, making it complicated and time-consuming to obtain the analytical signal from seemingly simple setup. On the other hand, it opens up vast possibilities for signal amplifications with nanomaterials such as metal nanoparticles, carbon-derived nanostructures (tubes, rods, etc.), or quantum dots [97]. Immunoassays, in general, are characterized by high specificity, reproducibility, and sensitivity; however, they most frequently require a multistep preparation protocol. Therefore, they are frequently utilized in clinical diagnostics in the form of rather costly kits combined with sophisticated analytical instrumentation, and their potential for "in-home" use or as POC tools is limited. Moreover, the method of Ab immobilization is crucial for the performance of immunosensor and maintaining bioreceptor activity – if negatively affected by inappropriate bioreceptor spatial orientation and density, it results in a drop in sensitivity [110]. Hence, overcoming steric hindrance, which occurs when the binding site of an antibody cannot form a complex with an antigen, is one of the challenges in designing and developing immunosensors.

2.2.2. DNA-based sensors and aptasensors

Deoxyribonucleic acid (DNA) is a naturally occurring structure composed of smaller units called nucleotides [111]. Each nucleotide contains a nitrogen base, deoxyribose, and phosphoric acid residues. The nitrogen bases consist of purines (adenine – A, guanine – G) and pyrimidines (thymine – T, and cytosine – C) that pair up to form complementary base pairs: A-T and G-C. Physiologically, DNA exists as a double-stranded helix (*ds*DNA) that is typically curved clockwise and referred to as B-DNA. The structure is held together by hydrogen bonds, van der Waals forces, and hydrophobic interactions. The DNA framework has distinct features, including major and minor grooves between the strands that differ in width. These grooves have different molecular electrical potential distributions, which enable electrostatic interactions with other molecules. Additionally, the spatial arrangement and number of functional groups allow for hydrogen bonding between DNA and proteins or drugs. There are several types of interactions between DNA and other molecules, including groove binding, electrostatic attraction, and intercalation [101,112]. The DNA-based affinity-type molecular recognition system relies exactly on DNA's ability to specifically interact with other molecules – mechanisms presented in Fig. 8. For instance, the early anticancer drugs were based on their capability to bind to the double helix in major or minor grooves or slide between base pairs (intercalation). Regarding controlling immobilization, which is a critical aspect of biosensor performance development, DNA oligonucleotides are easier to immobilize than antibodies due to their smaller size and linear-like shape [113]. Moreover, the structure of DNA allows for more straightforward modification of functional groups without affecting biological activity. Additionally, the manufacturing cost is significantly reduced with the rapid advancement of DNA synthesis technology in recent years. Except for the simple structure of DNA as a biorecognition element, much more sophisticated DNA-derived bioreceptors are in use for biosensing. Deoxyribozymes, known as DNAzymes, are short DNA strands that can catalyze specific biochemical reactions. They have a modular structure with a central catalytic core and two substrate-binding arms [103]. DNAzymes with specific catalytic activity can be obtained from billions of DNA candidates through SELEX. In the presence of metal ions, DNAzymes can cyclically catalyze reactions, making them ideal for designing sensor structures for signal amplification. DNAzymes have many advantages, including easy synthesis, high sensitivity, specificity, and signal amplification, making them highly versatile in detecting metal ions, nucleic acids, and

bacteria. Moreover, DNAzymes can be successfully combined with aptamers and nanomaterials to develop multiplex bioassays.
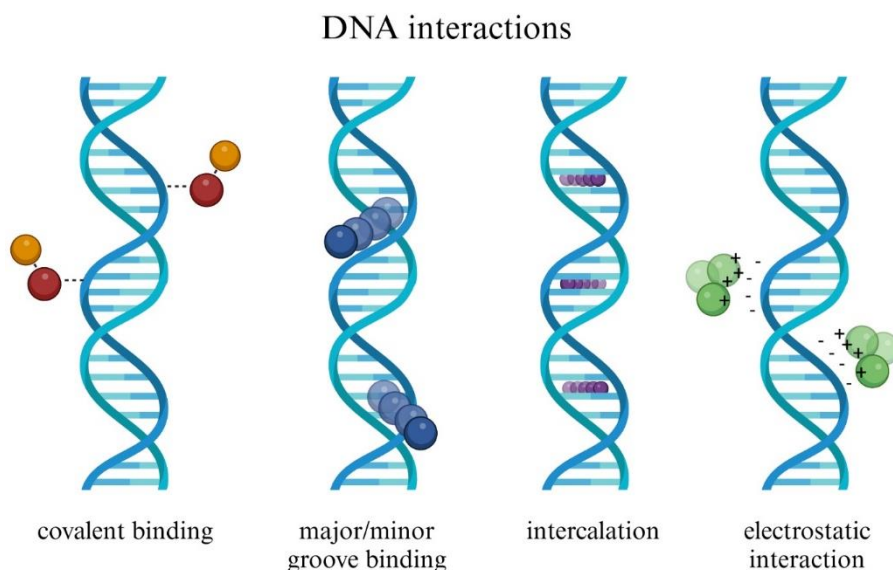

Fig. 8. Mechanisms of molecular interactions with DNA – covalent binding, groove binding, intercalation, and electrostatic forces.

G-quadruplex (G4) is a three-dimensional secondary structure formed by guanine-rich strands of nucleic acids through intermolecular or intramolecular Hoogsteen hydrogen bonds [74,114]. It is another DNA-derived molecule that demonstrates high stability and ease of chemical modification, making it useful as a functional nucleic acid. The G4 structure resembles quadrilateral hollow tubes with periodic pockets and has a central carbonyl-lined channel that can accommodate alkali metal ions. The presence of potassium ions further stabilizes the structure of the G-quadruplex. This makes G4 widely used as a molecular recognition unit in biosensors for metal ions. G4 can also interact with various substances, such as porphyrins and organic dyes, via π–π stacking. Combining organic dyes with G4 enhances the structural rigidity and planarity of the organic molecules, resulting in enhanced fluorescence of organic dyes. Moreover, the complexes effectively stabilize the G-quadruplex structure. Thus, G4 can be used as fluorescent probes to construct DNA biosensors [115]. DNA-walkers are an emerging trend that is used to enhance electrochemical response. They are a type of molecular machine that moves along a designed track, usually two or three-dimensional. These movements are based on strand displacement cascade or nuclease-mediated DNA hydrolysis mechanism, which can go continuously and automatically, resulting in considerable signal amplification. The development of

nanomachines, specifically DNA walkers, has received extensive attention since the Nobel Prize in chemistry was awarded in 2016 for achievements related to nanomachines [116–118], also described in [119,120]. However, the limited library of building blocks in DNA, only four types of nucleobases, compared to the 20 amino acids that Abs can be made of, is a major drawback. This limits the flexibility of designing DNA-type bioreceptors concerning chemical diversity. Nonetheless, nucleic acids can be easily produced and regenerated compared to other biorecognition elements. They provide exceptionally high selectivity due to sequence-based identification and sensitivity, making them highly useful in biosensing applications. Aptamers refer to synthetically produced single-stranded DNA (or RNA) oligonucleotides. These tertiary structures are created through an *in vitro* combinatorial process called SELEX [121,122]. Although there are multiple modifications of the SELEX protocol, the traditional approach involves repetitive cycles of 5 to 15 steps, which include incubation of a random pool of oligonucleotide sequences with the target molecule (library usually up to 10^{15} oligonucleotides), binding of the target molecule to some oligonucleotide, partitioning of bound and unbound sequences, and amplification of target-bound sequences by polymerase chain reaction for DNA sequences or reverse transcription polymerase chain reaction for RNA sequences. The purpose of the whole procedure is to select the sequence that exhibits the highest affinity towards the target molecule, such as complementary sequence, protein, peptide, drug, etc. Therefore, selected aptamers are characterized by binding affinity, secondary structure, and free energy. Compared with the traditional bioprobes like the Abs, aptamers could better adapt to extremely high temperatures, pH values, and high ionic concentrations [71,123]. The most used strategy to detect a biotarget with aptamer is to functionalize it with a reporting molecule (ferrocene, methylene blue) and an immobilization molecule (alkane thiol, alkane amino, streptavidin, and hydrazoate) at the 5′ end and 3′ end of the strand. The change of aptamer construction could be read out by detecting the electrochemical change on the electrode surface. An aptamer can also be decorated with conjugated polymers, which have been widely applied as the reporting tags in fluorescent and colorimetric biosensors because of their excellent optoelectrical properties. For DNA aptamer biosensors, the dynamic range and sensitivity, which the Langmuir isothermal adsorption model limits, are not flexible enough to suit the different ranges of detection concentration required. Some strategies, such as mixing different aptamers, can extend the concentration range; however, it often causes a drop in sensitivity. Compared with Abs or biomimetic sensors, aptamers' tertiary structure is highly dependent

on solution conditions, and they are easily degraded in contact with biomolecules present in real samples such as blood [124]. The chemical diversity of their structure is limited with nucleobases, while antibodies are built with 20 accessible amino acids. On the other hand, aptamers are more stable than antibodies and have a longer shelf life. Also, their synthesis is less laborious nowadays than it is for Abs. Nevertheless, compared to classical DNA structures, the SELEX protocol needs to be employed to synthesize aptamers, which still results in a multistep process of aptamers fabrication. The schematic representation of discussed NA-type molecules is shown in Fig. 9.
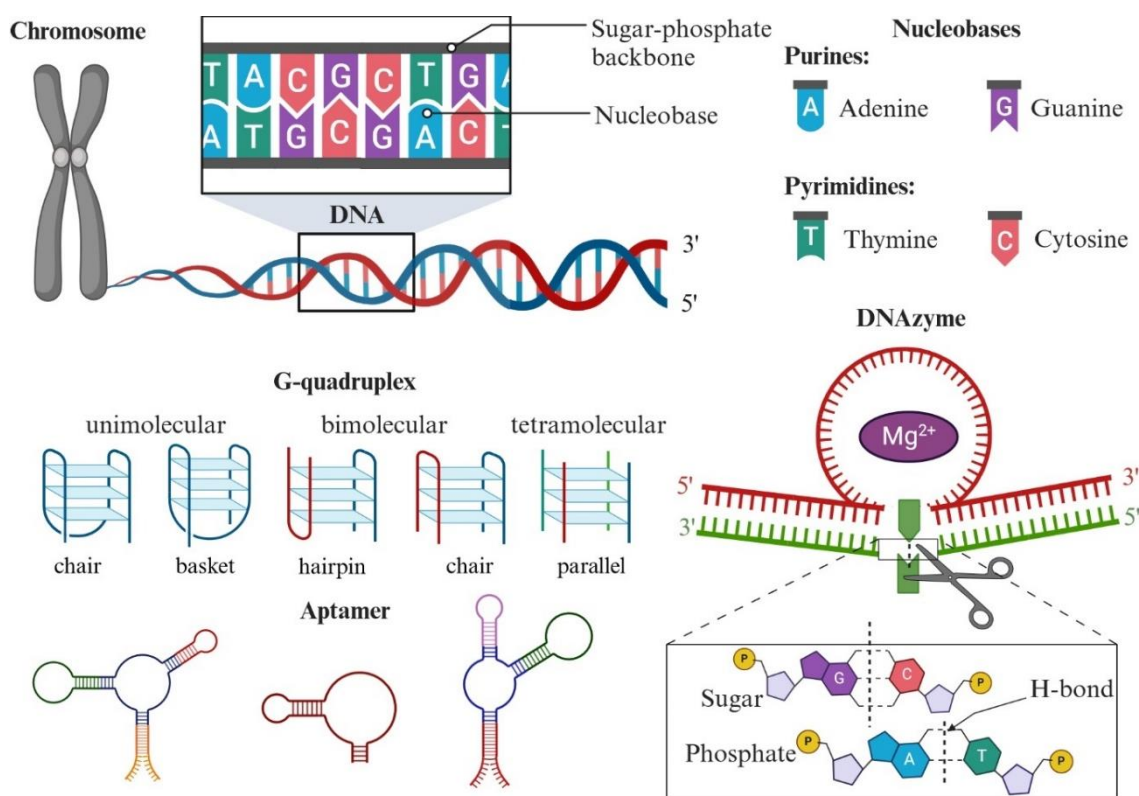

Fig. 9. Illustration of NA-type structures used in biosensing applications: DNA, aptamers, G-quadruplexes, DNAzyme.

2.2.3. Biomimetic sensors

Biomimetic sensors are equipped with an artificial recognition layer called molecularly imprinted polymer (MIP). It contains molecular cavities that interact specifically with target molecules [125,126]. The biomimetic layer is produced using a molecular imprinting technique to design tailored binding sites with predictable structures and specific recognition capabilities in shape, size, and functional groups. Biomimetic layers are relatively

inexpensive, easy to produce, reusable, and have good long-term stability. Unlike biomolecules, MIPs exhibit good chemical resistance and can be produced using a wide range of functional monomers, including naturally occurring monomers or conducting polymers. The role of the artificial cavity is to mimic the functional role of the bioreceptor in contact with the target molecule. This can be achieved using several imprinting strategies, such as bulk imprinting, in which the entire target is templated, or epitope imprinting, in which part of the target molecule that constitutes the selectivity is templated. Epitope imprinting is, therefore, suitable for large analytes (>1 kDa). Various methods, like grafting or microcontact imprinting, can create biomimetic binding sites depending on the desired transducing technique. The synthesis process follows the key-lock principle in three steps: (1) self-assembly of template molecule and functional monomer; (2) photopolymerization or thermal polymerization with cross-linkers and initiators, forming a network structure with a high degree of cross-linking and a particular three-dimensional space; and (3) separation of the template molecule from the polymer, leaving matching three-dimensional cavities on the substrate's surface [127]. Molecular imprinting is schematically shown in Fig. 10. The process of imprinting is classically performed at the planar support, however, molecularly imprinted nanoparticles (nanoMIPs) are another, more recent approach [128,129]. The imprinted polymer contains stereo cavities with specific recognition functions. These cavities can be combined with templates from complex samples to achieve detection and separation. The process is straightforward, fast, and easy to manage. MIP-based biomimetic sensors were used to detect antibiotic and pesticide residues, toxins, food additives, environmental pollutants, and heavy metal ions. MIPs have the potential to function as recognition elements, but achieving an extremely low limit of detection (LOD) is still a challenge. MIPs can have irregular morphology, low yield, and template leakage, which can cause issues. Moreover, no specific method exists for imprinting a particular class of molecules. Therefore, the synthesis process and choice of functional monomers must be determined experimentally, which can be laborious and resource-intensive [130]. Researchers mainly rely on incorporating nanostructures in biosensing layers to enhance MIP sensitivity. It is also necessary to investigate functional monomers, which can collaborate with other advanced technologies. For instance, computational studies are increasingly being used to select suitable functional monomers, which can be helpful in this regard.
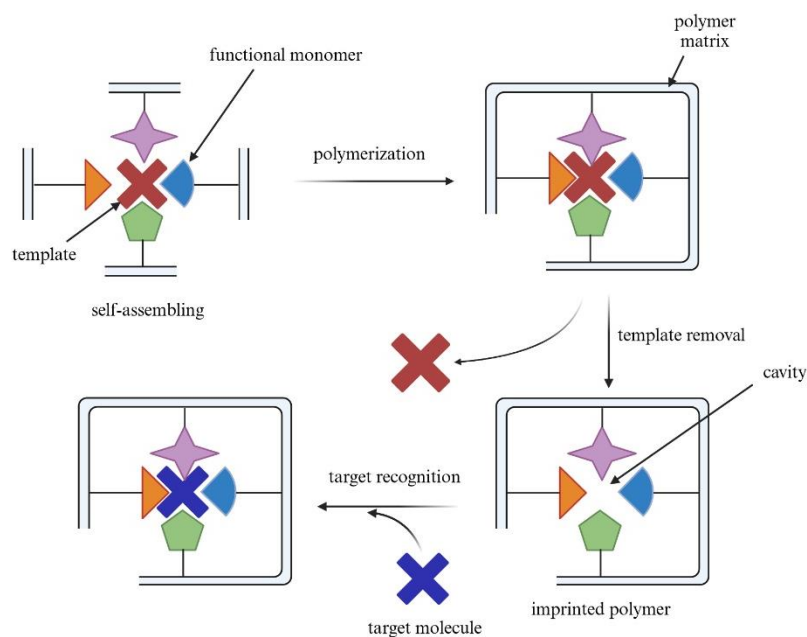
Fig. 10. Schematic view of the synthesis procedure of the molecularly imprinted polymer.

2.2.4. Others

Affinity biosensors have the potential to use various types of molecules as recognition elements, including peptides, proteins, dyes, and other compounds that exhibit affinity for a molecular target. While antibodies, nucleic acids, and biomimetic layers are commonly used, proteins are rarely utilized due to their size, which makes immobilization challenging and can affect biosensing performance. Thus, a more feasible approach is to select a specific protein fragment, such as a peptide, to serve as a biorecognition molecule [131,132]. Peptides are similar to proteins in their composition, as they are made up of amino acids. However, peptides have a rigid secondary structure, which makes their immobilization more reproducible than proteins. As mentioned earlier, immobilization is a critical factor affecting biosensors' effectiveness. Peptide structures that are artificially synthesized are known as peptide aptamers, and they can be used as recognition elements in biosensors, inhibitors, biological therapeutic agents, and so on. Organic and inorganic compounds are sometimes used as protein recognition elements through their interaction capability [133,134]. However, such solutions are rarely selective since metal-binding protein lactoferrin can capture di- and trivalent ions other than Fe^{3+}, e.g. Cu^{2+} or Mn^{3+}. Proteins can be detected through whole cells because many proteins interact with other protein-type receptors present on the cell membrane surface [135]. However, incorporating complex biological structures to design and develop biosensors is difficult and unprofitable compared to more

43

straightforward solutions. Therefore, in protein biosensing applications, using a peptide aptamer designed based on a cellular surface protein is easier. On the other hand, whole-cell biosensors are typically used to observe the effects of the analyte on living cells rather than provide detailed information about the analyte. They reveal details about the functional consequences of the analyte interacting with the cell or measure the total bioavailability towards the analyte.

3. Methods of lactoferrin detection – review

Lactoferrin is a protein that is present in body fluids and plays a vital role in the host defense system and regulation of immune processes. To understand the mechanisms of lactoferrin's action and to effectively monitor its level, it is crucial to use precise and reliable detection methods. As the interest in lactoferrin gradually grows, new biorecognition elements and methods for their development are being reported. Most of these methods are based on utilizing antibodies as Lf bioreceptors. However, recently, an aptamer-type biosensing approach has been frequently implemented. Concerning biomimetic sensing layers, only a few studies have been presented so far in which lactoferrin was quantitatively determined using artificial binding sites. As discussed in the previous sections, the biorecognition element is an essential part of the biosensor. Nevertheless, the readout method is another crucial factor for the overall success of the biosensing tool. It is worth noting that there are different methods to detect proteins, such as lactoferrin. These methods vary in their principles, complexity, instrumentation, time consumption, sample preparation requirements, the need for additional labels, and eventually costs. Among common methods used for lactoferrin detection are instrumental techniques. These techniques have high accuracy, require a small sample volume, and can be automated. However, it may be difficult to separate and distinguish lactoferrin from other components in the matrix using these techniques. Additionally, preparing such an analysis is time-consuming, requires qualified staff, and involves costly instruments. Instrumental methods are mainly used for samples and products in the food industry, where lactoferrin is present in raw materials such as milk or supplements. Commercially available kits for Lf detection are mostly enzyme-linked immunosorbent assays (ELISAs) using two antibody types. A primary antibody is used for the target antigen, and a secondary labeled antibody is used against the primary antibody. The analytical signal is obtained through spectrofluorimetry or UV-Vis spectrophotometry, depending on the type of label used (fluorophore, enzyme, etc.). These analyses are known

for their high selectivity, low limit of detection, and usefulness for a variety of real samples, such as urea and plasma. However, the accuracy of the analysis depends on the class of the detecting instrument, and the analysis itself can be laborious and expensive. Sensors, such as electrochemical and optical sensors, offer the highest diversity in biorecognition element type utilized for the Lf quantification. Fluorescence-based sensors are a cost-effective tool that can provide high sensitivity results. However, they are prone to generating noise signals and can be affected by the environment due to their light-sensitive nature. Furthermore, the process of labeling with a fluorescent dye is challenging and requires multiple steps, making sensor preparation a laborious procedure. Optical methods, such as SPR, are highly accurate and sensitive for analyzing numerous targets simultaneously in a multi-component matrix. However, the main drawback is the relatively high cost of instrumentation and the limitations associated with size-dependent analysis. In contrast to other sensor types, electrochemical sensors are more affordable, easy to operate, and have a higher potential for commercialization. However, the drawback is that most electrochemical methods require electrochemically active species, which limits their use to a narrow range of analytes or the use of electrochemically active labels. The exception is electrochemical impedance spectroscopy, which allows analysis for electrochemically neutral targets, similar to the case of SPR. Notably, both methods are label-free, meaning that indirect detection labels such as enzymes or dyes are not required. The major methods utilized for Lf detection are summarized in Fig. 11, concerning the generated signal. The upcoming sections will introduce and compare various methods for detecting lactoferrin based on the detection principle and the type of biorecognition layer used. These methods will be evaluated based on their metrological parameters, advantages, and limitations, considering the sample type and the target protein's physiological level. The review will include papers published since 2013 onwards, with a few exceptions of older reports. Finally, the chapter will be summarized by comparing the metrological parameters in table form.
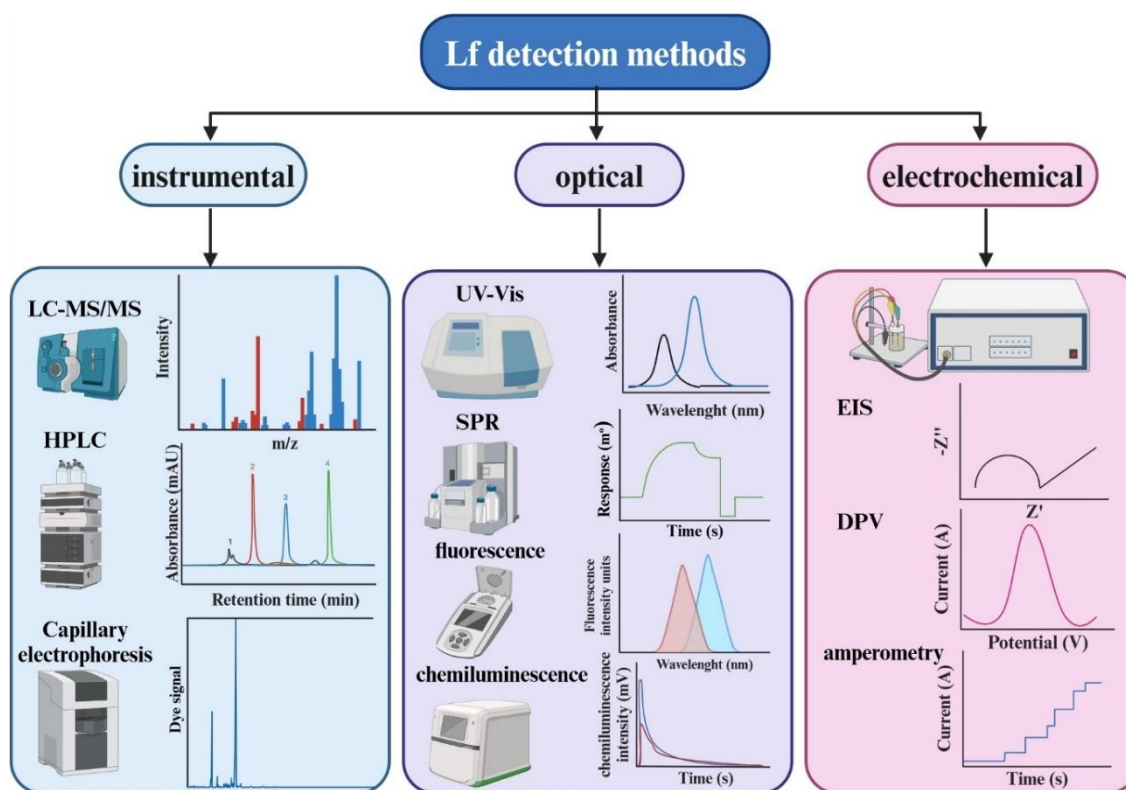
Fig. 11. Summary of major methods used for Lf detection and the schematic view of generated analytical signals.

3.1. Instrumental methods

Instrumental methods rely on the physiochemical properties of substances, such as mass-to-charge ratio in mass spectroscopy or retention time in chromatographic methods. In contrast to other analytical techniques, the advantages of instrumental analysis include the ability to examine small amounts of sample, the possibility to examine complex matrices either with or without separation, reliability, and fast analysis. Instrument methods are often the only choice if non-instrumental methods are not feasible. Although the results of instrumental methods are highly accurate and sensitive, these features depend upon the type of instrument, which can be costly. Expenses arise not only from the usage of the apparatus but also from maintenance and personnel training for handling the instrument. Instrumental methods may not always be specific for multicomponent analyses, so they often need to be verified with other methods. Several reports have suggested instrumental methods such as high-performance liquid chromatography (HPLC) [136,137], monolithic cation exchange HPLC [138], reversed-phase HPLC [139,140], capillary electrophoresis [141–143], or liquid chromatography-tandem mass spectrometry (LC-MS/MS) for this purpose [144–146]. Lactoferrin was determined in milk with high-performance liquid chromatography (HPLC)

equipped with HiTrap™ Heparin Column HP. In this method, heparin, as a negatively charged molecule, captures positively charged Lf from the milk sample [147]. The authors, however, do not provide a selectivity study, therefore, the developed method might be useful exclusively for milk samples. This is because heparin's interaction with lactoferrin is not specific and can bind to positively charged proteins like growth factors and cytokines in plasma [148]. Another proposed method for lactoferrin purification is a simple immunoaffinity method supported by HPLC and fluorescence readout for detecting bovine lactoferrin, which was suggested by Pang and his team [149]. Ostertag *et al.* utilized reversed-phase HPLC (RP-HPLC) with a diode array detector to measure lactoferrin in dairy products [139]. Molecular imprinting was introduced in order to obtain specific artificial binding sites for lactoferrin recovery with the native polyacrylamide gel electrophoresis (PAGE) method [150]. Notably, the authors presented the bulk imprinting method in vinylpirydin as a functional monomer, in which the whole lactoferrin molecule was imprinted, and the template was washed off using an acetic acid-methanol mixture. None of the metrological parameters are provided except the selectivity test vs. serum bovine albumin. Most of the available instrumental methods for measuring lactoferrin focus on milk or dairy products, where the protein composition and content are already known. As a result, many methods lack selectivity since they do not use any affinity-based biorecognition molecules for Lf. Among others, such analyses are the least used in clinical practice.

3.2.   Optical methods

Optical methods are a diverse set of techniques that include basic methods like UV-Vis spectrophotometry, as well as more advanced methods such as Raman spectroscopy, surface-enhanced Raman spectroscopy (SERS), surface plasmon resonance (SPR), spectrofluorimetry, or chemiluminescence. Optical biosensing offers high accuracy and sensitivity and does not affect the properties of the receptor or the molecular target during detection. Optical detection coupled with recognition layers such as antibodies, biomimetic layers, or aptamers is the most common method for lactoferrin detection. Sandwich ELISA was proposed for the detection of human nitrated lactoferrin by Alhalvani *et al.*, using a polyclonal anti-Lf capture antibody paired with a monoclonal anti-nitrotyrosine antibody labeled with detector tandem streptavidin-horseradish peroxidase (streptavidin-HRP) and TMB (3,3′,5,5′-tetramethylbenzidine) substrate [151]. Absorbance and fluorescence spectra were acquired in the range 200-500 nm at 2 nm resolution. The obtained LOD equal to 0.065

$\mu g \cdot mL^{-1}$ was remarkably lower than for any instrumental method. The point-of-care lactoferrin ocular detection in tears was proposed by Shi and co-authors [133]. They utilized the ability of $TbCl_3$ to interact with lactoferrin and developed a simple sensing approach supported by a smartphone to visualize fluorescence intensity resulting from the interaction. Similar approach was presented by Gao *et al.* [152], who utilized $TbCl_3$ dye to detect Lf onto an inversed opal crystal fiber-based sensor. The recent work of Mukhametova and others showed lactoferrin selective nanobodies (single-domain antibodies) conjugated with a fluorophore, which allowed the detection of lactoferrin in a relatively narrow range of 3-10 $\mu g \cdot mL^{-1}$ using the fluorescence polarization method [153]. Similar approach was presented in other reports, where the lowest LOD value of 1.25 pM was obtained for the bivalent aptasensor enhanced with the use of silver nanoparticles [154,155]. Label-free fluorescent aptasensor was introduced by Liu and co-authors [156], showing relatively good selectivity toward target vs. other milk proteins. However, the signal was inhibited significantly when measurements were performed in the mixture of milk proteins. Eventually, the study lacks cross-examination with reliable reference methods. In the work of Zhang and Zhang [157], a fluorescence resonance energy transfer (FRET) based aptasensor was reported for Lf measurements in artificial saliva. This work suffered from relatively poor selectivity – other salivary proteins, such as β-casein, interfered with analytical response. Colorimetric tests for the detection of Lf in milk and dairy products were reported: ELISA [158,159], and enzyme-linked aptamer [160]. Goicolea *et al.* proposed a protocol similar to ELISA, where the antibody was replaced with linear polymer [161], which gave a relatively low limit of quantification (LOQ) for the narrow concentration range of 0.1-0.25 nM. An interesting work was published by Kudo and colleagues [162]. A microfluidic paper-based sensor for lactoferrin detection was proposed based on lactoferrin's affinity to iron ions. The authors used a colorimetric complex of 2-(5-bromo-2-pyridylazo)-5-diethylaminophenol with Fe^{3+}, which was encapsulated in water-dispersible poly(styrene-block-vinylpyrrolidone) particles, that were entrapped in cellulosic fiber network. Due to the sequestration of Fe^{3+} from the complex in the presence of lactoferrin, a change of color was registered. The drawback of this solution is that it is only useful for iron-free forms of lactoferrin. Moreover, the interference of serum albumin was noted, and the study lacked measurements in real samples. An indirect competitive ELISA protocol was established using a monoclonal antibody designed with hybridoma technology, which allowed to obtain low LOD of 0.01 $ng \cdot mL^{-1}$ and a relatively wide linear concentration range of 9.76-625 $ng \cdot mL^{-1}$ of bovine Lf

in milk [163]. Works based on immunoreaction with colorimetric detection were also presented by Li *et al*. [164], who used a silver enhancement amplification system, and Zhang and Echegoyen [165]. A boronate affinity amplified dynamic light scattering immunosensor was proposed by Zhu and co-workers, in which gold nanoparticles coated with monoclonal Ab were used to separate and enrich Lf from milk and output the scattering signal [166]. The nanoparticles with Ab-Lf conjugates were aggregated onto bovine serum albumin modified with polyvalent phenylboronic acid scaffolds via the interaction of boronic acid groups with Lf. The immunosensor was characterized by high selectivity toward Lf in the presence of other whey proteins. The chemiluminescence phenomenon was utilized by Xu *et al*. to develop an immunoassay for lactoferrin detection in synovial fluid [167] for the diagnosis of periprosthetic joint infection. The immunoassay allowed determining Lf in a wide concentration range from 20 to 10000 ng·mL^{-1}, which, according to the authors, meets the criteria for clinical applicability. The selectivity vs. transferrin, hemoglobin, and bilirubin was proven. The combination of chemiluminescence with electrochemistry was utilized in the work of Lu *et al*., who developed a ratiometric electrochemiluminescence resonance energy transfer platform equipped with aptamer-BODIPY dye conjugate for selective detection of Lf. The biosensor was applied to Lf measurements in tears toward a diagnosis of dry eye disease [168]. Surface plasmon resonance was frequently used for lactoferrin detection since, as a real-time method, it allows the control of the immobilization process and observes receptor-analyte association and dissociation directly. Immunosensors based on the SPR method for lactoferrin detection in dairy products were reported by Tomassetti *et al*. [169] and Billakanti and co-workers [170]. Jia and colleagues utilized SPR imaging to develop Lf-specific aptamers [92,171], however the quantitative analysis with established metrological parameters was not provided. Culver *et al*. suggested using a poly(*N*-isopropylacrylamide-co-methacrylic acid) hydrogel as a recognition layer for Lf [172]. They highlighted its advantages, such as low cost and feasibility. Nevertheless, such non-imprinted layers deprived of molecular cavities lacked selectivity, as hydrogel interacts with molecules charged oppositely to it. Considering lactoferrin detection with optical methods, the predominant group is immunoassays with colorimetric or fluorescence readout, as they provide operational simplicity, high sensitivity, and accuracy. On the other hand, the online SPR technique recently gained interest as it allows the observation of every step of assay development (immobilization, interaction) in real-time mode. The limitations of optical methods, such as sensitivity to environmental changes (temperature, humidity, light),

susceptibility to noise and crosstalk, and their complexity, often are deciding factors diminishing their use in developing clinically applicable biosensing tools.

3.3. Electrochemical methods

Electrochemical methods, apart from optical ones, constitute a large group of analytically valuable techniques, including voltammetry (differential pulse voltammetry – DPV, cyclic voltammetry – CV, square wave voltammetry – SWV), chronoamperometry, conductometry, or electrochemical impedance spectroscopy (EIS). Electrochemical methods, in general, are embedded in the transformation of biological response resulting from bioreceptor and analyte interaction in measurable electrical signals. Compared to other methods, electrochemical ones are characterized by simplicity, the ability to extract multiple analytes simultaneously, high sensitivity and the possibility to study mechanisms of a redox reaction, low cost in relation to the majority of optical and instrumental methods, as well as fast and feasible analysis, including post-processing. Moreover, they stand with the flexibility of materials used and amplification strategies, e.g., using nanostructures, since metal nanoparticles and carbon-based nanomaterials exhibit excellent electrical properties and allow to significantly enlarge the active surface area, directly improving sensitivity. Electrochemical detection of lactoferrin has been performed so far using an immunosensing approach and aptamer-based sensing. Tomassetti and co-workers compared SPR biosensing with classical amperometric and screen-printed electrodes [169] in milk samples. In this simple approach, redox indicator Prussian Blue was used to obtain electroactive species H_2O_2 and indirectly determine Lf concentration with biotin-avidin–peroxidase conjugate onto the screen-printed platinum working electrode. The linear range from 0.05 to 25 μM and limit of detection equal to 0.025 μM were established for classical amperometric setup, while screen-printed immunosensor allowed to obtain 0.015 μM of LOD and linear concentration range 0.03-2.5 μM. The study was completed with the affinity study of antibody-lactoferrin, indicating a slight advantage of electrochemical detection over SPR. This study was based on the previous one from the same group [173]. Another electrochemical immunosensor was proposed by Huang *et al.* [174], using gold metallic electrode and monoclonal antibodies against lactoferrin. The examination was performed with cyclic voltammetry and electrochemical impedance spectroscopy, showing a linear lactoferrin range of 0.01-1000 ng·mL^{-1} and LOD of 4.9 pg·mL^{-1} in milk. The immunosensor exhibited 4-week shelf life, however it required over 1 hr of incubation in 37℃. The

impedimetric immunosensor was successfully implemented to measure lactoferrin to diagnose urinary tract infections [175]. The LOD value obtained using EIS was 145 pg·mL^{-1}, and the immunosensor was cross-examined with ELISA tests, showing satisfactory compatibility in results and utility. The electrochemical immunoassay operating in microfluidic mode was developed by Zitka and co-authors [176]. The paramagnetic beads covered with antibody against lactoferrin allowed to separate Lf from the milk sample, and the stopped-flow injection analysis with electrochemical detection resulted in LOD of 0.1 μg·mL^{-1}, compared with ELISA with spectrophotometric readout (LOD 5 ng·mL^{-1}). A calibration curve with a linear DPV current vs. Lf concentration correlation was obtained in the range 0.195-100 μg·mL^{-1}. Interestingly, a mixture of three different antibodies against Lf was used simultaneously as a biorecognition element. The same team published the results obtained using screen-printed carbon electrodes, where the limit of detection was 10 μg·mL^{-1} for the linear concentration range from 0 to 100 μg·mL^{-1} [177]. The CV method was applied to the immunosensor fabricated using a gold electrode functionalized with an anti-Lf antibody [178]. The indirect detection was possible due to the utilization of a sandwich setup of primary antibody conjugated with secondary antibody labeled with alkaline phosphatase. The study was performed in urea samples toward a diagnosis of urinary tract infection (UTI). The proposed immunoassay was characterized by a LOD of 1 ng·mL^{-1} and a concentration range of 1-729 ng·mL^{-1}, relevant for the Lf levels associated with UTI. This research aimed to integrate the multi-technique electrochemical immunosensor with smartphones and other wearable technologies toward the POC tool. The issue of diagnosis of UTI potential biomarkers was undertaken by Naseri *et al*. [179], who proposed a multivalent aptamer as a selective biorecognition element. The DPV and EIS methods were applied to investigate the performance of the aptasensor. The screen-printed gold electrodes were modified with a specifically designed aptamer, which allowed for selective DPV measurements in the laboratory and Lf-spiked urea samples. The metrological parameters: linear concentration range from 10 to 1300 ng·mL^{-1}, and LOD of 0.9 ng·mL^{-1} were obtained in acetate buffer, and 0-200 ng·mL^{-1} of linear range; 1.2 ng·mL^{-1} of LOD in artificial urine. The selectivity of aptasensor in the presence of human serum albumin as a major interferent was confirmed. A non-affinity electrochemical sensor for Lf detection in milk was developed by Devi and co-authors [180], who proposed utilization of methylene blue and Lf co-immobilization iron-impurity containing multiwalled carbon nanotube (MWCNT) and Nafion (Nf) modified glassy carbon electrode (GCE), designated as

GCE/Nf-MWCNT-MB-Lf, as an in-situ bio-electrocatalytic reduction system for H_2O_2 in milk, where the reduction signal is proportional to the amount of immobilized protein. Hence, it indirectly allows the determination of milk Lf. The hydrogen peroxide reduction current against the dilution factor of milk samples had linear characteristics with two slope values. However, the metrological parameters such as concentration range and LOD were not provided, suggesting that the method is suitable at most for qualitative analysis. Recently, another non-affinity impedimetric sensor was developed by exploiting a mixed monolayer of (S)-1-(3-mercapto-2-methyl-1-oxopropyl)-L-proline/3-sulfanylpropan-1-ol (MOP-SP) for Lf detection [181]. The EIS measurements in faradaic setup assisted by $[Fe(CN)_6]^{3-/4-}$ redox probe allowed to determine Lf in the range of 125 nM to 3.250 μM and with LOD of 65.2 nM, while reduction of time analysis through usage of single frequency mode showed linear relationship of signal vs. concentration from 500 nM to 3.250 μM and limit of detection equal 375 nM. The authors applied the developed platform to colostrum samples and confirmed satisfactory selectivity toward analyte in the presence of other milk proteins. As the electrochemical methods provide remarkable sensitivity, ease of miniaturization, disposable and simple operation mode, fast analysis, and post-processing, these features indicate a great applicatory potential. Nevertheless, in the case of electrochemically neutral molecules such as proteins, the label-free electrochemical impedance spectroscopy method seems to be the most promising one as it enables the establishment of electrical properties at the interface as well as quantitative analysis. In the next subsection, the label-free methods will be indicated in the reports that have already been discussed, and the characteristics of label-free technology will be briefly explained.

3.4. Label-free methods

Analytical techniques in biosensing applications can be grouped according to different criteria. The ability to transduce the physical event of binding between the recognition element and analyte can be realized directly, excluding additional reactants – as label-free, while label-based methods are indirect and require the addition of signal-generating factor called label, e.g., fluorophore, enzyme, quantum dots, nanoparticles, redox-active molecules, etc. [89,182,183]. The label can be attached to the target molecule or biorecognition unit, and its role is to act as a reporter and facilitate or amplify the detection. On the other hand, label-free detection is direct, meaning that it enables monitoring of changes that occur when the analyte binds to a recognition element immobilized on the biosensor surface without any

artificial manipulation of individual assay components. Table 1 summarizes all the previously described reports aimed at developing lactoferrin quantification methods, including division into instrumental, optical, and electrochemical methods. Among label-free methods utilized for the detection of lactoferrin, except instrumental techniques, one can mention electrochemical impedance spectroscopy [174–177,179,181], surface plasmon resonance [169,172,184], and dynamic light scattering – one report [166]. Label-free biosensing methods offer significant benefits over label-based methods. They allow the bioreceptor to maintain its natural conformation and biological activity, providing more physiologically relevant insights into the underlying biology. This is especially beneficial for developing new biosensing systems as it provides quantitative information on binding kinetics. Additionally, label-free methods eliminate the risk of unwanted background signals that could arise when labels bind non-specifically to other bioassay components. This is critical when working with complex or unpurified samples, such as real body fluids, which contain numerous components apart from the analyte of interest. Label-free technology is suitable for monitoring biomolecular interactions and more accurately represents the underlying biology than label-based methods [185]. Combining the advantages of real-time SPR analysis and the feasibility of EIS, these two label-free methods were used to develop a new biosensor for selective lactoferrin determination. The features of SPR have already been discussed in the previous chapter of the dissertation. The following section will introduce the characteristics and utility of the EIS method for studying the electric properties of biosensing interfaces and for developing a selective, feasible, and label-free assay for the quantification of biomolecules.

Table 1. Summary of metrological parameters and details on methods of lactoferrin detection.

No.	Type of (bio)receptor	Lf origin	Detection method	Sample	Concentration range	LOD	LOQ	Selectivity	Label	Ref.
					Instrumental					
1	heparin	bovine	HPLC- UV	milk	2-100 mg·L^{-1} (25-1250 nM)	0.57 mg·L^{-1} (7.13 nM)	1.90 mg·L^{-1} (2.38 nM)	declared in milk	-	[147]
2	antibody	bovine	HPLC-fluorescence	dairy products	0.8-30 µg·mL^{-1} (10-375 nM)	0.25 µg·mL^{-1} (3.13 nM)	-	-	-	[149]
3	heparin	bovine	HPLC-UV	dairy products	10-1000 µg·mL^{-1} (125-12500 nM)	0.6 mg·(100 g liquid sample)$^{-1}$ / 3 mg/100 g solid sample	-	-	-	[136]
4		ovine, caprine, bovine, donkey, human	HPLC-UV	milk	50-1200 µg·mL^{-1} (625-15000 nM)	35.4 µg·mL^{-1} (443 nM)	-	-	-	[137]
5	trypsin digestion – peptide assay	bovine	LC-MS/MS	dairy	10-1000 nM	0.3 mg ·100 g^{-1}	-	-	-	[145]
6	trypsin digestion – peptides assay	bovine	LC-MS/MS	infant formula	1-100 nM	0.02 nM (0.05 mg·100 g^{-1})	-	-	-	[144]
7	poly (2-methyl-2-oxazoline)-random-glycidyl methacrylate copolymer	bovine	Capillary electrophoresis-UV	Infant formula	10-500 µg·mL^{-1} (125-6250 nM)	5 µg·mL^{-1} (62.5 nM)	16.7 µg·mL^{-1} (209 nM)	-	-	[141]
8	aptamer	bovine	Capillary electrophoresis-UV	milk powder	4-128 nM	1 nM		-	-	[143]
9	monolithic cation exchange column	human	HPLC	milk	1-25 µg·mL^{-1} (12.5-313 nM)	-	-	-	-	[138]
10	none	human	RP-HPLC DAD	whey	0.03-0.15 g·L^{-1} (375-1880 nM)	6 mg·L^{-1} (75 nM)	19 mg·L^{-1} (238 nM)	-	-	[139]
11	none	camel	UHPLC-MS/MS	milk	10-500 nM	3.8 mg·kg^{-1}	11 mg·kg^{-1}	-	-	[146]
					Optical					
12	antibody	Human nitrated Lf	UV-Vis, fluorescence	laboratory sample	0.18-25 µg·mL^{-1} (2.25-313 nM)	0.065 µg·mL^{-1} (0.813 nM)	-	-	HRP	[151]
13	dye trivalent terbium TbCl$_3$	human	fluorescence	tears	0-5 mg·mL^{-1} (0-62500 nM)	0.57 mg·mL^{-1} (lateral flow sensing)	-	not selective	-	[133]
14	TbCl$_3$	human	fluorescence	tears	0.1-5 mg·mL^{-1} (1250-62500 nM)	-	-	not selective	-	[152]
15	nanobody	human	Fluorescence polarization	milk	3-10 µg·mL^{-1} (37.5-125 nM)	2.1 µg·mL^{-1} (26.3 nM)	-	-	fluorophore	[153]
16	bivalent aptamer	bovine	Fluorescence polarization	milk powder	0.2 ng·mL^{-1} – 25 µg·mL^{-1} (2.5 pM – 313 nM)	1.25 pM	-	-	fluorophore	[154]
17	aptamer	human	Fluorescence polarization	tears	0.6-3.32 mg·mL^{-1} (7.5-400 µM)	1.397 µg·mL^{-1} (17.5 nM)	-	-	fluorophore	[155]
18	aptamer with immobilized fluorophore	bovine	Fluorescence intensity	milk powder	20-500 nM	3 nM (2.4 mg·kg^{-1})	-	selective vs. milk proteins	fluorophore	[156]
19	aptamer	human	FRET	artificial saliva	4-16 µg·mL^{-1} (50-200 nM)	2.48 µg·mL^{-1} (31 nM)	-	-	fluorophore	[157]
20	antibody	bovine	ELISA UV-Vis	milk-derived products	100-520 ng·mL^{-1} (1.25-6.5 nM)	62 µg·L^{-1} (0.775 nM)	-	selective vs. other milk proteins	HRP	[158]
21	aptamer	bovine	colorimetric	milk	25-500 nM	14.01 nM	-	selective vs. other milk proteins	HRP	[160]
22	linear polymer	human	ELISA like	artificial urea	0.1 nM-0.25 µg·mL^{-1} (0.1-3.13 nM)	-	1.5 nM	-	HRP	[161]
23	Fe^{3+}	bovine	Colorimetric, microfluidic	laboratory sample	0-700 µg·mL^{-1} (0-8750 nM)	110 µg·mL^{-1} (1.38 µM)	-	selectivity vs. ions and proteins except serum albumin	(5-Br-PADAP)-Fe^{3+} complex	[162]

No.	Type of (bio)receptor	Lf origin	Detection method	Sample	Concentration range	LOD	LOQ	Selectivity	Label	Ref.
24	antibody	bovine	SPR	laboratory sample	0-100 µg·mL⁻¹ (0-1250 nM)	3.7 µg·mL⁻¹ (46.3 nM)	-	-	-	[184]
25	antibody	bovine	Indirect competitive ELISA	milk	9.76-625 ng·mL⁻¹ (0.122-7.81 nM)	0.01 ng·mL⁻¹ (0.125 pM)				Au NPs	[163]
26	antibody	bovine	Visual microarray	milk	0.05-25 µg·mL⁻¹ (0.625-313 nM)	0.03 µg·mL⁻¹ (0.375 nM)				Au NPs	[164]
27	antibody	human	Lateral flow paper-based	tears	-	10 ng·mL⁻¹ (0.125 nM)	-	-	Au NPs	[165]
28	antibody	bovine	Dynamic light scattering	milk	1.5-10000 ng·mL⁻¹ (18.8 pM – 125 nM)	1 ng·mL⁻¹ (12.5 pM)		selective vs. other milk proteins	-	[166]
29	antibody	human	chemiluminescence	synovial fluid	20-10000 ng·mL⁻¹ (0.25-125 nM)	-	-	selective vs. hemoglobin, transferrin, and bilirubin	alkaline phosphatase	[167]
30	antibody	bovine	SPR	dairy	0.5-3.5 µM static system / 0.1-10 µM flow system	0.28 µM static system / 0.05 µM flow system	-		-	[169]
31	poly(N-isopropylacrylamide-co-methacrylic acid) hydrogels	human	Localized SPR	tears	20-216 µg·mL⁻¹ (0.25-2.7 µM)	-	-	declared semi-selectivity	-	[172]
32	hairpin aptamer	bovine, human	SERS	milk, serum	0.5-100 µg/L (6.25 pM – 1.25 nM)	0.14 µg/L (1.75 pM)	-	declared in milk and serum	quantum dots and NPs	[186]
Electrochemical										
33	antibody	buffalo	amperometry	milk	0.07-1000 µM	0.035 µM	-	-	HRP	[173]
34	antibody	bovine, goat	amperometry	milk	0.05-25 µM / 0.03-2.5 µM	0.025 µM classical electrode / 0.015 µM screen-printed electrode	-	-	HRP	[169]
35	antibody	bovine	CV, EIS	milk	0.01-1000 ng·mL⁻¹ (0.125 pM – 12.5 nM)	4.9 pg·mL⁻¹ (0.0613 pM)	-	-	-	[174]
36	antibody	human	EIS	urine	-	145 pg·mL⁻¹ (1.81 pM)	-	-	-	[175]
37	antibody	bovine	amperometry	laboratory samples	0-100 µg·mL⁻¹ (0-1250 nM)	10 µg·mL⁻¹ (125 nM)	-	-	-	[177]
38	antibodies	bovine	SFIA, DPV	laboratory samples	0.195-100 µg·mL⁻¹ (2.44-1250 nM)	0.1 µg·mL⁻¹ (1.25 nM)	-	-	-	[176]
39	antibody	human	CV	urea	1-729 ng·mL⁻¹ (12.5 pM – 9.11 nM)	1 ng·mL⁻¹ (12.5 pM)	-	-	alkaline phosphatase	[178]
40	aptamer	human	DPV	Lf-spiked urea / laboratory samples	0-200 ng·mL⁻¹ (0-2.5 nM) / 10-1300 ng·mL⁻¹ (0.125-16.3 nM)	1.2 ng·mL⁻¹ (15 pM) / 0.9 ng·mL⁻¹ (11.3 pM)	-	vs. human serum albumin	-	[179]
41	MOP-SP	human	EIS, DPV	colostrum	125 nM – 3.250 µM / 500 nM – 3.250 µM	65.2 nM / 375 nM.	-	vs. milk proteins	-	[181]

## 3.5.	Electrochemical impedance spectroscopy as a label-free method for quantification of large molecules

Electrochemical impedance spectroscopy (EIS) is an electrochemical method that principally works by perturbing an electrochemical system that is in equilibrium or steady state. This is done by applying a sinusoidal stimulus, such as alternating current (AC) voltage or current, over a range of frequencies. The response of the system, whether it is current or voltage, is recorded [187]. EIS is able to provide a wealth of information about various electrical, electrochemical, and physical processes that occur in an electrochemical system. These processes include the resistance of the liquid electrolyte, conductivities of liquid/solid boundaries, charging/discharging of the electric double layer at the interfaces, dependence of capacitance behavior of the double layer on the morphology of electrode surface and electrolyte composition, kinetics of the electrode charge-transfer reaction, adsorption/desorption phenomena, mass transfer phenomena, and more. EIS measurements can be simulated to an equivalent electrical circuit, which comprises common passive components such as resistances, capacitors, and inductors, along with other more complicated distributed elements arranged in various ways [188]. Each process can be considered analogous to an equivalent electrical circuit characterized by a different time constant. Some of these processes are challenging to analyze when using voltammetric techniques like cyclic voltammetry in the time domain. However, by operating in the frequency domain, EIS simplifies a complex electrochemical system by separating it into individual processes with different time constants, making it easy to analyze [187]. In a three-electrode EIS system, the voltage is applied between the working and reference electrodes. Under voltage perturbation, the impedance to current flow is determined by three factors: (1) the ohmic resistance of the electrolyte, R_s, defined by the distance between the reference and the working electrodes, (2) under AC conditions, the electrical double layer behaves like a capacitor and is symbolized as C_{dl}, (3) the voltage/current curve slope at steady-state measurements defines the polarization resistance, R_p. Faradaic EIS setup corresponds with the presence of a redox couple, where a small sinusoidal voltage perturbation is added to a DC potential that matches the redox reaction's standard potential. In this case, the current passing through the R_u is divided into two parts: I_C related to charging/discharging of the electrical double layer and I_F related to the faradaic process. The general impedance, Z_F, accounts for both the kinetics of the redox reaction and the diffusion of the redox species to the surface of the working electrode. Z_F can be divided into two

components: (1) R_{ct} related to the kinetics of the heterogeneous electrochemical process, assuming that the redox species does not absorb on the electrode surface, and (2) Z_W, which is the Warburg impedance expressing the difficulty of mass transport of the redox species to the electrode surface, considering a semi-infinite linear diffusion. To get a Nyquist plot, the negative imaginary impedance $-Z''$ is plotted versus the real part of the impedance Z'. It illustrates an impedance spectra, where a time constant τ is represented as a semicircle, and Z_W is shown as a 45° line in the low frequency range. The Nyquist plot is complex and relatively incomprehensible, but due to practical reasons, it is more popular in electrochemistry. One reason is that the Nyquist plot is very sensitive to changes, and another is that some parameters can be read directly from the plot for the most common circuits.
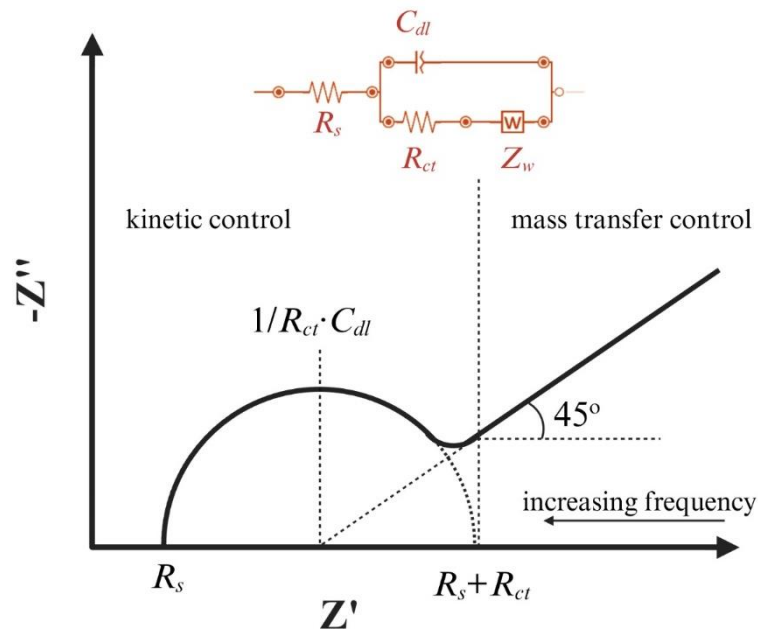
Fig. 12. Nyquist plot with corresponding Randles electrical equivalent circuit.

In actual electrochemical systems (as shown in Fig. 12), the Nyquist plot pattern for a faradaic impedance spectrum over a wide range of frequencies typically includes both a semicircle and a straight line. The semicircle represents the frequency region in which the electrochemical process is controlled by charge transfer phenomena, while the straight line represents the frequency region in which mass transfer phenomena control the electrochemical process. The characteristics of these parts can vary depending on the values of C_{dl}, R_{ct}, and Z_W. In systems where the capacitance of the double layer is not ideal, a constant phase element (Q) replaces the C_{dl}. It occurs due to the uneven distribution of various properties like solution resistances, interfacial capacitances, and current densities

across the surface of solid electrodes, which is common in most actual electrochemical systems [189]. EIS is a technique that can be used to study, optimize, and develop various applications, including label-free biosensing, due to its unique capabilities. In impedance measurements, the biosensor is prepared on an electrode that selectively modulates the electron-transfer rate by the analyte [190,191]. The electrode surface can be chemically modified to change its properties and to immobilize biorecognition elements. Self-assembled monolayers or conductive layers were intended to ensure effective immobilization of the recognition molecules and provide appropriate electrode properties. However, the specific electrical properties of biomolecules and surface defects cause the whole structure of the electrode description by a model in the form of an electrical equivalent circuit consisting of nonideal electrical elements, such as capacitors, constant phase elements, resistors, Warburg impedance [192,193]. Consequently, faradaic impedance measurements have been considered an alternative method for studying biomolecule interactions in the presence of a redox couple in the measuring solution. In this method, the impedance spectra can be modeled by a Randles circuit, where the charge-transfer resistance (R_{ct}) varies in a concentration-dependent manner. This variation depends on the flow rate of the redox molecules to the electrode surface that is being polarized to the formal potential of the redox couple, e.g. $[Fe(CN)_6]^{3-/4-}$ [194]. The flow rate of the redox probe is controlled by the extent of the formation of the receptor-analyte complex, which acts as a physical barrier, causing a concentration-dependent decrease in redox species flow, eventually increasing the charge-transfer resistance. As such, the size of the receptor-analyte complex directly influences charge-transfer resistance – the bigger the conjugate, the higher the resistance. Hence, EIS is frequently used in setups with large molecules involved in complex formation, such as proteins. The flow rate is also affected by the attractive or repulsive forces of columbic nature between the biosensor's surface and the molecules of the redox probe, depending on the measuring pH and the pI of the biomolecules such as proteins [187,195]. Label-based techniques are typically used for protein quantification, while label-free methods provide more direct information describing phenomena taking place at the sensor surface. EIS, as a label-free assay, is easy to use, relatively fast, and enables miniaturization of the setup. Compared to voltammetric or amperometric methods, it ensures gentle analysis conditions that do not interfere with the molecular interaction or the activity of the biorecognition molecules. Principally, by measuring the double-layer capacitance and resistance associated with electron transfer, insight into the electrical properties of each consecutive layer

introduced onto the electrode surface is acquired. The detection method is remarkably simple and relies on the fact that binding the target protein to the immobilized bioreceptor brings changes to the electrical properties at the electrode surface/solution interface. The electrical equivalent circuit parameters correspond to the system's physical quantities. One of the advantages of EIS in protein quantification is that it requires a low volume of sample and simplified preparation, making it especially useful for real sample measurements. Therefore, impedimetric protein detection has been demonstrated for clinically important proteins such as transcription factor [196], human serum albumin [197], apolipoprotein E [198], SARS-CoV-2 antibodies [199], or C-Reactive Protein [200].

4. Summary and motivation for looking for a new lactoferrin receptor

Lactoferrin is a cationic protein abundant in various body fluids such as milk, blood, plasma, saliva, or urea [201]. It is secreted from secondary granulocytes when the organism is under stress conditions, followed by inflammation. This protein has immunomodulatory properties and acts as a protective factor by regulating the cell cycle, activating transcription factors and gene expression, and acting on DNA. One of the unique abilities of Lf is its ability to recognize the immune status of the host and act accordingly. It can up- or downregulate by acting at different levels and on various targets, such as microbial fragments, iron ions, or cell surface receptors [10]. The complex feedback mechanism of Lf action is not yet fully understood but plays a key role in regulating the immune system and preventing inflammation. Although Lf is linked to autoimmune inflammatory diseases, it has not yet been included in routine diagnostics. The detection of Lf is usually done indirectly with an immunosensing approach using a variety of readout systems [202]. Antibody-antigen assays are characterized by specificity, but they show lower sensitivity due to the need to label the bioreceptors for indirect detection. Instrumental methods are also used, especially for dairy and milk samples, but their bottleneck is the high cost of apparatus, reagents, and complex handling. Some studies have attempted to use aptamer-based detection methods for lactoferrin, but these methods are costly and time-consuming and have not shown significantly higher sensitivity compared to immunoassays. A challenge in developing a specific bioreceptor for lactoferrin is its relatively bulky and unsymmetrical structure. The interactions of Lf are mostly non-specific, even though lactoferrin can bind to membrane proteins of various cells [203], bacterial toxins (e.g. LPS) [40], phenothiazine dyes [204], low density lipoproteins [205], proteoglycans [30], interleukins [206], nucleolin [207],

naringin [208], heparin [209], etc. Nevertheless, according to He and Furmanski [61], Lf binds to specific sequences of DNA, similarly to DNase, and activates transcription. They identified Lf binding sequences: (1) GGCACTT(G/A)C, (2) TAGA(A/G)GATCAAA, and (3) ACTACAGTCTACA. However, the literature data on the nature of DNA interactions with Lf is highly limited and has not been sufficiently evidenced experimentally. In contrast, multiple reports on Lf indicate its clinical significance, especially in the context of inflammation due to multiple causes, such as bacterial and viral infections [27], cancer [3], or autoimmune diseases [49]. Recent research also suggests that salivary Lf could be an early marker of cognitive decline and correlates its level with cortical amyloid-beta load, cortical integrity, and memory in aging [4,6,14]. The antimicrobial activity of Lf was shown in oral infections by *Streptococcus mutans* [17]. Since 2019, Lf antiviral activity has been extensively investigated, as it was found that it binds to the spike protein of the SARS-CoV-2 virus [45]. Given the complex nature of Lf and its diagnostic value, there is a need for a new stable bioreceptor that would enable selective biosensing of this protein. In order to obtain high sensitivity and selectivity in biosensing applications, it is essential to investigate the interaction between DNA bioreceptor and the target protein. These considerations became a premise for research towards a new DNA-based Lactoferrin molecular biorecognition system aiming to develop a new analytical method for Lactoferrin determination using dedicated DNA-based biosensing layers. An experimental approach utilizing preselected sequences, which were based on the existing literature, was used to identify the DNA oligonucleotide sequence that has the highest affinity to Lf. The goal was to design a unique DNA molecule that could specifically interact with Lf and evaluate its utility as a potential Lf bioreceptor. The mechanisms and driving forces of binding between reactants at the supramolecular level were studied through kinetic and thermodynamic analyses, and the selectivity was examined versus potential interferents – selected proteins. The developed DNA-type bioreceptor was further used as a biorecognition element in an impedimetric biosensor established for quantitative measurements of Lf in saliva samples. Since Lf is linked to autoimmune inflammatory diseases, it is necessary to directly determine its concentration in real samples and pharmaceuticals. This would aid medical decision-making, improve the efficiency of treatments, and ensure patient safety. The research carried out in this dissertation offers a better understanding of the mechanisms behind the interaction between Lf and DNA. Besides its cognitive value, this study also paves the way for further

research on selective biosensing layers for clinically relevant markers. This is particularly important for the detection of large proteins that are not routinely determined.

Experimental

5. Materials and instrumentation

5.1.   Materials

All sensors were purchased from two vendors: XanTec bioanalytics GmbH (Germany) and KE Instruments, the Netherlands. The sensors have a 50 nm thick gold layer deposited on borosilicate glass with 2 nm titanium transition layer. Two types, bare gold chips (KEI BK-7 SPR Sensors) and chips with linear polycarboxylate hydrogel layer of 200 nm and medium charge density modified with streptavidin (SAHC200M, XanTec), were used. Laboratory plastics that met the requirements of the analytical laboratory and biological samples were used, including falcons, Eppendorf vials, sterile syringes, and pipette tips. The laboratory glassware was cleaned with appropriate solutions (nitric acid ~ 1%) or sonicated (hemicylinder of SPR instrument) in order to avoid contaminants. Additionally, buffer solutions were filtered using a membrane filter with a cut-off of 20 μm prior to use.

5.2.   Chemicals

DNA oligonucleotides listed in Table 2 were purchased from FutureSynthezis, Poznań, Poland. The DNA sequences that were used in the experiments were subjected by the vendor to a thorough desalination and purification process using the HPLC method to ensure their purity. To prepare the stock DNA solutions, lyophilized reagents were dissolved in 10 mM Tris-HCl containing 0.1 mM EDTA at pH 8.5. The prepared stock solutions were then aliquoted and stored in a refrigerator according to the supplier's instructions. For daily use, working DNA solutions were prepared by diluting the stock solutions, and they were stored at a cool temperature of 4°C throughout the day. Shortly before use, the DNA solutions were transferred to ambient temperature to ensure their effectiveness. This process was repeated daily to ensure that the DNA solutions used in the experiment were fresh and optimal for the desired outcomes.

Reagents: ethanol (99.5%, HPLC), ammonia (30%), Na_2HPO_4, KH_2PO_4, KCl, NaCl, ethylenediaminetetraacetic acid (EDTA) disodium salt, potassium hexacyanoferrate(III) ($K_3[Fe(CN)_6]$), potassium hexacyanoferrate(II) trihydrate ($K_4[Fe(CN)_6]$), acetic acid min.

99%, HCl (35%), and NaOH, were provided by Chempur, Poland. Human Lactoferrin ELISA kit (ab200015) was purchased from Abcam.

Table 2. List of DNA oligonucleotides.

ssDNA biotinylated	Length (nb)	MW (Da)
I.1. biotin-5'GGCACTTGACTAGAAGGATCAAA3'	23	7540
I.2. 5'TTTGATCCTTCTAGTCAAGTGCC3'-biotin	23	7406
I.3. biotin-5'TTTGATCCTTCTAGTCAAGTGCC3'	23	7431
I.4. biotin-5'GAGAGAGAGAGAGAGAGAGAG3'	21	7127
I.5. biotin-5'$(G)_{23}$3'	23	7935
I.6. biotin-5'$(A)_{23}$3'	23	7567
I.7. biotin-5'$(C)_{23}$3'	23	7040
I.8. biotin-5'$(T)_{23}$3'	23	7385
ssDNA nonmodified, complementary strands		
II.1. 5'TTTGATCCTTCTAGTCAAGTGCC3'	23	6981
II.2. 5'AAACTAGGAAGATCAGTTCACGG3'	23	7106
II.3. 5'GGCACTTGACTAGAAGGATCAAA3'	23	7106
II.4. 5'CTCTCTCTCTCTCTCTCTCTC3'	21	6161
II.5. 5'$(C)_{23}$3'	23	6589
II.6. 5'$(T)_{23}$3'	23	6935
dsDNA biotinylated, hybridized with respective complementary strands	Length (bp)	
III.1. biotin-5'GGCACTTGACTAGAAGGATCAAA3'	23	14537
III.2. biotin-5'TTTGATCCTTCTAGTCAAGTGCC3'	23	14537
III.3. biotin-5'$(G)_{23}$3'	23	14524
III.4. biotin-5'$(A)_{23}$3'	23	14502
III.5. biotin-5'$[GGCACTTGCAAA]_4$GGCACTTGC3'	57	35548
III.6. biotin-5'$[TAGAGGATCAAAAAA]_4$TAGAGGATCAAA3'	72	44799
III.7. biotin-5'$[ACTACAGTCTACAAAA]_4$ACTACAGTCTACA3'	77	47892

Reagents: 11-mercaptoundecanoic acid (MUA), 6-mercapto-1-hexanol (MCH), *N*-(3-dimethylaminopropyl)-*N'*-ethylcarbodiimide hydrochloride (EDC), *N*-

hydroxysulfosuccinimide sodium salt (sulfo-NHS), 4-(2-hydroxyethyl)-1-piperazine ethanesulfonic acid (HEPES), ethanol (99.8%, HPLC), H_2SO_4 (98%, HPLC), Tween-20® viscous liquid, Triton X-100, sodium dodecyl sulfate, 2-(*N*-morpholino)ethanesulfonic acid hydrate (MES) ≥99.5%, guanidine, Tris base, sodium acetate, human lactoferrin (iron saturated, >90% SDS–PAGE), *L*-glutamate oxidase (from *Streptomyces sp.*, ≥5 U/mg protein), urease type IX (from *Canavalia ensiformis*), horseradish peroxidase (~150 U/mg), and bovine serum albumin (≥98% GE), poly(amidoamine) dendrimer (PAMAM) 2G 20% wt. in methanol, PAMAM 4G 20% wt. in methanol, PEGylated bis(sulfosuccinimidyl)suberate (BS(PEG)9), suberic acid bis(3-sulfo-*N*-hydroxysuccinimide ester) sodium salt (BS3) ≥98%, glutaraldehyde (GA) 50% wt. in H_2O, polyclonal anti-lactoferrin antibody (pAb against human Lf, recombinant, expressed in rabbit, L3262), and dopamine hydrochloride (DA) were purchased from Sigma–Aldrich. All chemicals used were of analytical grade and were used without further purification. For all aqueous solution preparations, freshly obtained deionized water with a resistance of 18.2 MΩ was used. All chemicals used within the research were of analytical grade and used without further purification.

5.3.　　Instrumentation

The electrochemical investigations, which included electrochemical impedance spectroscopy (EIS), cyclic voltammetry (CV), and open circuit potential (OCP) method, were carried out employing a PalmSens system potentiostat/galvanostat with PSTrace 5.59 software (PalmSens BV, The Netherlands). The SPR Springle instrument from KE Instruments (The Netherlands) was utilized for all SPR measurements, such as optimization of surface modification conditions, affinity, kinetics, thermodynamics, and selectivity measurements, and additional comparative optical measurements of real samples. The raw data of SPR were processed using the TraceDrawer software provided by XanTec bioanalytics GmbH. Fourier Transform Infrared (FTIR) spectrometric analysis of surface functional groups using Nicolet Summit X FTIR spectrometer, Thermo Scientific (USA), was carried out for modified SPR sensors. Transmittance spectra were collected under 0.5 cm^{-1} resolution in the wavelength range of 600-4000 nm. Fourier Transform Infrared (FTIR) spectra were analyzed and evaluated to detect peaks associated with specific surface functional groups of DNA oligonucleotides and proteins for validation and confirmation of each modification step. Similarly, contact angle measurements were taken at each

modification step using OCA 25 goniometer, DataPhysics Instruments GmbH (Germany). The Eppendorf MiniSpin centrifuge was applied to prepare real samples for analysis. A commercial lactoferrin ELISA kit using microplate UV-Vis spectrophotometer Synergy HT (BioTek, USA) was used for referential colorimetric measurements. Within the research, Origin 8 Pro and Biorender software were employed for data processing and visualization.

6. Methodology

In this chapter, detailed information on the leading and supporting methods, conditions, and developed protocols is provided. The leading measurement methods are SPR and EIS, both label-free. However, there are many supportive measurement methods that were used, including FTIR spectroscopy for surface analysis at each step of sensor (bio)functionalization and ELISA tests as a reference method for Lf determination. The methodology includes developed protocols for surface modification, bioreceptor immobilization, measuring procedures, saliva sample preparation, and others. The scheme describing the research methodology is presented in Fig. 13.

6.1. DNA as a biorecognition element for lactoferrin

Interaction of lactoferrin with DNA was first reported by Bennett *et al*. in 1982 [57]. Although a few works discussed the ability of lactoferrin to interact with DNA, such as in the nuclei of pathogenic bacteria [210], with bacterial CpG motifs [211], with plasmid DNA [212], at the cell surface of neutrophils, B cells, and monocytes [213,214], with CpG-containing oligonucleotides on human B cells [215], or using *ss*DNA on agarose gel [216], only He and Furmanski identified experimentally three specific short sequences using CASTing method [61]. These sequences are (1) GGCACTT(G/A)C, (2) TAGA(A/G)GATCAAA, and (3) ACTACAGTCTACA, derived from 64 clones of a 30-mer long random sequence. The calculated binding constants for identified sequences were around $1.24 \cdot 10^{-8}$ M, and saturating molar ratios Lf:DNA were 1.96:1 for low Lf concentrations and 4.02:1 for high Lf concentrations. Within the research, the preference for iron-saturated lactoferrin over apo-Lf to bind DNA was confirmed, indicating that DNA binding is non-dependent on protein form, which is encouraging to utilize DNA as a potential Lf-specific bioreceptor. DNA-binding proteins recognize specific target DNA using two mechanisms: nucleobase sequence and shape.
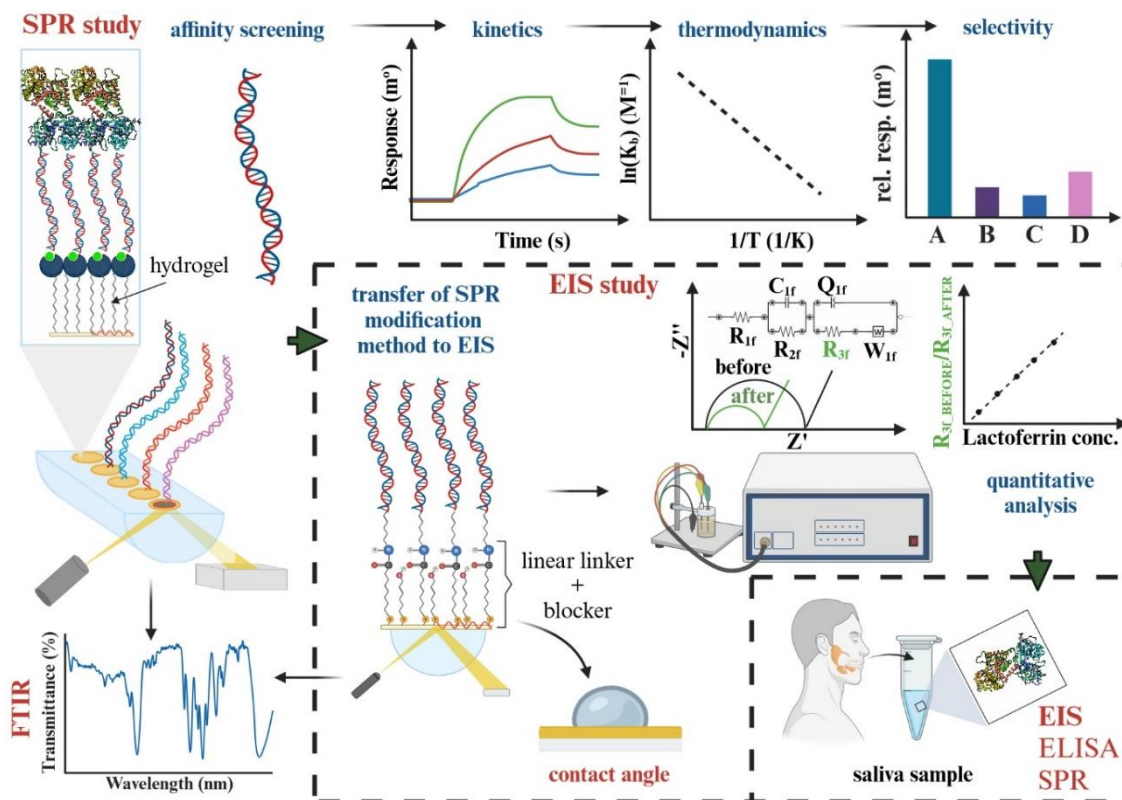
Fig. 13. Scheme of research methodology including leading and supporting methods and analyses performed throughout the course of investigation.

These mechanisms differ in specificity, suggesting different levels of biological significance for such complexes. DNA can bind non-specifically, such as when it wraps around histones [217]. Specific or highly selective interactions with the protein recognition site, however, strictly depend on nucleotide sequence and occur under intrinsic conditions. Recent theoretical studies have shown that there are two types of protein-DNA binding based on different forces [218–220]. The first type is pure electrostatic attraction between differently charged DNA and protein molecules. The second type is associated with specific motifs of DNA sequence that strengthen the attraction. This combination of other weak forces, such as van der Waals, hydrogen, steric interactions, and electrostatic charge patterns recognition, as well as strong covalent bonding. According to Kanyshkova *et al*. [62], Lf possesses two DNA binding sites, and one of them is localized on the N-lobe of the protein. The study has proven the interaction between lactoferrin and non-specific versus a specific DNA sequence, indicating about a 20-fold higher binding constant for the specific oligonucleotide. Moreover, the authors attempted to identify potential interferents such as microbial RNA and polyanions – their binding sites partially overlap with lactoferrin DNA binding sites, which was confirmed later on in a thermodynamic study performed for identical

oligonucleotide [221]. Soboleva and co-authors studied the DNase activity of Lf, including a computational spatial model of the Lf-DNA complex [47]. Although there is no straightforward explanation for the correspondence between DNA nucleobases (nb) and protein amino acids, some pairings are enriched, such as arginine with guanine or glutamine/asparagine with adenine. The negative charge of DNA promotes the creation of salt bridges with positively charged proteins due to electrostatic attraction between nucleobases and amino acids such as lysine and arginine, while more negatively charged proteins interact with DNA in major grooves via aspartate and glutamic acid residues [222]. It is suggested that additional significant factors, besides DNA and protein motifs, influence the affinity and spatial organization of DNA-protein attachment [223,224]. The most recent studies of Lf-DNA binding concern a molecular dynamic study of Lf-derived peptides' interactions with the specific DNA sequence, however, it was none of the sequences identified by He and Furmanski [61]. The data on interaction mechanisms at the supramolecular level is highly limited and has not been experimentally evidenced yet [132,225]. The mechanism of recognition, strength, and driving forces define the affinity between DNA and protein molecules, which has a significant impact on the sensitivity and selectivity of the DNA-based biosensor [83]. Therefore, when developing a bioreceptor for biosensing applications, it is important to consider both the mechanism of interaction and the specificity resulting from it. DNA exhibits tremendous variability in terms of the sequence of nucleobases and length. It is resistant to a relatively wide range of environmental conditions such as pH (5-9) or temperature (up to 40) and has structure flexibility that increases with DNA length increment [217]. Except for programmability and dynamic behavior, DNA ensures precise molecular recognition due to its unique composition and structure, making it a molecule of choice for the development of selective biosensing layers. In this study, He and Furmanski's [61] specific sequences were used in various combinations as well as multiplications (up to 4 times, separated with $d(A)_3$ spacers), to address the affinity of potential bioreceptors to Lf. Along with literature-based oligonucleotides, random sequences rich in GC or AT base pairs were applied to the study. The reason behind this is the structure of human Lf, where arginine (~49/691 amino acids) and glutamine (~41/691 amino acids) are relatively frequent, according to crystallographic studies at 2.5 Å resolution [226]. The spatial configurations, obtained by controlled immobilization, were aimed to expose particular oligonucleotides' fragments for target protein in a free state in solution.

6.2.   Modification of SPR sensors

For investigation of DNA-protein interactions *in vitro* using the SPR method, either DNA or protein has to be immobilized as a biorecognition element [227]. However, each approach has its own advantages and disadvantages. The choice of the appropriate strategy for interaction studies depends on its purpose, such as drug development, biomarker discovery, quantitative assay development, etc. It is also crucial to consider the differences in interactions between free reactants in a solution and immobilized ligand with a free analyte. The number of degrees of freedom is smaller for the latter, making the choice of ligand and its spatial orientation towards free analyte crucial for successful binding. In this study, DNA oligonucleotides were immobilized on the SPR chip surface for two reasons. Firstly, modification of DNA end with terminal groups (e.g., NH_2) or binding molecule (e.g., with biotin) is easy to perform, allowing immobilization in an oriented fashion [228], while for protein molecules, it is much more complex. The second reason is related to the characteristics of the hydrogel surface itself, especially its pK_a, which is approximately 4.5 for polycarboxylate matrices. This implies that the surface is negatively charged, similar to DNA oligonucleotides. Hence, the process of immobilizing DNA might be slowed down due to electrostatic repulsion. However, this wouldn't affect the following interaction measurements. If DNA were used as the analyte, such electrostatic repulsion could significantly affect the kinetic data, leading to an incorrect picture of complex formation. To better comprehend this, one can refer to the schematic diagram presented in Fig. 14, which explains the idea of lactoferrin interaction with immobilized DNA. Commercial SPR chips (SAHC200M, XanTec) with a polycarboxylate hydrogel were proposed with streptavidin as a capture molecule and biotinylated DNA strands as ligands. Streptavidin-biotin's high affinity ensures surface stability over time and avoids the need for harsh regeneration, making it ideal for affinity screening of DNA sequences. In all SPR experiments, the sensing surface was pre-activated and stabilized for at least an hour with an appropriate buffer solution before immobilizing ligand molecules. This was done to obtain a stable and reliable baseline before interaction measurements. All buffer solutions were freshly filtered before use. The SPR conditions for capturing ligand and interaction processes were adjusted based on the type, composition, ionic strength, and pH of buffer solutions (Table 2).
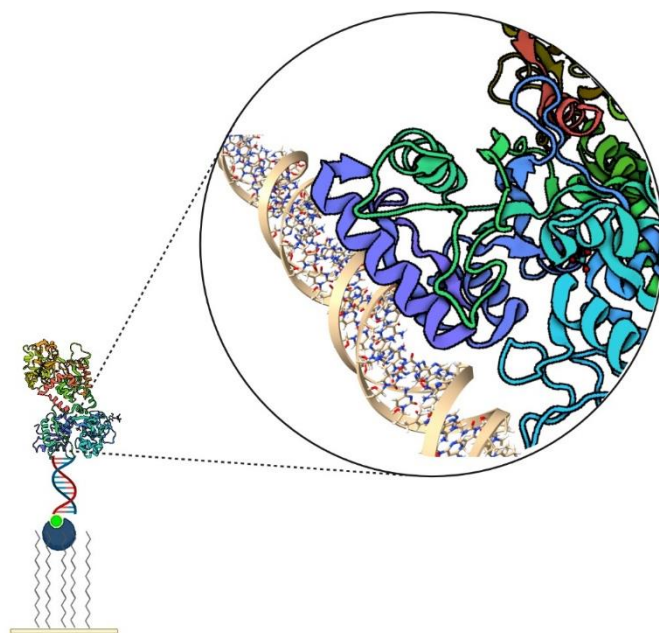
Fig. 14. Schematic design of DNA-based Lf biorecognition referring to the spatial orientation of DNA ligand and protein analyte in relation to each other.

This was done to ensure high immobilization yield and reduce non-specific binding. To prevent protein aggregation, relatively high concentrations of monovalent ions were used along with surfactants. To adjust modification conditions, immobilization of I.1 23 nb *ss*DNA was followed by hybridization with complementary II.1 DNA sequence was carried out using buffer solutions listed in Table 3. A volume of 50 µL of 10 µM DNA of each type was injected and mixed for 10 minutes in each particular buffer solution of different ionic strength and pH. To minimize non-specific binding, unconjugated streptavidin binding sites were blocked with a 10 µg/mL biotin solution in a coupling buffer. The amount of immobilized bioreceptor per mm^2 was directly appointed by SPR results. The hybridization efficiency W_{hybr} (%) was estimated as the percentage ratio of hybridized complementary DNA over *ss*DNA for each type of buffer solution.

When selecting the buffer for interaction analysis, it is important to consider the pI of the target protein in relation to the net charge of the biosensing layer. Typically, for molecular interactions, the pH should be equal to the pI minus 0.5 in order to increase the electrostatic attraction between the ligand and analyte. Nevertheless, all proposed buffer solutions were cross-examined for utility in interaction measurements by injecting 50 µL of Lf sample at a fixed concentration (100 mg·L^{-1}) onto a DNA-modified spot. The association and

dissociation were 100 seconds each, and the relative response was calculated as the difference between the SPR angle after and before interaction.

Table 3. Buffer solutions used upon optimization of modification conditions of SAHC200M sensors.

Buffer solution	pH	Composition
10 mM HBS-EP	7.4	10 mM HEPES, 137 mM NaCl, 3 mM EDTA, and 0.05% v/v Tween-20
10 mM HBS-EP	8	10 mM HEPES, 137 mM NaCl, 3 mM EDTA, and 0.05% v/v Tween-20
25 mM MES	6	25 mM MES hydrate
10 mM PBS	7.4	10 mM Na_2HPO_4, 1.8 mM KH_2PO_4, 137 mM NaCl, 2.7 mM KCl
10 mM PBST	6	10 mM Na_2HPO_4, 1.8 mM KH_2PO_4, 137 mM NaCl, 2.7 mM KCl, 0.05% v/v Tween-20
10 mM acetate buffer	4.5	5.5 mM acetic acid and 4.5 mM sodium acetate salt

The bulk effect was checked by injecting buffer solution instead of the analyte sample. Negative controls were performed using SPR sensors prepared according to a different modification protocol in which the ligand immobilization step was omitted. The schematic representation of the hydrogel-based biosensing layer is shown in Fig. 15. The quantitative results of ligand density and interaction relative response were processed using a conversion factor equal to 122 m°·mm²·ng⁻¹. The mass of the immobilized ligand (*m*) was calculated using the surface area of the immobilization spot (7.9 mm²). At the same time, the number of functional bound molecules (dsDNA) Nδ was obtained from the equation eq.1, where NA is Avogadro number (6.022·1023 mol⁻¹). M is a molar mass of immobilized *ss*DNA and complementary hybridized DNA strands.

$$N_\delta = \frac{(m_{ssDNA} + m_{complementaryDNA})}{(M_{ssDNA} + M_{complementaryDNA} \cdot \frac{W_{hybr}}{100})} \cdot N_A \qquad \text{(eq.1)}$$

In SPR measurements, choosing an appropriate immobilization yield is crucial as different loading densities are required for different research purposes. Therefore, the characteristics of immobilization parameters versus loading density were used for designing biorecognition layers for each particular analysis: affinity, kinetic, and thermodynamic [96]. The nuances

of dynamic parameters of the interaction can be assessed while the biosensing layer is weakly packed with ligand molecules since too densely packed ligand molecules can result in mass transport limitations, especially for the setup where the size of both ligand and analyte differ tremendously. On the contrary, high ligand density is necessary for binding affinity screening measurements, particularly to ensure obtaining an equilibrium state of interaction and to address the electrostatic repulsion between negatively charged DNA and the hydrogel layer. The modifications of SPR hydrogel-based sensors for affinity and dynamic investigations were performed similarly as described before, taking into account the final ligand immobilization yield, which was controlled by adjusting contact time.
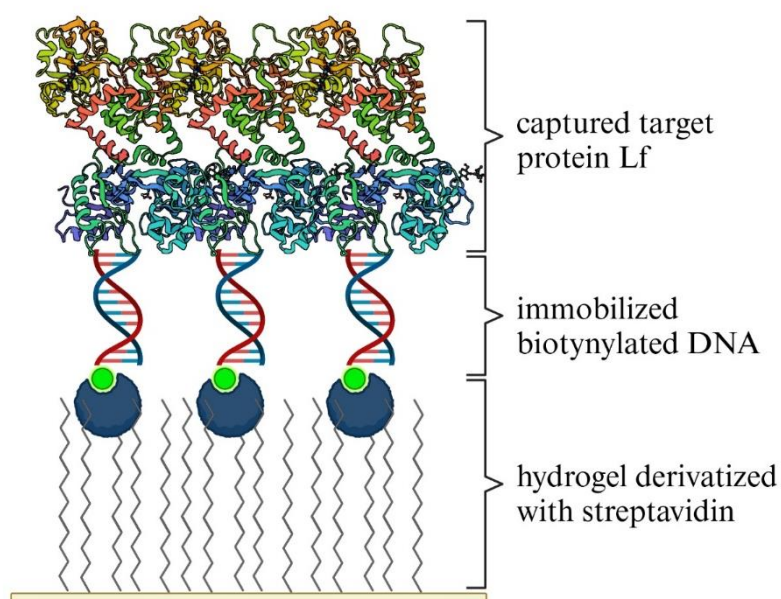
Fig. 15. Scheme of biofunctionalized DNA-based lactoferrin SPR sensor with 3D hydrogel interlayer and streptavidin-biotin conjugate, where streptavidin acts as capture molecule for biotinylated ligand.

6.3.   Affinity screening

The binding affinity screening measurements were conducted for oligonucleotides listed in Table 1 using SPR gold sensors with a streptavidin-derivatized hydrogel layer. The (1) GGCACTTGC, (2) TAGAGGATCAAA, and (3) ACTACAGTCTACA DNA sequences were utilized in various combinations and different spatial configurations, either single-stranded or double-stranded, exposing one of the ends for the interaction with the analyte. The random and monobasic sequences, both types (single-stranded and hybridized), were applied to examine their affinity towards Lf. The experiments were performed under

controlled conditions – adjusted supporting buffer solution, densely loaded biorecognition layers, and fixed high concentration of Lf sample (50 µL of 1.25 µM). Before taking measurements, the surfaces modified with DNA were conditioned by running buffer solution to establish a stable baseline. The baseline was then recorded, after which the sample (coupling buffer containing Lf) was injected for 100 seconds, followed by dissociation with the running buffer (without Lf) for the same duration. It is worth noting that the running and coupling buffers were the same. Blank measurements were also taken by injecting running buffer solution into the DNA-modified surface and subtracting it from the analytical signal. All experiments were carried out at 25°C, and the chips were stored dry in their original containers at 4°C between the measurements. The collected data were processed to obtain normalized relative response values (relative response divided by loading density of the ligand) and select the best DNA oligonucleotide-lactoferrin configuration for further development of Lf-specific DNA-type bioreceptor. The stoichiometry of interaction for each type of DNA used was calculated as the ratio of the number of captured Lf molecules to the number of immobilized DNA molecules after the full association/dissociation cycle. The sequence with the highest ratio was indicated.

6.4. Kinetic and thermodynamic analyses

Dynamic analysis of supramolecular interactions, especially between biomolecules, is essential to designing and developing new selective and stable biorecognition elements for biosensing applications. It can be performed using a variety of methods, including surface plasmon resonance, isothermal titration calorimetry (ITC), and biolayer interferometry (BLI) [229]. Although these methods are similar in that they are label-free, they differ in principle. ITC is a physical method used to assess kinetic and thermodynamic data. It involves measuring the enthalpy of binding directly using two cells, one containing water and acts as a reference cell, while the other includes the sample. The cells are kept at the same temperature throughout the experiment, and the temperature difference between the sample cell and the reference cell is recorded and compensated for. The observations are then plotted as the power needed to maintain the temperature of both cells against time. Unlike SPR and BLI methods, ITC does not require immobilization, and the measurements are performed entirely in a solution state. The isothermal titration calorimetry technique can be used to determine the reaction enthalpy, equilibrium constants, and stoichiometry of binding [230]. One of its advantages is that the size of the molecules forming the complex

is unlimited. SPR technique consumes a higher sample volume and requires higher concentrations of reactants. Additionally, it is a low-resolution and throughput technique. Biolayer interferometry uses fiber optic biosensors with a proprietary bioreceptor layer at the tip. The binding of molecules to the biosensor surface leads to changes in optical interference between light waves that reflect from an internal surface and the external interface between the biosensor and sample. As a result, it measures the binding kinetics of biomolecular interactions through the physical principle of optical interference [231]. Essentially, one biosensing tip is exposed to light and buffer conditions and then used as a reference, while the remaining tips are exposed to experimental conditions. The experimental tips will have one binding receptor immobilized, thus forming a layer, and analytes are located in 96-well plates. Once the ligand is immobilized, the tips are dipped into the wells, and when an interaction between the two binding reactants takes place, the change in thickness of the layer's tip reflects a change in wavelength. In this respect, binding kinetics are measured in real time. The primary benefit of BLI is its ability to perform high throughput analysis. However, it is not very reproducible, which means that reference measurements with other techniques, typically SPR, are necessary. On the other hand, SPR is known for its high reproducibility, minimal sample usage, and user-friendliness, as explained in the previous section. While SPR is limited by technology design, BLI is limited by sample evaporation during the experiment. Other than label-free methods, techniques like stopped-flow analysis, capillary electrophoresis, or affinity chromatography are used to assess kinetic data of biomolecular interaction [232]. Each of these methods has advantages and limitations. Still, SPR stands out as it allows for determining the broadest range of rate constants (association rate constants from 10^2 to 10^8 M^{-1}, dissociation rate constants from 10^{-6} to 1 s^{-1}). SPR is a versatile method that provides reproducible results and reusability for immobilized bioreceptors. Thus, within the dissertation, SPR was utilized for affinity screening, dynamic analysis, selectivity investigation, and quantitative measurements.

6.4.1. Kinetic analysis

To characterize the interactions between DNA and Lf, a kinetic analysis was performed on a 3D biorecognition layer obtained by selecting a DNA sequence based on the results of affinity screening. To obtain a lower density of bioreceptor, 50 µL of 10 µM DNA in coupling/running buffer solution was injected onto a streptavidin-derivatized hydrogel sensor for only 30 seconds, reducing contact time by 20 times. This created a low-

capacitance ligand density surface with δ around 1 ng·mm^{-2}. After blocking and stabilization, the biosensing surface was extensively stabilized to minimize the bulk effect and baseline drift between consecutive injections, producing the most reliable experimental data for analysis. The evaluation was conducted over a broad analyte concentration range of C_{range} ~0.1÷10 K_D, corresponding to 10 to 500 mg·L^{-1} or 0.125 to 6.25 µM, to cover the data requirements. It included a curve of initial interaction as well as a curve in the steady state, where the association is balanced with dissociation. As part of the procedure, blank (running buffer) samples were taken. All measurements were carried out separately in triplicate using multi-cycle kinetics mode (MCK). This mode is less sensitive to signal drift and capture dissociation compared to the single-cycle kinetics mode (SCK). Although the architecture of the SPR system used already allows for a decrease in mass transport limitations, relatively high values of association/dissociation flow rates (33.3 µL·s^{-1}) were set further to reduce the putative analyte concentration gradient and diffusion distance. All kinetic measurements were conducted at 25°C. The complex formation scheme describes the 1:1 interaction according to eq.2, where k_a and k_d are association/dissociation rate constants, while Lf, DNA, and COMPLEXDNA-Lf represent protein, DNA, and DNA-Lf complex, respectively.

$$\text{Lf} + \text{DNA} \underset{k_d}{\overset{k_a}{\rightleftharpoons}} \text{COMPLEX}_{DNA-Lf} \tag{eq.2}$$

The differential rate equation eq.3 that describes how fast the complex is formed is:

$$\frac{d[COMPLEX_{DNA-Lf}]}{dt} = k_a \cdot [DNA] \cdot [Lf] - k_d \cdot [COMPLEX_{DNA-Lf}] \tag{eq.3}$$

To calculate all phases of interaction, the maximal loading (R_{max}) was set locally as a concentration-dependent parameter, while the other parameters were set globally as concentration-independent. The association and dissociation rate constants (k_a expressed in M^{-1}·s^{-1} and k_d with the unit of s^{-1}) were established, which allowed for the calculation of the dissociation constant (K_D). The dissociation constant was calculated as the ratio of k_d/k_a (in mol·L^{-1}).

6.4.2. Thermodynamic analysis

The study aimed to investigate the DNA-Lf complex formation by conducting a thermodynamic characterization using the SPR method. This would help to gain a deeper understanding of the driving forces behind the supramolecular interaction. A hydrogel-based SPR chip was used, along with the chosen DNA as the biorecognition element. The same

surface preparation protocol as the affinity screening was followed. The analysis was carried out at temperatures ranging from 18°C to 32°C, and the concentration of Lf solutions used for the study varied from 40 to 300 mg·L^{-1}. The experimental data was processed to obtain a van't Hoff plot, which helped in calculating thermodynamic parameters such as binding enthalpy change (ΔH^o), binding entropy change (ΔS^o), and Gibbs free energy change (ΔG^o) in molecular structural events. It was ensured that the complete thermal equilibrium was reached for each individual measurement. The values of the binding constant, K_b (L·mol^{-1}), were calculated according to equation eq.4:

$$K_b = \frac{k_a}{k_d} \hspace{4cm} \text{(eq.4)}$$

The change in standard Gibbs free energy of binding ΔG^o (J·mol^{-1}) was calculated using the equation eq.5, where R is the universal gas constant (8.314 J·mol^{-1}·K^{-1})), and T (K) is the temperature.

$$\Delta G^o = -RTlnK_b \hspace{4cm} \text{(eq.5)}$$

The plot of ln(K_b) versus 1/T is a graphical solution of the van't Hoff equation (eq.6), based on which the parameters of the linear curve, namely the slope and the intercept, are determined.

$$\ln(K_b) = -\frac{\Delta H^o}{RT} + \frac{\Delta S^o}{R} \hspace{4cm} \text{(eq.6)}$$

The standard enthalpy change ΔH^o was determined using the DNA-Lf complex's thermodynamic properties. It was calculated as the slope of a linear curve multiplied by the universal gas constant (eq.7). The parameter $T\Delta S^o$ (J·mol^{-1}) was estimated using equation eq.8, where ΔS^o representing standard entropy change expressed in J·mol^{-1}·K^{-1} was obtained according to the equation eq.9.

$$\Delta H^o = -slope \cdot R \hspace{4cm} \text{(eq.7)}$$

$$T\Delta S^o = \Delta H^o - \Delta G^o \hspace{4cm} \text{(eq.8)}$$

$$\Delta S^o = intercept \cdot R \hspace{4cm} \text{(eq.9)}$$

6.5. Selectivity SPR analysis of bioreceptor

The biorecognition layers, fabricated using DNA sequence identified by affinity screening, were evaluated regarding selectivity toward the target protein. The selectivity study followed the same conditions as those adjusted in the screening process. Various interfering proteins were chosen based on their common characteristics or differences compared to lactoferrin, such as their biological origin, molecular weight, and isoelectric point. Lactoferrin has MW of 80 kDa, pI of 8.7, and is a glycoprotein of the transferrin group that captures two metal ions. The list of interfering molecules is as follows: urease, which has MW of 200 kDa and a pI of 5-5.2, is a nickel-containing metalloenzyme with enzymatic activity over urea and has no reported DNA binding ability; bovine serum albumin (BSA), which has MW of 66.5 kDa, a pI of 4.5-4.8, and is the major serum protein found at a physiological level of around 40 mg/mL in blood. BSA maintains colloidal osmotic pressure, binds a wide variety of compounds, and has no reported DNA binding ability; glucose oxidase (GOx), which has MW of 160 kDa and a pI of 4.2, is an oxidase with enzymatic activity over glucose. There is no data available on its interaction with DNA; glutamate oxidase (GluOx), which has MW of 120 kDa and a pI of 6.2, is an oxidase with enzymatic activity over sodium glutamate, and has no reported DNA binding ability; horseradish peroxidase (HRP), which has MW of 40 kDa and a pI of 9, is a glycoprotein that catalyzes various reactions using hydrogen peroxide (H_2O_2) as a substrate, but does not interact with DNA; human lactalbumin (LA), which has MW of 14.2 kDa and a pI of 4.5-5, is a globular protein that forms part of the lactose synthase enzyme and is capable of binding DNA under intrinsic conditions. Measurements were taken separately for both the interferents and the analyte, with each measurement being repeated three times. The concentration of each protein in the injected sample was 100 mg·L^{-1}, and for the second set of experiments, it was reduced to 5 mg·L^{-1}. The results were then processed to determine the mean selectivity percentage for each interferent, calculated using equation eq.10.

$$Selectivity = \frac{Mean_{rel.response\ to\ interferent}}{Mean_{response\ to\ Lf}} \cdot 100\% \qquad \text{(eq.10)}$$

where the reference value was mean relative response obtained in the Lf sample after full association/dissociation cycle.

6.6. Preliminary SPR quantitative analysis on hydrogel-based biosensor

In order to preliminarily examine the utility of developed biorecognition element for quantitative Lf measurements, a concentration analysis was conducted on laboratory samples using the SPR method. Hydrogel-based SPR sensors were used to evaluate two *ds*DNA oligonucleotides, III.1 (23 bp long) and III.6 (72 bp long), which were chosen based on previous analyses. The 23 bp long sequence was used to compare the calculated metrological parameters. Both ligands were immobilized in a similar manner as affinity screening in HBS-EP pH 7.4 to achieve the desired loading density and maximize the final response. Thus, the immobilization process of respective *ds*DNA was performed similarly to the affinity screening in HBS-EP pH 7.4. The binding of each type of ligand was tested in triplicate at various analyte concentrations: 0.0125, 0.0625, 0.125, 0.25, 0.375, 0.5, 0.625, 0.938, 1.25, 2.5, and 6.25 μM for III.6, and 0.0125, 0.125, 0.25, 0.625, 1.25, 2.5, 6.25, and 12.5 μM for III.1. The contact and washing time was kept constant for both cases at 100 seconds each, with the final relative response being a normalized value after the complete association and dissociation cycle. Mild regeneration was carried out using 10 mM HCl as required to preserve the activity of the ligand molecules. The linear concentration range, correlation coefficient R2, sensitivity (slope of mean relative response vs. Lf concentration within linear range), and repeatability (expressed as standard deviation) were determined. The LOD values were calculated by multiplying the value of blank SD by 3 and dividing it by sensitivity.

6.7. Transfer of modification toward impedimetric measurements

The optical investigation on Lf-selective DNA-type bioreceptors was followed by an electrochemical study. Therefore, the procedure of DNA oligonucleotide bioreceptor immobilization was adjusted to the electrochemical method. Streptavidin-derivatized hydrogel sensors were replaced with bare gold sensors modified with a linear linker aiming to covalently attach the bioreceptor [96,233]. Furthermore, to achieve optimal loading density, additional SPR measurements were conducted, in which linear linker-to-blocking agent molar ratio was adjusted in the range of MUA:MCH 1:5, 1:10, 1:25, and 1:50. The sensors were pre-modified with MUA:MCH mixture outside of the SPR instrument. To introduce surface carboxyl functional groups, bare gold chips were immersed in a mixture of MUA:MCH in ethanol for 30 minutes. Then, rinsed thoroughly with a 10% ammonia solution in ethanol, followed by another wash with ethanol. The density of these functional

groups was defined by the molar ratio of MUA:MCH used. Activation of the surface -COOH groups was carried out by injecting a mixture of EDC and sulfo-NHS (molar ratio 40 mM:10 mM in deionized water) for 10 minutes. Immobilization was performed with 10 µM DNA (*ds*DNA of 23 bp) in 10 mM HBS-EP buffer solution of pH 7.4 for another 10 minutes. After immobilizing DNA oligonucleotides, the unconjugated functional groups were blocked with 1 M ethanolamine-HCl pH 8.5. The biofunctionalized sensors were stabilized with an appropriate buffer solution to obtain a reliable and stable baseline. The relative response of ligand-analyte interaction for each MUA:MCH ratio was recorded in three repetitions using a fixed volume and concentration of the analyte (50 µL of 1.25 µM Lf). The contact time and washing with running buffer were 100 seconds each. To eliminate bulk effect, blank measurements were taken by injecting running buffer solution into the surface and subtracting it from the analytical signal. The loading density δ (ng·mm^{-2}) of either ligand or analyte (after interaction) was directly obtained by SPR measurements (Δ *angle* expressed in m°) and processed using a conversion factor 122 m°·mm^2·ng^{-1}. All experiments were performed at 25°C, and all the chips were stored dry in their original containers at 4°C between the measurements. The second set of modification procedures was focused on preparing planar biosensing layers, particularly for electrochemical measurements, using DNA oligonucleotide as a biorecognition element. The original 25 mm diameter SPR chips were employed for SPR loading density and interaction studies, whereas they were diced into quarters for all electrochemical experiments (EIS, CV, OCP). The advantage of using a planar surface lies in the ease of modification, where the density of introduced functionalities can be controlled during the initial step of biosensing surface preparation. This approach is particularly beneficial in the case of DNA-Lf complex formation toward biosensing application because it minimizes steric hindrance, which can result from over-dense immobilization of ligand molecules. Additionally, an overpacked receptor layer can influence kinetics through mass transport and diffusion limitations [234,235]. The modification in this case was fully performed entirely outside of the SPR instrument, on the basis of analysis of MUA:MCH ratio influence on immobilization and interaction. Firstly, a linear linker/blocking agent mixture in ethanol was introduced to the surface, according to the result from the loading density analysis. Then, the sensors were immersed in an EDC/sulfo-NHS mixture for 30 minutes. They were washed with HBS-EP buffer of pH 7.4 and then incubated in 1 µM DNA solution dissolved in HBS-EP pH 7.4 for 24 hours. After the incubation period, the Au-MUA:MCH-DNA biosensors were gently rinsed with HBS-

EP buffer pH 7.4 and left to dry at room temperature. Fabricated biosensors, schematically presented in Fig. 16, were used for Lf quantification in both laboratory and real samples, utilizing the EIS method.
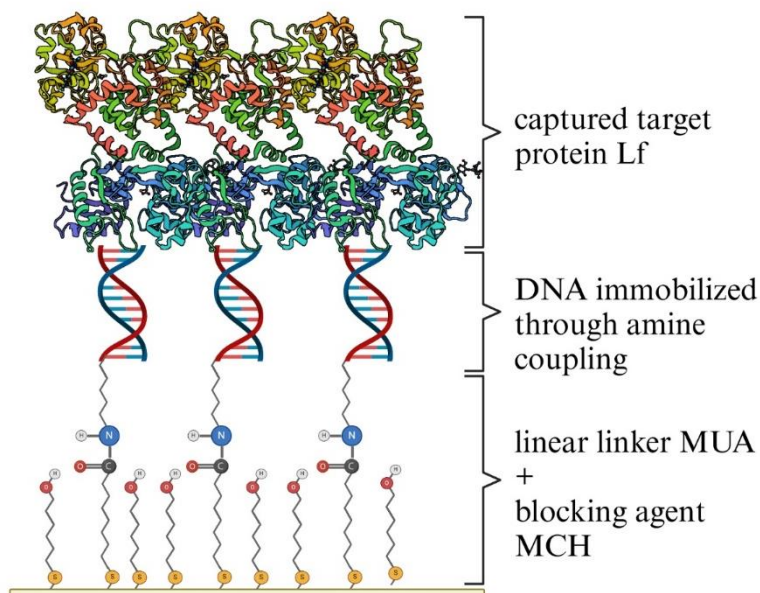
Fig. 16. Scheme of biofunctionalized DNA-based lactoferrin SPR sensor with 2D planar biorecognition layer obtained through covalent immobilization of DNA with linear linker/blocking agent.

6.8. Verification of modification for hydrogel and linear-linked bioreceptor

FTIR analyses were carried out for biorecognition layers of both types, hydrogel-based and linear linker-based. The transmittance spectra were collected with the 0.5 cm^{-1} resolution in the wavenumber range of 4000-600 cm^{-1}. The analysis served as an additional validation of each modification step, confirming the presence of surface functional groups after each modification step for both hydrogel-based and linear linker-based biosensing layers. Additionally, the wettability analysis was conducted after introduction of linker/blocker, DNA immobilization and interaction with Lf. The static contact angle was calculated as the mean value of 20 measurements.

6.9. Cyclic voltammetry and open circuit potentiometry measurements

The cyclic voltammetry method was employed to get the oxidation/reduction potential of the redox probe $[Fe(CN)_6]^{3-/4-}$. The CV measurements were performed in 2 mM $[Fe(CN)_6]^{3-/4-}$ dissolved in 10 mM HBS-EP buffer of pH 7.4 for different values of scan rate. The three-electrode system consisted of an Ag/AgCl reference electrode with liquid junction,

platinum counter electrode, and gold working electrodes. The CV parameters were set as potential step, E_{step} = 5 mV, potential range from -0.6 to 0.7 V, number of scans, n_{scans} = 3, and the scan rate range from 5 to 100 mV·s^{-1}. To assess the possible shift of oxidation/reduction potential of the redox probe, the open circuit potential (OCP) passive method was used, and the measurements were performed after each modification step. Lastly, the DNA-modified biosensors were subjected to OCP measurements for fixed lactoferrin level of 25 mg·L^{-1} (incubation for 2 minutes, measurement in 2 mM [Fe(CN)$_6$]$^{3-/4}$ in 10 mM HBS-EP pH 7.4) in 4 repetitions. Importantly, the OCP experiments examined the open circuit potential of each working electrode with respect to a reference electrode. Thus, the calculated mean potential of 4 OCP repetitions was set as the E_{DC} for further EIS measurements.

6.10.   EIS measurements

Electrochemical impedance spectroscopy is a method that enables characterize the interface sensor surface/solution. It gives an insight into the electrical properties of the interface. The impedance data are used to build an equivalent electrical circuit that consists of resistances, capacitors, or constant phase elements combined in series or parallel, representing various processes. The Randles circuit models a simple electrochemical reaction of a faradaic model, including electrolyte resistance (R_s), charge-transfer resistance (R_{ct}), double-layer capacitance (C_{dl}), and Warburg impedance (Z_W). The R_s depends on its conductivity and the reaction cell's geometry, while C_{dl} depends on the electrode's area, nature, ionic strength, and permittivity. R_{ct} reflects charge transfer kinetics, and the Warburg element reflects oscillating diffusion-related processes [189]. A detailed description was provided in the previous chapter, 3.5. EIS method, as a label-free non-disruptive technique, was employed complementarily to SPR to confirm the interaction between DNA-type biorecognition element and target protein and to quantitatively measure this protein. The EIS system used for the experiment had a fixed-space three-electrode configuration that included a Pt plate serving as a counter electrode, an Ag/AgCl reference electrode, and a gold SPR chip serving as a working electrode. Preliminary verification of DNA-Lf interaction with EIS was performed for faradaic setup in 2 mM [Fe(CN)$_6$]$^{3-/4-}$ in 10 mM HBS-EP pH 7.4, and 0.625 µM Lf sample incubated for 2 minutes. The frequency was set in the range 25 kHz – 0.1 Hz, with 10 mV AC and 200 mV DC amplitudes, respectively. Electrical parameters of surfaces were characterized using EIS measurements, which were conducted for non-faradic (0.1 M KCl) and faradaic (2 mM [Fe(CN)$_6$]$^{3-/4-}$ in 10 mM HBS-EP pH 7.4) processes at a fixed

concentration of analyte (0.625 µM = 50 mg·L^{-1}). For faradaic processes, the EIS method's frequency range was from 25 kHz to 0.1 Hz, while for non-faradaic processes, the frequency range was from 100 kHz to 10 Hz. Except for preliminary verification, all other EIS measurements were carried out with a 10 mV AC amplitude and a DC offset that depended on the OCP result. Prior to any EIS measurements, each experimental spot was conditioned for 10 minutes using the respective electrolyte (10 mM KCl or redox probe in HBS-EP buffer). Quantitative measurements of the analyte were performed as described in the below protocol. Firstly, the DNA-based biosensor was placed in 3 mL of electrolyte containing the redox probe and incubated for 10 minutes. The potential value was recorded for 10 minutes, and the average was calculated from 500 to 600 seconds. Secondly, EIS measurements were conducted at a frequency range of 25 kHz to 0.1 Hz, using a 10 mV AC signal and fitted DC amplitude. The biosensor surface was then washed gently with 1 mL of buffer solution and dried with gaseous nitrogen. After that, the biosensor was incubated in 3 mL of lactoferrin solution for 2 minutes, followed by another gentle wash and drying. Once the interaction with lactoferrin was completed, the biosensor was again incubated in 3 mL of electrolyte with the redox probe for 10 minutes. The potential value was measured for 10 minutes, and finally, EIS measurements were conducted with fitted DC amplitude. Calibration-aimed experiments were carried out to compare the performance of a 72 bp DNA bioreceptor with a 23 bp dsDNA sequence. Lactoferrin concentration was measured for both sequences – ranging from 0.1 to 75 mg·L^{-1} (1.25 to 937.5 nM) for the 72 bp oligonucleotide and from 5 to 200 mg·L^{-1} (62.5 nM to 2.5 µM) for the 23 bp DNA. Measurements were repeated thrice for each concentration using fresh redox probe solution in the electrolyte. A 1 g·L^{-1} stock of lactoferrin was prepared daily and diluted with appropriate buffer solution. The EIS spectra were analyzed to obtain electrical equivalent circuits using electrical elements (resistor, capacitor, constant-phase element) and electrochemical elements (semi-infinite diffusion, restricted diffusion, bounded diffusion) configured in series or parallelly. Then, a fitting tool was used to find the parameter values for which the simulated impedance data and the experimental impedance data were the closest, expressed by fitting coefficient χ^2. The fitting was considered sufficient when the $\chi^2 < 0.001$. These parameters were established to correspond to the physical quantities of the considered system. Eventually, the developed biosensors were subjected to durability tests by measuring the analytical signal for a fixed concentration of Lf after 1, 7, 14, and 21 days from the biosensors' preparation.

6.11. Reference tests

Two techniques were employed to carry out reference measurements on actual samples: SPR and spectrophotometric. In the case of SPR measurements, dsDNA immobilization was performed in HBS-EP (pH 7.4) outside of the SPR device, just like impedimetric biosensors. The interaction was repeated three times for the analyte concentrations, which were 0.1, 0.5, 1, 5, 10, 25, 50 mg·L^{-1} (1.25, 6.25, 12.5, 62.5, 125, 312.5, and 625 nM, respectively). The contact and washing period was kept consistent at 100 seconds each, and the average relative response was obtained after the entire association/dissociation cycle. When necessary, mild regeneration was performed with 10 mM HCl to preserve the DNA ligand's activity. The mean relative response value was related to Lf concentration to build the calibration curve. The linear concentration range, correlation coefficient R^2, sensitivity (slope of mean relative response vs. Lf concentration within the linear range), and repeatability (expressed as standard deviation, SD) were determined. The LOD was calculated by multiplying the SD for blank by 3 and dividing it by the biosensor's sensitivity. The measurements of real samples were carried out by following the earlier protocol, using saliva samples diluted ten times in HBS-EP buffer solution (pH 7.4). Spectrophotometric measurements were conducted using a commercial one-step ELISA kit, following the supplier's protocol. The endpoint absorbance at 450 nm was measured thrice for the ELISA experiments, and the calibration curve was determined. The raw absorbance signal obtained for human saliva samples was recalculated for a dilution of 1:25000.

6.12. Biological samples

Saliva contains antimicrobial properties, which come from its various components, including mucins, lactoferrin, lysozyme, lactoperoxidase, statherin, histatins, and secretory immunoglobulin A [236]. Salivary lactoferrin is considered a marker of neurodegenerative diseases, such as Alzheimer's disease [14,237], and it has been confirmed to have antiviral activity against pathological bacteria [17,238]. In order to collect human saliva samples, three volunteers from age 26 to 34 had their saliva directly collected from their oral cavity using sterile 2 mL syringes (Polfa Lublin S.A., Poland). All saliva samples were collected while fasting, at least 30 min before liquid consumption at the fixed time, and tested on the same day. The volunteers were two healthy females, and one male who suffers from Leśniowski-Crohn disease. The collection and testing protocol was strictly defined to maintain the salivary glands unstimulated, thus preventing the risk of uncontrolled

fluctuations in daily experimental data. The process of preparing the saliva samples involved centrifuging them for 10 minutes at 8000 rpm, which effectively removed heavy fractions of saliva, such as bacteria, epithelium, mucins, clustered proteins weighing 1-10 million Da, bacteria, and secretory immunoglobulin A, a polymer of 2-4 immunoglobulin monomers linked by two additional chains, with a total molecular weight of around 385 kDa. These fractions could deposit on the sensor-chip surface. The supernatant was collected, leaving the residue at the bottom of the vial, in order to prepare the saliva samples for testing. Lactoperoxidase and lactoferrin are enzymes of similar molecular weight, around 78 kDa and 80 kDa, respectively, but their structures are significantly different, and lactoperoxidase has a higher isoelectric point (pI = 9.6). On the other hand, statherin and histatins have much lower molecular weights, weighing approximately 5.3 kDa and 3-5 kDa, respectively. None of these proteins have been found to interact with DNA. Lysozyme, a strongly basic protein with a pI of 10.7 and a molecular weight of around 14 kDa, is known to interact with bacterial components, including bacterial DNA, but it is only active under acidic conditions (pH 5-6). Saliva has a normal pH range of 6.2 to 7.6, but it can become more acidic due to consuming food and drinks that contain carbohydrates, which are broken down by bacteria and release lactic, butyric, and aspartic acids. Noteworthy, the biosensor surface was blocked using 6-mercaptohexanol as a standard procedure to minimize non-specific interactions. As a result of the adjustments to the saliva sample collection, preparation, and examination procedures, the potential for interference was eliminated.

6.13. Alternative biorecognition elements – surface modification and measurements

Various methods can be considered to develop recognition layers for determining Lf, starting with immunolayers wherein polyclonal or monoclonal antibodies capture the target molecule. Other type of sensors relies on artificial synthetic recognition elements, but data on such molecularly imprinted polymers for Lf is highly limited. To meet the requirements of sensitive and selective analytical measurements for detecting Lf in real samples, three different strategies for obtaining Lf sensing layers with antibodies and artificial cavities are presented. Fig. 17 shows a schematic view of three different approaches for gold SPR chip modification. In strategy I, polyclonal antibodies were immobilized directly onto the gold surface of an SPR chip using a bifunctional linear linker with thiol and carboxyl terminated groups (MUA). Initially, the gold SPR chip was incubated overnight with 1 mM MUA in

ethanol, rinsed with ethanol and deionized water, and then left to dry. In the next step, the surface carboxyl groups were activated using a 0.4 M EDC/0.1 M sulfo-NHS mixture (1:1, v/v), followed by incubation with an antibody solution. If the ligand is directly immobilized, SPR measurements for a wide range of analyte concentrations – in this case, lactoferrin – were performed along with the calculation of the linear calibration curve. Strategy II aimed to increase the saturation of the chip surface with antibodies. This was achieved by introducing an additional hyperbranched dendrimer layer between the linear linker and the antibodies. In this study, PAMAM dendrimers of different generations (2 and 4G), or a mixture of both, were attached to the linear linker via EDC/NHS cross-linking, which had been previously described. Each dendrimer contained amine functional groups, the number of which depended on the dendrimer's generation.
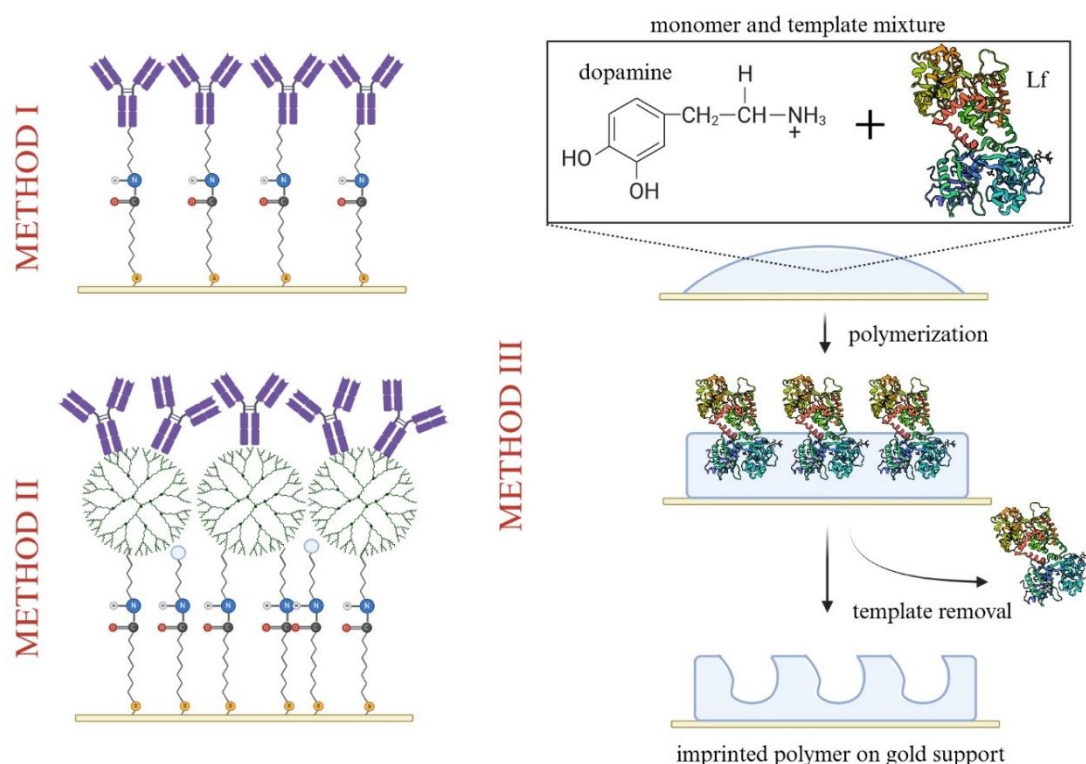
Fig. 17. Schematic view of modification approach: method I with linear linkers, method II using hyperbranched linkers, method III based on molecular imprinting in polymer.

Briefly, dendrimers are three-dimensional polymer structures that have a spherical shape with branching chains and a core. These structures can be functionalized to obtain peripheral functionalities, making them versatile [239]. Due to their flexible structure, dendrimers can cushion and protect immobilized biomolecules from deformation. However, dendrimers are

sensitive to changes in pH. In acidic conditions, dendrimers tend to shrink, while in alkaline media, they tend to expand [240]. The polyclonal antibodies were attached to the PAMAM functionalities through amine-to-amine coupling with reagents such as BS3, BS(PEG)9, or glutaraldehyde at different concentrations. The attachment via -COOH antibody groups was also performed using EDC/NHS. The immobilization procedure had various parameters that affected the antibody-antigen interaction analytical response, such as running buffer, PAMAM generation and ratio, cross-linker type between PAMAM and antibody, and eventually ligand dilution. These parameters were tested to determine the best conditions for obtaining sufficient surface saturation. Notably, every step of modifications I and II, except for the prior functionalization of bare gold SPR chips with linear linker MUA, was conducted using the SPR instrument. The prepared biosensors were tested in a lactoferrin solution of fixed concentration (0.125 µM) to compare the analytical signal of antibody-antigen interaction resulting from methods I and II. This allowed the evaluation of the influence of introducing a dendrimer interlayer on the biosensors' performance. The third strategy was based on molecular imprinting in a polymeric matrix made of polydopamine (PDA). The biomimetic layer was created using the bulk imprinting method, where the whole protein was imprinted. Here, a mixture of $2g \cdot L^{-1}$ of functional monomer (dopamine) and a 7.5 µM solution of the template (analyte) was prepared and further auto-polymerized under basic conditions (10 mM Tris-HCl buffer of pH 8.5) for 5 hours at 25°C. After that, the template was removed using a 5% (v/v) solution of acetic acid, and the performance of the sensing layer was evaluated with SPR measurements. Additionally, a template removal procedure was investigated using UV-Vis spectroscopy at 96-well plates, and the affinity of the analyte towards non-imprinted PDA was measured to evaluate the possibility of lactoferrin non-specific binding.

Results

7. Interaction of human lactoferrin with DNA

7.1.   Influence of experimental conditions on immobilization and interaction

Influence of immobilization conditions on loading density of ligand

Optimizing SPR measurement conditions mainly focused on adjusting the buffer solution, particularly its composition and pH. This is crucial for immobilization as electrostatic interactions initially affect ligand attachment efficiency. Capturing the biotinylated sequence (I.1) was used for immobilization, followed by hybridization with a complementary strand

(II.1), which provided additional insight into the impact of immobilization conditions on hybridization efficiency. The entire process was performed online using the SPR instrument, and full sensorgrams were recorded. The immobilization procedure was consistent in terms of the type of sensors used (hydrogel-based), contact time for each step, the type of blocking agent, and the concentration of ligand. The protocol is illustrated in Fig. 18.
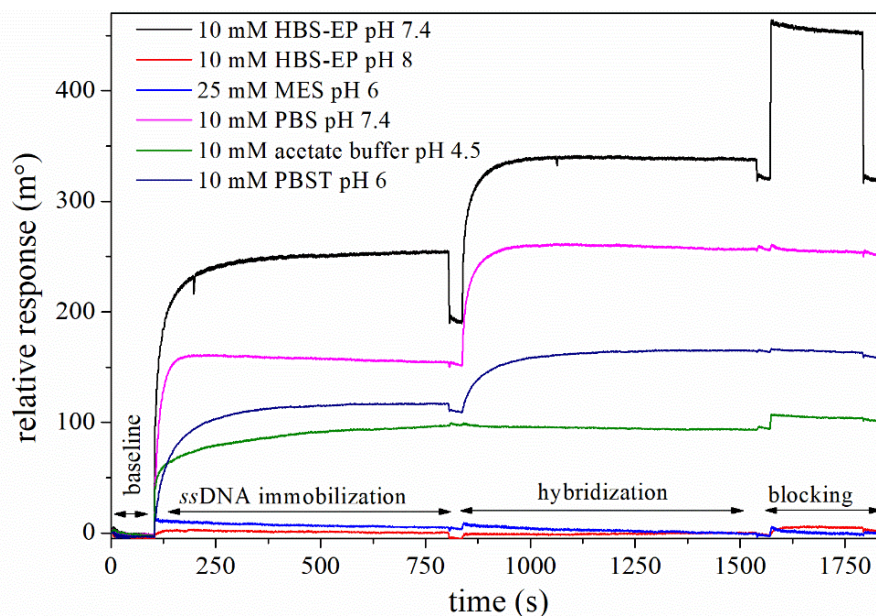
Fig. 18. Sensorgrams of streptavidin-derivatized hydrogel layers during immobilization with *ss*DNA and complementary strand (I.1 + II.1) under different conditions [65].

Table 4 summarizes the quantitative results of the density of ligands for each specific buffer solution. The immobilization of biotinylated DNA was most effective in neutral pH environments. The results obtained from acidic media showed fewer immobilized ligand molecules when compared to neutral pH environments. On the other hand, alkaline conditions led to significant inhibition of immobilization. The surface of polycarboxylate hydrogel is negatively charged under neutral pH, just like DNA molecules. Therefore, when buffer pH increases, the repulsiveness between the support and ligand also increases. However, under pH 4.5, the overall net charge of DNA is closer to neutral, resulting in electrostatic attraction [241]. Using the capture molecule method for ligand immobilization is likely the best way to reduce the negative effects of the solution on immobilization yield, compared to conventional amine coupling. However, apart from pH, the buffer composition is another factor that affects the immobilization process. The ionic strength, as well as the content of salts and surfactants, have an impact on the final immobilization level. This is

especially evident when comparing the mean ligand loading density obtained in buffers containing non-ionic surfactant and those without it, where the immobilization yield is higher for the former case.

Table 4. Immobilization level of (I.1 + II.1) under different conditions, n ≥ 3. Ligand density was calculated according to the conversion factor $122\ m^o = 1\ ng \cdot mm^{-2}$.

Running/coupling buffer	Immobilization			
	Δ angle (m°)	δ (ng·mm^{-2})	amount, m (ng)	$N_\delta \cdot 10^{11}$ (-)
	mean ± SD			
HBS-EP pH 7.4	323.4 ± 33.7	2.7 ± 0.3	20.9 ± 2.2	11.0 ± 1.2
HBS-EP pH 8	6.5 ± 2.3	0.1 ± 0.0	0.4 ± 0.2	0.2 ± 0.0
25 mM MES pH 6	0.8 ± 16.5	0.0 ± 0.1	0.1 ± 1.1	0 ± (-)
PBS pH 7.4	179.7 ± 82.9	1.5 ± 0.7	11.6 ± 5.4	6.0 ± 2.8
10 mM acetate buffer pH 4.5	105.0 ± (-)	0.9 ± (-)	6.8 ± (-)	5.3 ± (-)
PBST pH 6	199.1 ± 45.1	1.6 ± 0.4	12.9 ± 2.9	7.3 ± 1.7

Ultimately, for optimal immobilization in terms of efficiency, stability, and reproducibility of the ligand layer, a HEPES-based buffer with surfactant, a high NaCl content, and physiological pH was selected for further preparation of a DNA-based layer for subsequent experiments.

Influence of conditions on hybridization efficiency

The results of the hybridization efficiency (W_{hybr}) analysis are presented in Table 5. The highest value was achieved at pH 8, while a decrease in pH resulted in a decrease in hybridization efficiency. Since ssDNA carries a negative charge, higher pH levels lead to repulsive steric forces between neighboring immobilized strands. This creates more space for target complementary strands. However, alkaline media promote duplex dissociation, which can inhibit hybridization and result in high SD. On the other hand, low acidic pH negatively affects hybridization efficiency. This is because it can lower solubility and cause depurination of bases, which can alter the native DNA structure [242]. The physiological pH environment provides relatively stable conditions for hybridization, resulting in a hybridization efficiency level near 60%.

Table 5. Hybridization efficiency (%) is calculated as the percentage ratio of hybridized complementary DNA (II.1) over *ss*DNA (I.1), obtained under different conditions, n ≥ 3.

Running/coupling buffer	W_{hybr} (%), mean ± SD
HBS-EP pH 7.4	55.8 ± 11.7
HBS-EP pH 8	85.7 ± 71.6
25 mM MES pH 6	0 ± (-)
PBS pH 7.4	58.3 ± 14.7
10 mM acetate buffer pH 4.5	3.8 ± (-)
PBST pH 6	44.4 ± 1.5

Influence of experimental conditions on DNA-Lf binding

The impact of buffer solution on the interaction with the target analyte was thoroughly cross-examined using surfaces obtained previously. To achieve a high interaction signal, the pH of the environment in relation to the isoelectric point of the target protein (which is 8.7 for lactoferrin) is crucial. The initial complex formation is governed by electrostatic forces, which allow the analyte to reach the ligand's vicinity and minimize the limitations of stationary reactants. While the pH of the media for interaction study is typically set according to pH = pI$_{analyte}$ − 0.5, the properties of the DNA ligand layer were considered in parallel to analyte features. To study the Lf-DNA interaction, experimental results recorded for different supporting buffers after association and dissociation (150 seconds each) are displayed in Table 6. It is important to note that the efficiency of hybridization was not considered in this analysis. The study includes the overall interaction of Lf with *ds*DNA, as well as alternative Lf-*ss*DNA binding. After washing off excess analyte during dissociation, the number of molecules bound to the bioreceptor is useful for quantitative analysis and estimation of the binding ratio. The binding ratio is defined as the number of analyte particles bound per ligand molecule, which practically means the stoichiometry of supramolecular interaction [243,244]. This information is vital in the detailed analysis of the kinetics and thermodynamics of binding. The biosensor was prepared at pH 7.4 with HBS-EP, and the cross-examination of buffer solutions during the association/dissociation processes was carried out for a fixed concentration of Lf. The results obtained after each interaction step showed that the buffers with acidic pH had high normalized mean signal values due to strong electrostatic attraction. However, the poor reproducibility and instability during measurements resulted in large standard deviations, making it unsuitable for further analysis. In contrast, buffers with alkaline pH close to the analyte's isoelectric point had the smallest

mean number of bound protein molecules. Among the buffer solutions with physiological pH, the best performance was observed for HEPES-based media containing a high concentration of salt and 0.05% (v/v) surfactant. This media showed a satisfactory response after both association and dissociation. It's essential to adjust the pH for the Lf-DNA interaction study because lactoferrin's structure changes depending on the concentration of H^+ ions.

Table 6. Influence of running buffer composition and pH on the interaction between immobilized DNA (I.1 + II.1) and 100 mg·L^{-1} lactoferrin, n ≥ 3. Immobilization was performed using a streptavidin-derivatized hydrogel SPR chip with a running/coupling buffer 10 mM HBS-EP pH 7.4.

Running/coupling buffer	Interaction	
	association rel. response (m°)	dissociation rel. response (m°)
	mean ± SD	
HBS-EP pH 7.4	648.5 ± 84.1	179.6 ± 55.5
HBS-EP pH 8	147.3 ± 59.3	40.5 ± 39.3
25 mM MES pH 6	1642.4 ± 792.5	1967.9 ± 966.7
PBS pH 7.4	281.1 ± 0.8	58.9 ± 29.0
10 mM acetate buffer pH 4.5	332.7 ± 998.1	332.7 ± 998.0
PBST pH 6	367.9 ± 63.3	88.4 ± 14.2

When the pH is acidic, the orientation of lobes changes, and the entire structure relaxes, which can lead to the release of iron ions [25]. According to the Nevinsky group, iron-saturated Lf is more potent than apo-Lf when it comes to binding with DNA. However, both forms can bind to single-stranded and double-stranded DNA [62]. Therefore, this ability of lactoferrin is an essential premise for DNA being a potential specific bioreceptor for Lf.

FTIR measurements – evaluation of surface modification

FTIR transmittance spectra were collected within the range of 4000-600 cm-1 to validate the immobilization of ssDNA, hybridization with a complementary strand, and interaction of dsDNA with lactoferrin at the hydrogel-modified SPR gold sensor, depicted in Fig 19A-B. The spectra obtained for the streptavidin-derivatized hydrogel layer, which was then biotinylated DNA modified (two-step process) and Lf modified, exhibit similar visible peaks

at the wavenumbers of broad bands 3400-3200 cm^{-1}, which can be attributed to the stretching O-H vibrations. Due to the hydrogel's nature, which accumulates water, the entire spectra are heightened. The slightly visible peaks at 2950-2770 cm^{-1} can be linked to the stretching C-H vibrations of the polycarboxylate hydrogel structure [245].
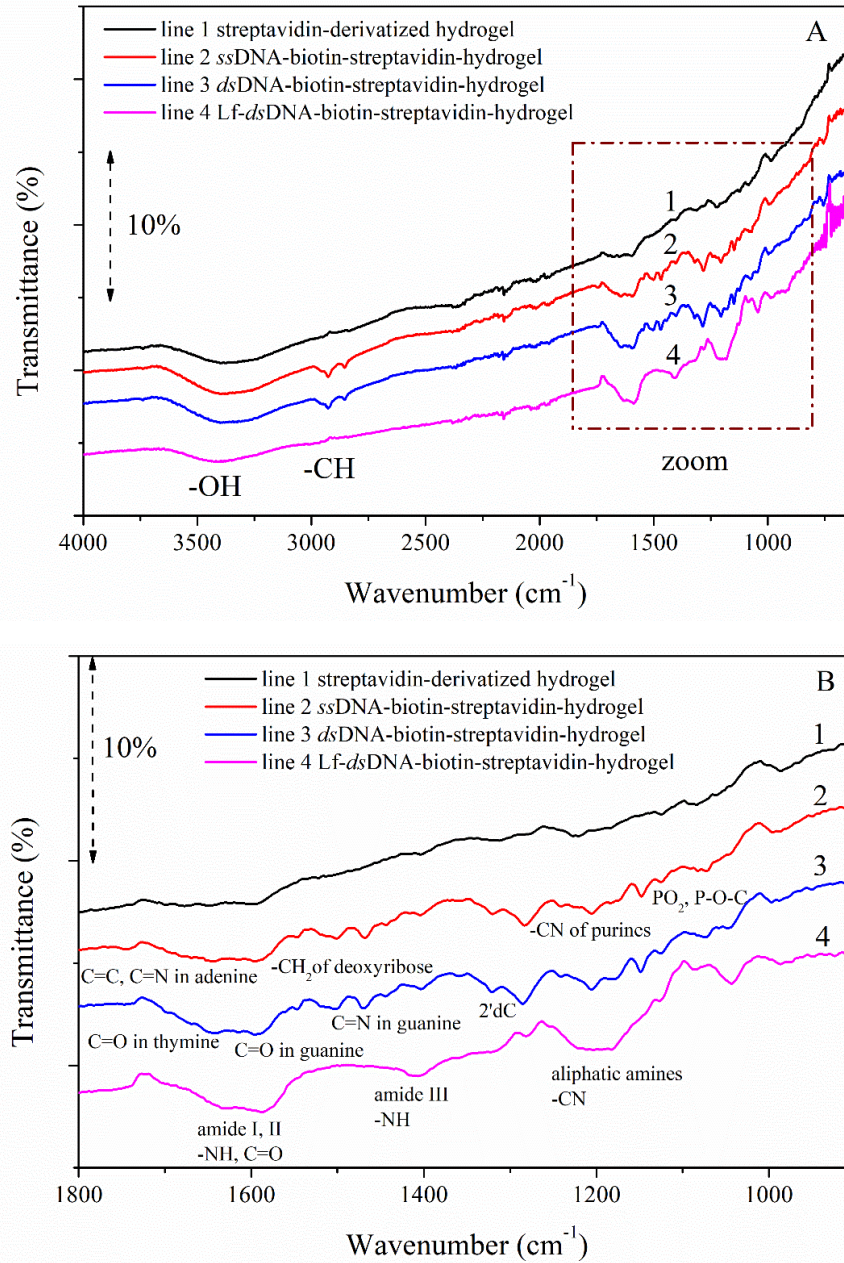
Fig. 19. FTIR spectra of consecutive modification steps of the SPR hydrogel layer taken from 600 to 4000 cm^{-1} (A) and magnified to 900-1800 cm^{-1} (B). Results of own research [65].

The bands at 1600-1550 cm^{-1} present in all spectra originate from peptide bonds, including amide I and amide II, which are characteristic of the proteins streptavidin (line 1) and

lactoferrin (line 4) [246].The vibrations of α-helices correspond to the peak of amide I, while the peak of amide II comes from the vibrations of N-H and C=O groups. Even though DNA is much smaller than streptavidin, the protein structure's vibrations can still be detected in the green and blue spectra. The peak at 1410 cm-1 in the red spectrum can be linked to amide III N-H vibrations while stretching C-N vibrations of aliphatic amines produce 1200-1100 cm^{-1} and 1020 cm^{-1} peaks. The spectra of layers modified with *ss*DNA (line 2) and *ds*DNA (line 3) display different peaks that are characteristic of DNA structure [247]. The following bands can be assigned to vibrations: around 1730 cm^{-1} from C=O vibrations and 1550 cm^{-1} from C=N of guanine rings; at 1350 cm^{-1}, the vibrations of bonds in 2'-deoxycytidine; vibrations of C-N bands of purines around 1260 cm^{-1}; around wavenumbers of 1090 cm^{-1} and 1220 cm^{-1}, symmetrical stretching vibrations from PO_2 and P-O-C are shown; peaks at 1460-1420 cm^{-1} are attributed to vibrations of CH_2 bands and C_2'-endo/anti of deoxyribose; around 1610-1570 cm^{-1}, the vibrations of C=C and C=N bands in adenine are present, while at 1720 cm^{-1} the C=O carbonyl groups of thymine are slightly visible. It can be concluded from the obtained transmittance spectra that the immobilization of *ss*DNA and its subsequent hybridization with complementary strands were successful. The peaks arising from bond vibrations originating in the protein confirm the presence of lactoferrin at the modified DNA surface. It is worth noting that the height difference between the corresponding peaks for hybridized and unhybridized DNA was up to 40%. This finding is consistent with the data obtained from SPR measurements.

Preliminary verification of DNA-Lf interaction with EIS

Complementary EIS analysis and the SPR interaction study were conducted to demonstrate the interaction between lactoferrin and DNA using an independent, label-free method. The measurements were taken on a biofunctionalized surface of sensing electrodes, with the addition of redox-active compounds to the solution. The sensing electrode's impedance controlled the system's overall impedance, resulting in a distinct charge transfer resistance visible in the Nyquist plot and equivalent circuit components calculated for the Randles model. The equivalent circuit model, displayed in Fig. 20, described the resistance of the solution R_s, as well as the diffusion processes in the low-frequency range (semicircle $R_{dl}QW$).
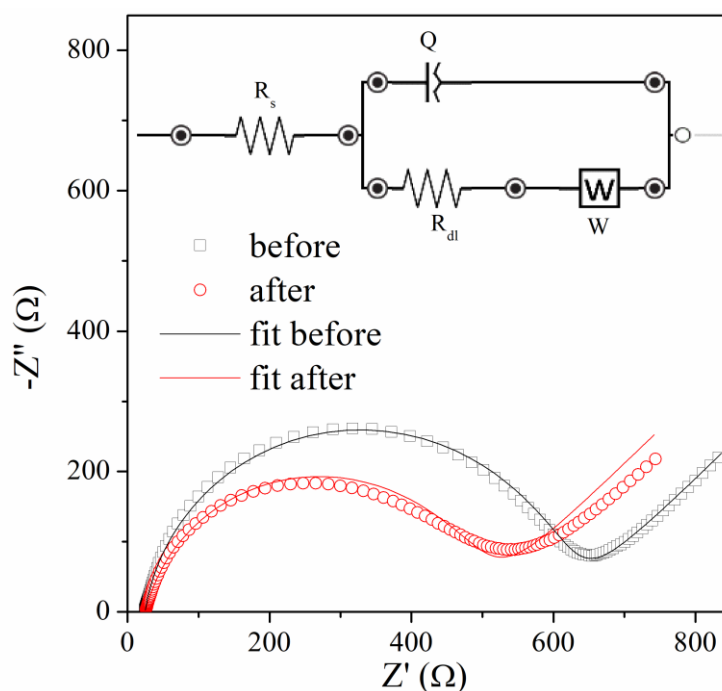
Fig. 20. Nyquist plots, an equivalent electric model and fitting for measurements of Au-MUA:MCH*ds*DNA (72 bp III.6 sequence) sensor in 2 mM K$_3$[Fe(CN)$_6$]/K$_4$[Fe(CN)$_6$] in HBS-EP pH 7.4 before and after incubation with 0.625 μM Lf in buffer solution for 2 minutes. Results of own research [65].

The parameters in Table 7 clearly indicated the change in the studied sensor's electrical properties after the interaction with lactoferrin compared to corresponding values before the interaction, confirming the formation of a complex between lactoferrin and immobilized DNA. Based on those results, the use of the EIS method for lactoferrin determination was established.

Table 7. Parameters of equivalent elements for applied faradaic model $R(Q[RW])$, including the fitting factor χ^2 of the model to the experimental data. Columns before and after refer to results obtained before and after interaction with Lf.

Element	before	after
R_s (Ω)	24.70	25.39
Q (μT)	6.91	11.10
n_1 (ϕ)	0.91	0.86
R_{dl} (Ω)	590.70	470.20
W (Ω·s$^{-1/2}$)	177.00	197.90
χ^2	$4.00 \cdot 10^{-4}$	$7.00 \cdot 10^{-4}$

## 7.2.	SPR affinity analysis

Experimental affinity screening is an important process when it comes to analyzing the interaction of biomolecules. This is particularly true when one of the biomolecules is immobilized on the sensor surface, as it is in biosensor design. The analysis results of the interaction between DNA sequences indicated in Table 2 and Lf are summarized as two relationships in Fig. 21. The first relationship is between the type of DNA used and the normalized mean relative response divided by the ligand density. The second relationship is between the $N_\delta^{Lf}/N_\delta^{DNA}$ ratio and the interaction results. This calculation allows for easy comparison of the results while assuming that the ligand density remains equal for each case. Furthermore, it eliminates the dependence of the interaction on the ligand immobilization yield. To design new DNA oligonucleotides, researchers used literature-recognized DNA sequences in various combinations, reversals, and multiplications separated with short spacers $d(A)_3$. Their goal was to discover a variant that would be suitable as a biorecognition element for Lf biosensing purposes. The results showed that the weakest interaction with lactoferrin occurred for the unhybridized mono$(A)_{23}$ sequence I.6. Another low response was recorded for the sequence containing an equal number of purines and pyrimidines arranged alternately (I.4 + II.4, hybridization efficiency 22%). The results obtained for the mono$(T)_{23}$ (I.8) and mixed sequence I.2 immobilized at the 3′ end were slightly higher. The bars in the next group on the chart are similar and include sequences I.1 + II.1, I.7, I.3, and III.2. When the I.3 sequence was hybridized with II.3, no improvement in interaction with Lf was observed. The relatively poor response for I.1 + II.1 may be due to partial hybridization (about 44%) obtained when the SPR method was used for modification. This could explain why the unhybridized sequence I.1 had a higher interaction result than the same sequence that was hybridized prior to immobilization onto the SPR chip (III.1). Lf had a higher affinity for the GC pair than for the AT pair, as observed when comparing the results obtained for the III.3 and III.4 sequences. Despite its low hybridization efficiency (only about 7%), the interaction of Lf with *ss* mono$(G)_{23}$ hybridized with mono $(C)_{23}$ (I.5 + II.5) was much higher than the response obtained for *ss* mono $(G)_{23}$ (I.5) and efficiently hybridized sequences mono$(A)_{23}$ with mono $(T)_{23}$ (I.6 + II.6, 74.5% hybridization efficiency). The results obtained from I.5 vs. III.3 show that hybridized oligonucleotides have an advantage over single-stranded ones, as the lowest ratio was found for the unhybridized sequence. The last batch of sequences used in the affinity screening process was based on literature and marked as III.5, III.6, and III.7. The first sequence, III.5, has a total of 57 base pairs (bp), while the

second one, III.6, which provided the highest normalized interaction signal, is 72 bp long. The third sequence is 77 bp long, and it gave a slightly lower response than III.6. The number of molecules that bind to the bioreceptor after washing off the excess analyte helps in quantitative analysis and calculation of the binding ratio. The binding ratio is defined as the number of analyte particles bound per ligand molecule, which practically means the stoichiometry of the supramolecular complex [243].
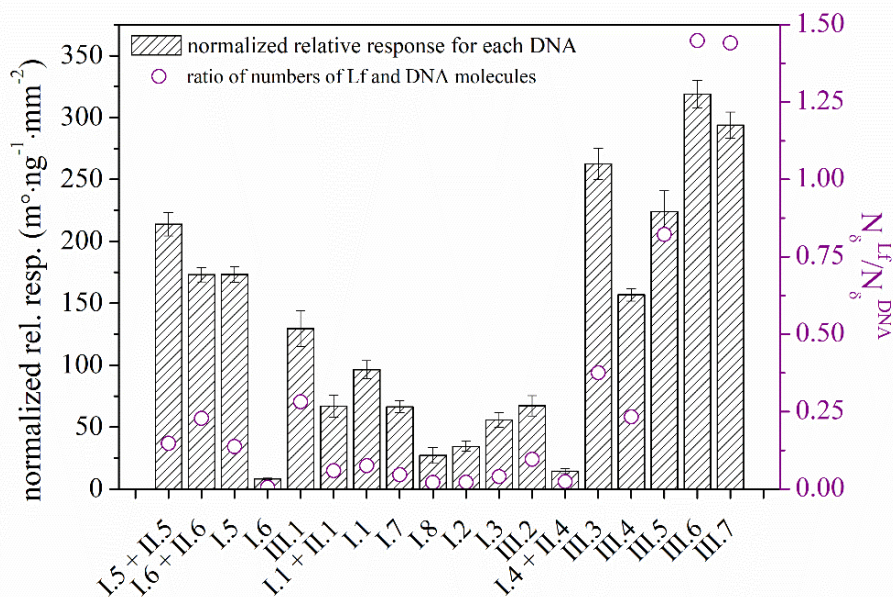
Fig. 21. Relative normalized response DNA-Lf interaction experiments, obtained for full association/dissociation cycle and the ratio of bound Lf molecules to immobilized DNA molecules vs. DNA oligonucleotides used, n $\geq$ 3. Results of own research [65].

In accordance with the affinity analysis, the $N_\delta^{Lf}/N_\delta^{DNA}$ ratio was found to be the highest for sequence III.6, indicating that it is the most suitable oligonucleotide for further analyses. Based on the data obtained, a suitable mathematical model was chosen to represent the experimental data. The results confirmed that Lf has a stronger affinity towards double-stranded oligonucleotides compared to single-stranded ones. Moreover, the study revealed that longer multiplied oligonucleotides are more advantageous than short sequences used as building blocks for oligonucleotides longer than 50 bp, as they offer higher flexibility and better exposure of the specific DNA sequence to lactoferrin.

7.3. Kinetics of lactoferrin-DNA interaction

The dynamic parameters of intermolecular interactions were obtained through the kinetic analysis, which provided vital information about the rate of complex formation and its stability, giving an insight into these processes. Measurements were performed in a wide range of analyte concentrations, from zero to saturation, to address the requirements of kinetic analysis. In general, the acquisition of kinetic data is extremely challenging for complex systems like biomolecular interactions. The simplifications have to be applied since oftentimes instrumentation imposes limitations such as data acquisition rate, which for SPR hardware is typically about several ms, while the biological process has multiple discrete steps of several µs or less. Hence, the experimental part was carefully designed and performed to obtain consistent and reproducible data. The low immobilization yield of utilized biosensing layers allowed for the avoidance of steric hindrance, while the high flow rate of sample injection and mixing enabled the minimization of the mass transport effects. The bulk effect was eliminated by injecting a buffer solution devoid of analyte molecules and subtracting from the relative response for each concentration.

Kinetic model

The research led to a one-on-one interaction between Lf and particular DNA, supported by stoichiometry findings. Fig. 22 illustrates the results obtained for one set of measurements, where the colored lines represent the experimental data and the mathematical fitting of the model is visible as black lines. The simplest model was created based on the significant size difference and the immobilization of the smaller DNA ligand, which formed a comparatively firm and uniform layer with no surface heterogeneity or conformational changes expected. As a result, it provides the most accurate reflection of the binding event. Generally, surface effects, such as immobilization heterogeneity or cross-linking and mass transfer or rebinding of analyte to the surface, can affect the kinetic data. However, the simplest one-to-one is the starting model and fits well for a majority of interactions, indicating good experimental performance.
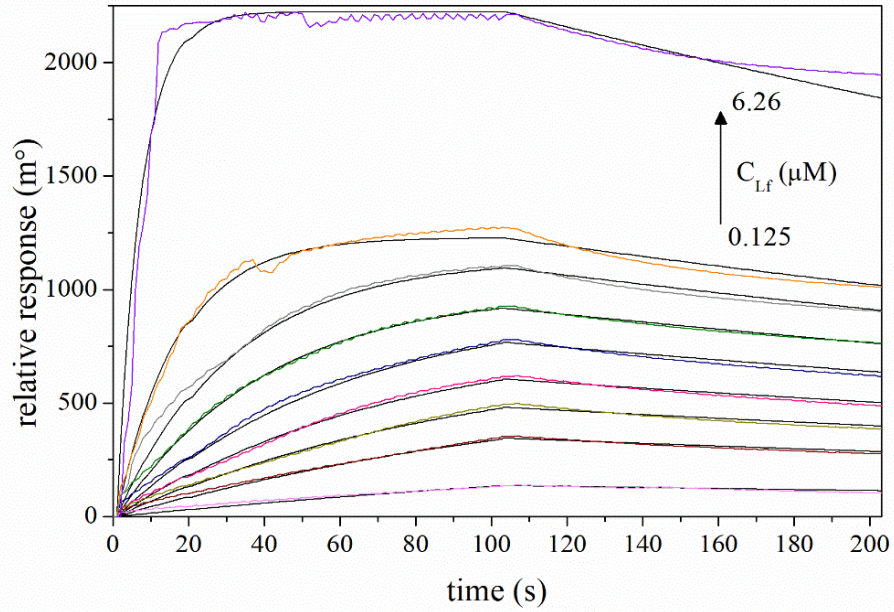
Fig. 22. Exemplary experimentally obtained kinetic curves (in color) of 72 bp III.6 and Lf, along with mathematically fitted one-to-one binding model curves (in black). The curves were obtained within a concentration range of 0.125 to 6.25 µM Lf in an HBS-EP buffer solution pH 7.4. TraceDrawer software was used to process the data. Results of own research [65].

Kinetic constants

A summary of the kinetic evaluation is presented in Table 8.

Table 8. The kinetic parameters of the one-to-one interaction between Lf and III.6 DNA sequence, n = 3.

C_{Lf} (µM)	R_{max} (m°)	$k_a \cdot 10^4$ (M$^{-1} \cdot$s^{-1})	$k_d \cdot 10^{-3}$ (s^{-1})	$K_D \cdot 10^{-8}$ (M)	$K_A \cdot 10^8$ (M^{-1})
0.125	549.6 ± 136.0				
0.25	800.3 ± 15.0				
0.375	848.9 ± 7.1				
0.5	908.0 ± 7.0				
0.625	1035.1 ± 3.3	2.49 ± 0.03	1.89 ± 0.002	7.61 ± 0.18	0.13 ± 0.05
0.938	1075.9 ± 1.8				
1.25	1204.1 ± 2.0				
2.5	1266.2 ± 1.2				
6.25	2250.3 ± 0.3				

The maximal immobilization yield, R_{max}, is unique for each concentration of Lf, while all other parameters remain independent of Lf concentration. The experiment was repeated three times, and mathematical modeling showed that the results were highly reproducible. This was indicated by the low SD of each parameter in the model. The rate constant for complex formation (k_a) was calculated to be $(2.49 \pm 0.03) \cdot 10^4$ $M^{-1}s^{-1}$, indicating a fast rate of binding. The dissociation rate constant (k_d) was found to be $(1.89 \pm 0.02) \cdot 10^{-3}$ s^{-1}, indicating that the breakdown of the complex was slow, which suggests that it was stable. The dissociation constant (K_D) was calculated to be $(7.61 \pm 0.18) \cdot 10^{-8}$ M, and the association constant (K_A, which is equal to the binding constant K_b at equilibrium $K_A = K_b$) was also determined. Both these constants indicate that there was high specificity in the intermolecular binding of Lf with the proposed oligonucleotide sequence [203,224]. The K_D values obtained in this study were relatively close to those obtained in other studies [221] where inhibition experiments were used. The authors of the study found that out of the literature-recognized sequences, the highest affinity was obtained for TAGAAGATCAAA, which was used as a building block for III.6 sequence. The values of the equilibrium constants obtained within the kinetic analysis confirmed the dynamic properties of the DNA-Lf setup and justified the premise of using specific DNA oligonucleotides to develop a functional biorecognition layer for Lf.

7.4. Thermodynamics of lactoferrin-DNA interaction

Direct experimental thermodynamic characterization of the formation of DNA-Lf complex was conducted using the SPR method. The aim was to gain a deeper insight into the driving forces that facilitate supramolecular interactions between DNA and Lf. The binding constants obtained for the range of Lf concentrations from 0.5 to 3.75 µM were used to compute the thermodynamic parameters. The considerations were carried out for the equilibrium state where association and dissociation rates are equal. The van't Hoff plot, which is a natural logarithm of K_b vs. $1/T$, describes the temperature dependence of the binding constant (visualized in Fig. 23).
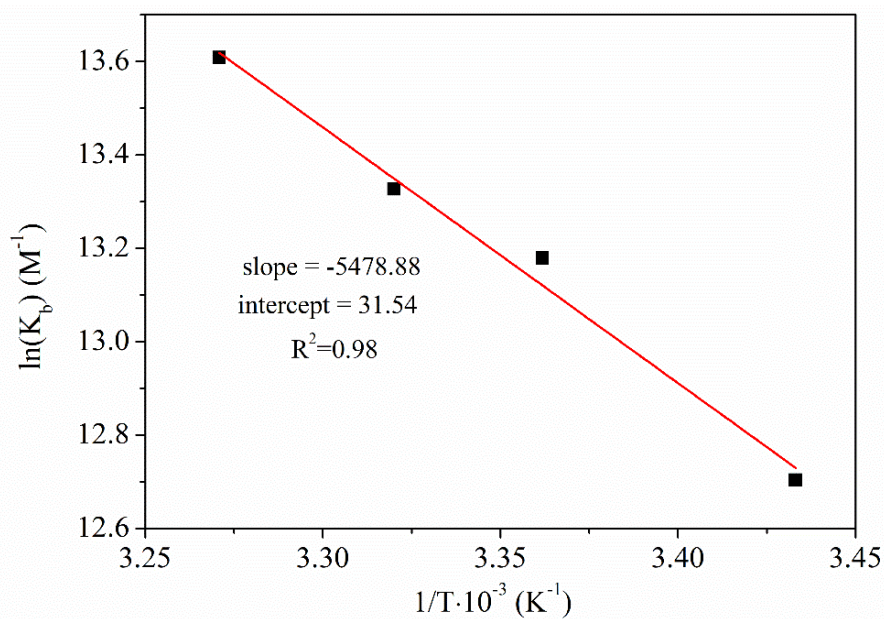
Fig. 23. The van't Hoff plot of DNA-Lf interaction under different temperatures as a linear function of $\ln(K_b)$ vs. inversed temperature. Results of own research [65].

Thermodynamic constants

The findings from the study have been collected in Table 9. The values for binding constants increased with temperature, suggesting that the process of DNA-Lf complex formation is endothermic within the temperature range studied. The binding constants for oligonucleotide sequences (1), (2), and (3) from literature-based studies [58] that used electrophoretic mobility shift assay [221] were of similar magnitudes, indicating consistency between EMSA and SPR techniques. However, the concentrations of Lf-DNA complexes for III.6 and Lf were at least one order of magnitude higher than those obtained in studies involving Lf-naringin [134] or Lf-phenothiazine dyes [204]. This implies that Lf binds to DNA more strongly than to flavonoids or dyes under comparable conditions, such as temperature range and pH. The study utilized Lf as an immobilized ligand that interacts with free naringin flavonoid or phenothiazine dyes. These results suggest that *ds*DNA has potential as a biorecognition element for human Lf.

Driving force for lactoferrin-DNA interaction

The stability of a non-covalent complex formed between a protein and a specific DNA site can be determined by the standard free energy difference during the association process, which is relative to the specified solution conditions such as pH, salt concentration, etc. This

is not an absolute quantity but is determined by the quality and quantity of non-covalent interactions between the protein, DNA site, and solvent components like water and ions [248].

Table 9. Thermodynamic parameters of DNA-Lf complex formation under different temperatures and pH 7.4 (HBS-EP buffer solution).

T (K)	$K_b \cdot 10^5$ (L·mol^{-1})	ΔH^0 (kJ·mol^{-1})	R^2	ΔG^0 (kJ·mol^{-1})	ΔS^0 (kJ·mol^{-1}·K^{-1})	$T\Delta S^0$ (kJ·mol^{-1})
291.15	3.29			-30.76		76.32
297.15	5.29	45.55	0.989	-32.59	0.26	78.14
301.15	6.13			-33.37		78.92
305.15	8.13			-34.59		80.14

A negative ΔG^o value suggests that the chemical equilibrium can be favorably reached at any temperature between 18-32°C (291.15 – 305.15 K). Furthermore, the characteristic of Gibbs free energy vs. temperature shows that the stability of DNA-Lf interaction increases with temperature. The obtained ΔH^o and $T\Delta S^o$ values are positive, indicating that the process is entropically driven in the range of used temperatures. Typically, positive enthalpy and entropy values are associated with hydrophobic-dominated intermolecular interactions of reactants, which relates to some extent to the properties of the proposed lactoferrin DNA-binding site [7,249]. The complex formed between DNA and Lactoferrin shows an increase in entropy, which is not necessarily indicative of a change in the conformation of the reactants during the conjugation process. Instead, it may result from the gain of configurational entropy associated with the release of water or the formation of ion solvation shells around the complex [82]. As the pI of lactoferrin is basic and the *ds*DNA exhibits a negative charge, under the condition used in the study pH 7.4, the electrostatic forces, including special cases such as van der Waals weak forces, seem to play an important role in the Lf-*ds*DNA binding [218,225]. The thermodynamic analysis results presented align with the data obtained by the Nevinsky group [62,221], which showed ΔG^o ca. -11.1 kcal·mol^{-1} (around -7.35 to -9.16 kcal·mol^{-1}), thus confirming the hypothesis that hydrophobic binding and weak electrostatic forces play a crucial role in the complex formation process. Although the proposed model assumes no change in the heat capacity with temperature increment upon binding, typically, the site-specific protein-DNA associations are characterized by a large negative standard heat capacity change, shifting the driving force from entropic to enthalpic with increasing temperature range [250,251].

However, the major contribution to the heat capacity change for protein interactions arises from changes in surface hydration, including apolar and polar parts [252]. Moreover, HEPES-based buffer solution utilized in the study is temperature-sensitive [253], nevertheless relevant for the binding event, according to results summarized in Table 4 of the previous section. Other buffer solutions, although having lower temperature dependence of pK_a values regarding thermodynamic quantities, were not compatible with the properties of the hydrogel matrix and pI of the target protein. The selection of buffers must guarantee the proper condition of interaction, taking into account, among others, the pH operation range. The decrease of pK_a of buffer with increasing temperature does not favor the ionization of the buffer solution [254,255]. Eventually, the temperature change in this study was rather small (18-32°C), so the changes in heat capacitance or pK_a of buffer solution are less obvious.

7.5.   Selectivity analysis of lactoferrin bioreceptor

The experiment investigated how a selected DNA interacts with various proteins with different features. The goal was to estimate the chosen DNA's relative response to these proteins compared to lactoferrin, which was used as a reference. Interfering proteins that might appear in real samples, such as plasma, urine, or saliva, were used. A hydrogel-based SPR sensor with a relatively high ligand capacity surface (1.77 ng·mm^{-2} of III.6) was utilized. The selectivity of the sensor was calculated for protein concentrations of 5 and 100 mg·L^{-1}, and the results are shown in Fig. 24. The data analysis showed that none of the used proteins exceeded 3% of the reference signal for Lf, regardless of the concentration used. The critical 10% threshold for clinical analysis was not crossed either, after taking into account the SD values. It is important to note that higher selectivity is achieved for interfering samples when they are present at low concentrations. This is because the matrix effect and nonspecific purely electrostatic interaction have a stronger effect at low concentrations. It should also be noted that negative results were obtained for urease and HRP at 100 mg·L^{-1} and for all proteins at 5 mg·L^{-1} (excluding Lf). These negative mean values are due to a slight signal drift that causes the baseline to decrease by several milli-degrees (m∘), which is considered a measurement error of the method. Most interferents are proteins that are commonly present in various biological samples. Therefore, at pH values above their pI and considering the negative charge of the biorecognition layer, electrostatic repulsion minimizes the possibility of interaction. However, HRP is an enzyme with a

strongly positive charge at pH 7.4, yet it did not interact with *ds*DNA. The literature reports that selectivity studies for aptamer-based analyses typically involve the use of proteins found in milk samples at high concentrations, such as Lf [171,179,186].
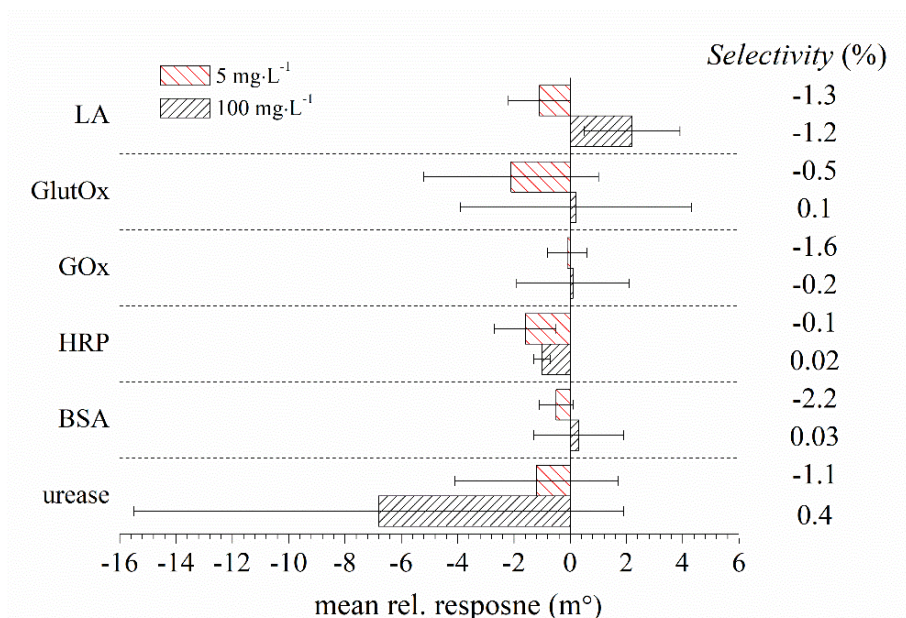
Fig. 24. Selectivity bars with RSD obtained for 5 and 100 mg·mL^{-1} interferent vs. lactoferrin in HBS-EP pH 7.4 buffer solution, n =3. Results of own research [65].

However, this study aims to develop a biorecognition element suitable for analysis in clinically significant samples, leading to the investigation of a different set of interferents. Furthermore, most aptamers do not exhibit satisfactory selectivity in quantitative analysis, which makes their use unfavorable, and their development process is rigorous and time-consuming compared to oligonucleotide synthesis. The mean relative responses are summarized in Table 10.

Table 10. Mean relative response with SD and calculated values of *Selectivity* obtained for each respective protein-type interferent in high (100 mg·L^{-1}) and medium concentration (5 mg·L^{-1}) in relation to the reference mean response to Lf after the full association/dissociation cycle. Samples injected separately, n = 3.

	mean relative response ± SD, (m°)	*Selectivity* (%)
	100 mg·L^{-1} of protein	
Lf	594.2 ± 53.2	100
urease	-6.8 ± 8.7	-1.2
BSA	0.3 ± 1.6	0.1
HRP	-1.0 ± 0.3	-0.2

100

	mean relative response ± SD, (m°)	Selectivity (%)
	100 mg·L^{-1} of protein	
GOx	0.1 ± 2.0	0.02
GlutOx	0.2 ± 4.1	0.03
LA	2.2 ± 1.7	0.4
	5 mg·L^{-1} of protein	
Lf	98.2 ± 7.8	100
urease	-1.2 ± 2.9	-1.3
BSA	-0.5 ± 0.6	-0.5
HRP	-1.6 ± 1.3	-1.6
GOx	-0.1 ± 0.7	-0.1
GlutOx	-2.1 ± 3.0	-2.2
LA	-1.1 ± 1.1	-1.1

7.6. SPR quantitative analysis

The results of SPR quantitative analysis are presented in Fig. 25. The measurements were carried out to verify the utility of dedicated 72 bp DNA oligonucleotide for lactoferrin determination, compared to other DNA sequences. The findings reveal a significant difference between the multiplied 72 bp long sequence and the shorter 23 bp long sequence. In order to conduct a comparative analysis, the experiments were performed for the following loading density of each respective ligand: 1.01 ng·mm^{-2} for III.1. and 1.05 ng·mm^{-2} for III.6. The calibration curves, plotted as a relationship between mean relative response and Lf concentration, indicate a linear concentration range from 12.5 to 625 nM for the longer (72 bp) dedicated DNA oligonucleotide, and shifted towards higher value ranges from 0.1 to 1.25 μM for III.1, both with satisfactory correlation coefficients. The findings indicate a significant improvement in sensitivity for biosensing with the use of the III.6 sequence compared to the value calculated for III.1, which was nearly 5 times lower. The results show that longer DNA sequences offer higher repeatability of measurements within the linear concentration range, as evidenced by the lower SD bars. Moreover, it is clear that the 72 bp *ds*DNA outperforms the 23 bp ds sequence in terms of calculated LODs, with values of 4.42 nM and 85.56 nM, respectively. These findings highlight the effectiveness of the chosen DNA oligonucleotide as an Lf biorecognition element, with favorable metrological parameters, particularly LOD, in comparison to other SPR studies utilizing the immonosensing approach [169,170,256].
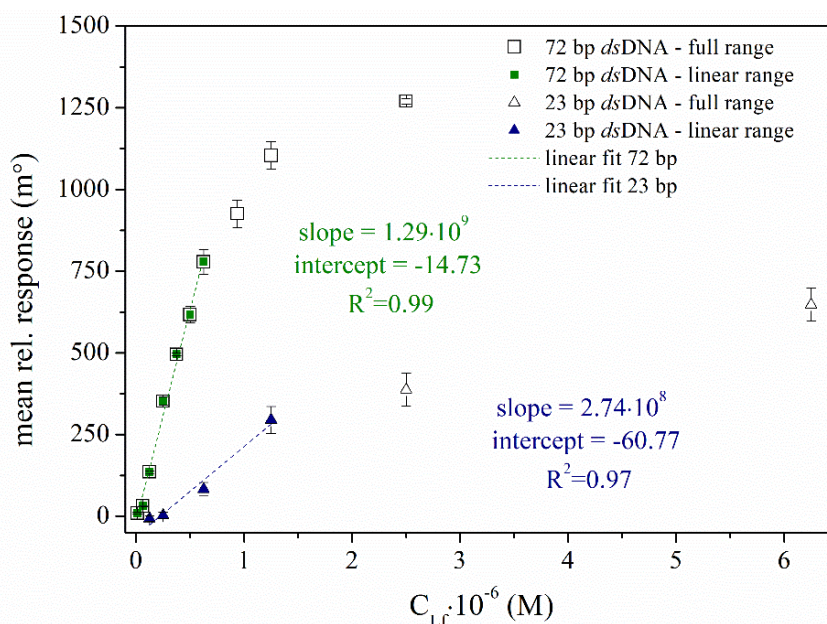
Fig. 25. Calibration curves obtained for Lf interacting with 72 bp *ds*DNA (III.6) and 23 bp *ds*DNA (III.1) immobilized on the SPR sensor chips. Results obtained in HBS-EP buffer of pH 7.4, n = 3. Results of own research [65].

8. DNA-based label-free impedimetric biosensor for determination of lactoferrin

The usage of a particular type of biorecognition element for the development of impedimetric biosensors for quantitative Lf analysis was fundamentally based on the research presented in the previous section. Briefly, the 72 bp DNA oligonucleotide was proposed among various sequences as the selective DNA-based bioreceptor for Lf. The choice was motivated by the results of affinity, kinetics, thermodynamics, and selectivity analyses. In this chapter, the results of the investigation on adapting the SPR sensor modification procedure to electrochemical sensors, characterization of the fabricated impedimetric biosensor, and quantitative analysis of Lf in laboratory samples and human saliva will be presented and discussed in detail.

8.1. Loading density of bioreceptor with SPR

The bioactivity of the recognition biomolecules immobilized on EIS biosensors poses a challenge for protein biosensing. Careful selection of the concentration of the compound providing functional groups for immobilization is necessary to avoid negative consequences, such as steric hindrance, which can directly reduce the activity of the bioreceptor. The SPR method was used to adjust conditions and achieve an optimal immobilization level of the bioreceptor, which enables efficient interaction. The concentration of the linear linker

(MUA) to the blocking agent (MCH) was compared in terms of immobilization level and normalized response for the fixed Lf concentration The primary function of MCH is to fill the free spaces between MUA functionalities, thereby reducing the non-specific binding of DNA to the sensor surface. MUA, on the other hand, binds to DNA that has been modified with primary amine using the EDC/NHS reaction. The results in Fig. 26 A-B show that a 1:10 MUA:MCH molar ratio provides the lowest ligand density and the highest interaction level, which is consistent with SPR theory [94,96].
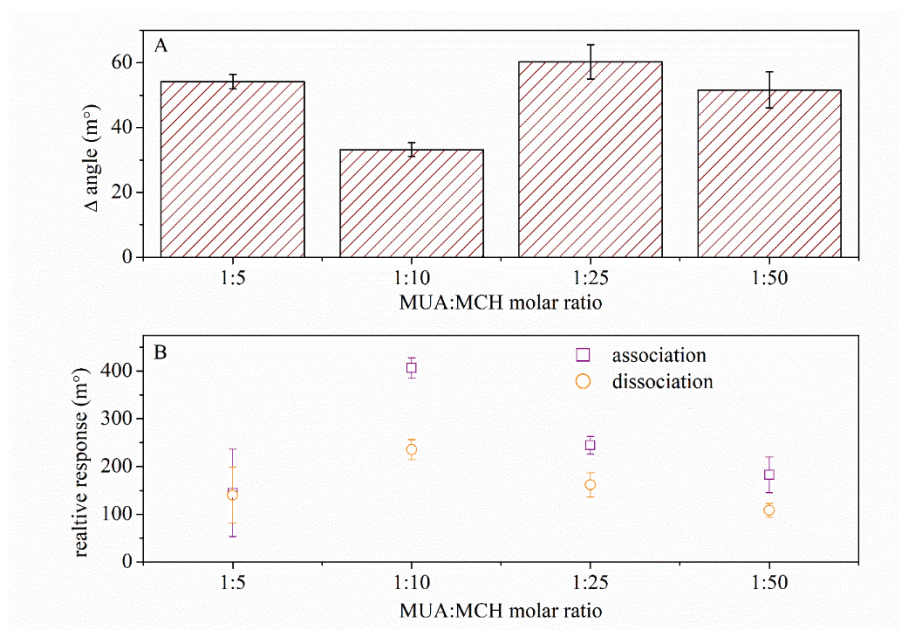
Fig. 26. (A) Relative response corresponding to immobilization level of dsDNA on 2D MUA:MCH-modified gold sensor, depending on the molar ratio of linker-to-blocker, n = 3; (B) the impact of linker-to-blocker ratio on Lf binding to immobilized DNA, n = 3. All experiments were carried out in HBS-EP pH 7.4 as a running/coupling buffer. Results of own research [257].

To carry out further analyses, a ratio of 1:10 was utilized. During the initial stage of biosensing surface preparation, the density of introduced functionalities was regulated by incorporating an appropriate quantity of blocking agent. This step was particularly advantageous in the formation of DNA-Lf complexes since it helped to minimize steric hindrance. This hindrance is often caused by the overcrowding of ligand molecules [235]. The interaction between molecules can be affected by the presence of a receptor layer that is highly packed or overpacked, which can introduce mass transport and diffusion limitations. To create a biosensing layer for EIS analysis, the modification protocol that was adjusted with SPR has been transferred and adapted.

8.2.   Characterization of new impedimetric biosensor

FTIR and contact angle analyses

The sensors' surface underwent characterization at each modification step using FTIR spectroscopy and water/air contact angle measurements (as shown in Fig. 27A-B). The initial hydrophobic surface of the bare gold was modified with a linker/blocker mixture, which caused its properties to become more hydrophilic (with a contact angle of around 65 degrees). The subsequent addition of DNA and protein layers further decreased the mean value of the contact angle to below 60 degrees, indicating their successful attachment. The presence of surface functional groups, which are characteristic of molecules captured on the sensor surface at each step, was confirmed by FTIR transmittance measurements. The spectra recorded for the MUA:MCH-derivatized gold that was further modified with dsDNA and Lf were found to share the same broadbands at 3400-3200 cm^{-1}, which are assigned to O-H stretching vibrations. The spectra of the MUA:MCH-modified gold (line 2) additionally exhibit vibrations assigned to C=O bands around 1710 cm^{-1}. The presence of dsDNA (line 3) is confirmed through various peaks that are characteristic of DNA structure [247]. These peaks are assigned to the vibrations of the following groups: approximately 1730 cm^{-1} from C=O vibrations and 1550 cm^{-1} from C=N of guanine rings; at 1350 cm^{-1}, the vibrations of bonds in 2'-deoxycytidine; and at 1720 cm^{-1}, a small band ascribed to the C=O carbonyl groups of thymine. Additionally, the peak corresponding to the vibration of the -OH group decreased, which resulted from the occupation of these functional groups by DNA strands. The presence of lactoferrin at the DNA-modified surface is indicated by distinct bands originating from bond vibrations of this protein (line 4). Small bands at 2950-2770 cm^{-1} are attributed to C-H stretching vibrations of protein structure. The bands observed at 1600-1550 cm^{-1} come from peptide bonds (amide I and amide II) [246]. The amide I band corresponds to the vibrations of α-helices, whereas the amide II band originates from the vibrations of N-H and C=O groups. In the 4th spectrum, the band at 1410 cm^{-1} is associated with amide III N-H vibrations, while 1200-1100 cm^{-1} and 1020 cm^{-1} result from C-N stretching vibrations of aliphatic amines.
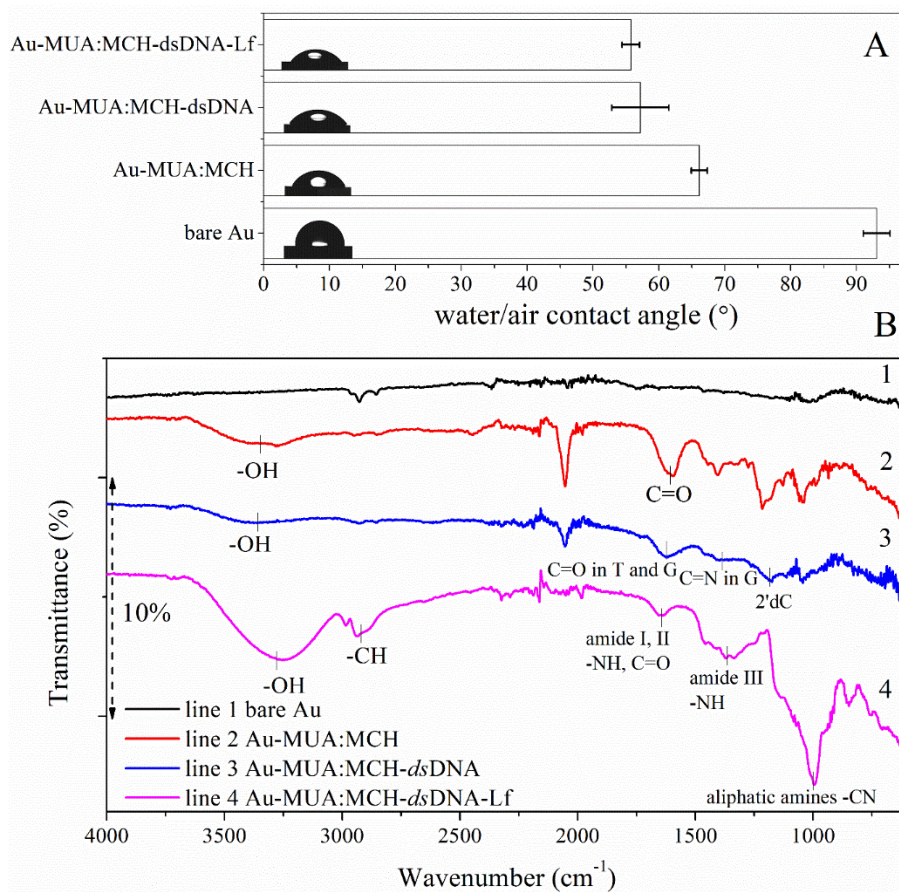
Fig. 27. (A) Contact angle (water/air), n = 20, and (B) FTIR spectra in wave number range 4000 to 600 cm^{-1} obtained for the sensors at consecutive modification steps, described as: bare Au, Au-MUA:MCH-derivatized, Au-MUA:MCH-dsDNA and Au-MUA:MCH-dsDNA-Lf. Results of own research [257].

8.3.   Faradaic and non-faradaic EIS experiments

Before conducting EIS measurements, the electrochemical behavior of redox probe 2 mM [Fe(CN)$_6$]$^{3-/4-}$ in 10 mM HBS-EP of pH 7.4 was examined onto DNA-modified sensors using CV and OCP methods. The mean value of the open circuit potential decreased slightly from 275 mV (± 2.9 mV) to 271 mV (± 0.6 mV), which suggests that the modified surfaces are highly stable. The characteristics of oxidation and reduction potentials (E_{ox}, E_{red}) and currents (I_{ox}, I_{red}) are illustrated in Fig. 16A-B. It was observed that the CV redox potentials were not significantly affected by the scan rate (v) above 20 mV·s^{-1}, whereas the smallest changes in CV current were obtained within the same scan rate range from 5 to 20 mV·s^{-1}. To describe the behavior of the electrochemical system investigated with EIS methods, the Randles model – an electrical equivalent circuit is commonly used [188]. For our purposes, the Randles model was modified and illustrated in Fig. 28.
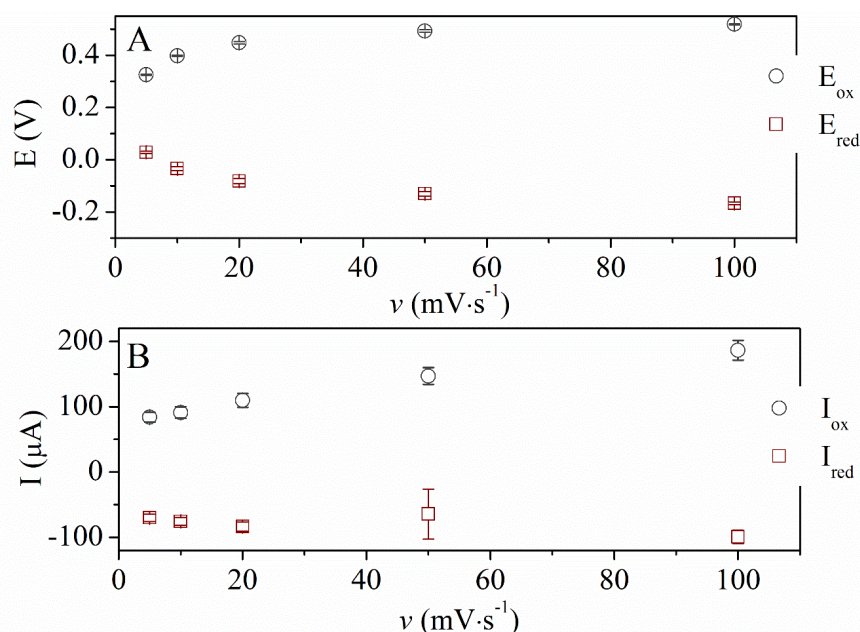
Fig. 28. Oxidation/reduction potential (A) and current peak (B) vs. scan rate of CV measurements, obtained using redox probe 2 mM $[Fe(CN)_6]^{3-/4-}$ after incubation with 312.5 nM Lf for 2 minutes, n = 3. Results of own research [257].

The fit of each model to experimental data can be determined by the chi-squared χ^2 parameter. Two approaches are used to study the electrical properties of interface biosensor surfaces/solution: faradaic reactions and non-faradaic processes. Faradaic processes require the use of a redox probe and the application of direct current (DC) conditions to promote the development of electrochemical reactions. An electrochemical probe ($[Fe(CN)_6]^{3-/4-}$ solution) is commonly used for this purpose [189]. To study the electrode-electrolyte resistance at equilibrium, which corresponds to the charge transfer behavior of the electrode, the open circuit potential (OCP) is first determined and then applied as the DC potential (E_{DC}). Thermodynamically stable conditions are maintained at or below the OCP. For non-faradaic processes, the use of redox couples is unnecessary. In such cases, a one-component 0.1 M KCl electrolyte solution without an electrochemical probe is sufficient [194]. The results of EIS measurements conducted for both models were analyzed, and the obtained electrical parameters were summarized in Table 11. The experiments were performed using bare Au, Au-MUA:MCH, and Au-MUA:MCH-*ds*DNA. The analysis of the non-faradaic model clearly shows the changes in electrical properties of the Au sensor-chips after being modified with an organic layer.
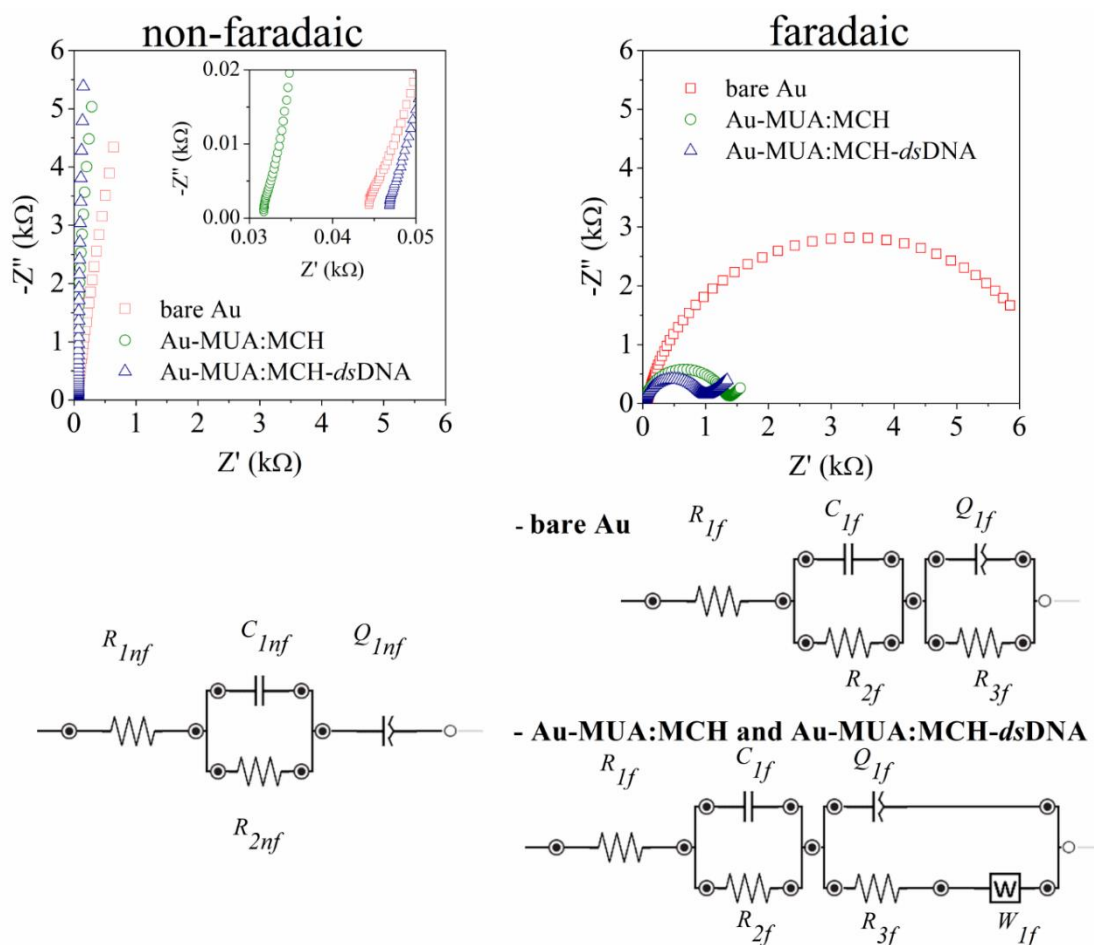
Fig. 29. Randles equivalent circuits for non-faradaic and faradaic processes; the results of electrical characterization of bare Au, Au-MUA:MCH, and Au-MUA:MCH-*ds*DNA presented as Nyquist plots. The inset graph for the non-faradaic process shows the high frequency range with partially developed semi-circles. Results of own research [257].

These changes are expressed by an increase in capacitance C_{1nf}. The resistance of the 0.1 M KCl solution was around 40 Ω. However, the presence of the organic layer, MUA:MCH, and further *ds*DNA limited the electron transfer, resulting in an increase in C_{1nf} capacitance. Additionally, the double-layer resistance increased due to the poor electrical conductivity of the linker and immobilized DNA. The calculated time constant $\tau_{nf} = C_{1nf} \cdot R_{2nf}$ increases with each consecutive layer added onto a surface. The deposition of consecutive layers was confirmed by SPR results, which also validated the impedimetric interpretation. In addition, changes in the phase angle and value of the constant phase element parameter Q_{1nf} can be noted within the low frequency range. This describes a non-ideal capacitor with a decreasing value as the deposited layer thickness increases. The exemplary impedimetric spectra in the form of Nyquist plots and the schemes of equivalent electrical models for non-faradaic and faradaic processes are depicted in Fig. 29.

Table 11. Parameters calculated using equivalent electrical circuit models for non-faradaic and faradaic processes.

	non-faradaic model (measurements in 0.1 M KCl)					
Element	**Au**		**Au-MUA:MCH**		**Au-MUA:MCH-*ds*DNA**	
	mean	**SD**	**mean**	**SD**	**mean**	**SD**
R_{1nf} (Ω)	42.543	2.127	35.340	2.624	42.465	4.615
C_{1nf} (μF)	2.747	0.690	4.833	0.724	5.452	0.095
R_{2nf} (Ω)	4.912	1.408	3.508	0.438	7.594	0.644
Q_{1nf} (μT)	4.396	0.747	3.389	0.363	3.112	0.020
n_{1nf} (-)	0.930	0.007	0.978	0.020	0.992	0.001
χ^2_{nf} $(\cdot 10^{-5})$	15.000	5.000	11.740	6.158	10.333	13.199
τ_{nf} (μs)	13.490	0.972	16.957	0.317	41.396	0.061
	faradaic model (measurements in 2 mM [Fe(CN)$_6$]$^{3-/4-}$ in HBS-PE pH 7.4)					
R_{1f} (Ω)	31.333	2.073	28.997	2.095	31.907	3.789
C_{1f} (μF)	6.913	1.001	9.205	2.082	9.027	1.003
R_{2f} (Ω)	28.430	1.687	2.555	0.702	2.741	0.414
Q_{1f} (μT)	64.767	4.984	5.718	0.912	5.438	0.198
n_{1f} (-)	0.840	0.043	0.938	0.009	0.944	0.002
R_{3f} (Ω)	8966.000	2084.759	1137.000	360.292	767.467	98.995
W_{1f} $(\Omega \cdot s^{-1/2})$	-----	-----	173.600	35.310	213.433	80.126
χ^2_f $(\cdot 10^{-5})$	113.333	30.912	6.557	2.557	6.547	2.225
τ_f (μs)	196.537	1.690	23.522	1.461	24.743	0.415

Each modification step was characterized using the faradaic model. The resistance of the electrolyte (2 mM [Fe(CN)$_6$]$^{3-/4-}$ in HBS-EP pH 7.4) was defined as R_{1f} and was around 30 Ω, lower compared to the non-faradaic setup due to the presence of the redox probe. The best fit of the experimental data to the model was obtained for the equivalent electrical circuit with the following configurations: $C_{1f}R_{2f}$ and $Q_{1f}R_{3f}$. In the case of results obtained after modifying Au sensors with (bio)organic layers (Au-MUA:MCH and Au-MUA:MCH-dsDNA), the equivalent electrical model was expanded by the Warburg element W_{1f}, which describes the mass transport of redox probe molecules from the solution to the electrodes' surface [187]. Limited diffusion within the examined electrochemical system is associated

with such behavior, which results from the presence of poorly conductive organic or bioorganic layers. Due to this, the W_{1f} value increases as the thickness of the (bio)organic layer increases. However, the capacitance of the double layer is greater for the surface with (bio)organic layers, which leads to a lower time constant defined as $\tau_f = C_{1f}R_{2f}$, indicating faster charge transfer to the electrodes' surface from the solution. The resistance R_{3f} is significantly lower for the bare sensor compared to the MUA:MCH-modified, and immobilization of another molecule, such as DNA oligonucleotide, results in further resistance drop. The constant phase element Q_{1f} of the faradaic process decreases after modifications with linker/blocker and DNA. Similarly, the change of phase angle is visible. The observed differences in electrical properties for each type of sensing surface confirm the modification steps, first with linear linker/blocker and second with DNA molecules.

8.4. Electrical equivalent circuit parameters vs. lactoferrin concentration

The data obtained with the use of the developed biosensor was processed by adapting an equivalent electrical model for the faradaic process. The experimental impedimetric signal was recorded before and after interaction with a fixed concentration of Lf. The changes in the impedimetric spectra confirmed the interaction between the DNA receptor and Lf. The calculated parameters were analyzed to identify the quantitative correlation between the changes in impedimetric spectra and the changes in Lf concentration. The results of this analysis are summarized in Table 12. Several types of parameters were taken into account: (1) ratio of time constant before and after the interaction calculated as $C_{1f}R_{2f}$, (2) ratio of resistance R_{2f} before and after the interaction, (3) difference between R_{2f} before and after the interaction, and (4) ratio of R_{3f} resistance before and after the interaction The analysis was conducted on four independent biosensors using two sets of AC offsets: 10 mV and 50 mV, respectively. The DC settings for each specific measurement were obtained from OCP experiments.

Table 12. Parameters of an equivalent electrical circuit resulting from EIS measurements aimed at finding the analytical relationship of the EIS response with lactoferrin concentration.

AC 10 mV	$\tau_{f\_before}/\tau_{f\_after}$	$R_{2f\_before}/R_{2f\_after}$	$R_{2f\_before}-R_{2f\_after}$	$R_{3f\_before}/R_{3f\_after}$
biosensor1	0.95	0.81	-1.22	1.14
biosensor2	0.97	0.87	-0.60	1.21
biosensor3	0.97	0.96	-0.14	1.31
biosensor4	0.93	0.92	-0.27	1.39
SD	0.017886	0.065271	0.482318	0.109055
AC 50 mV				
biosensor1	0.91	0.77	-1.11	1.17
biosensor2	0.97	0.86	-0.44	1.26
biosensor3	0.99	0.97	-0.07	1.39
biosensor4	1.24	1.58	1.09	1.17
SD	0.143866	0.366059	0.922415	0.10325

The results showed that the reproducibility of the data obtained from AC 10 mV was higher compared to those obtained from AC 50 mV. Eventually, the value of resistance R_{3f} was selected among other parameters, as it exhibited the most significant and reproducible changes, as evidenced by the lowest SD values. Fig. 30A shows the Nyquist spectra for the Au-MUA:MCH-*ds*DNA biosensor before and after interaction with Lf, as well as the SPR sensorgram (real-time recording of SPR angle change) in Fig. 30B indicating the complex formation between a 72 bp dsDNA oligonucleotide and Lf, are presented. The change in resistance R_{3f} was utilized as an analytical parameter to measure the Lf concentration in the EIS readout. An increase in analyte level leads to a decrease in R_{3f}. The binding of Lf molecules alters the charge transfer resistance of the model, which enhances the charge transfer kinetics by reducing the negative charge on the electrode surface. The reason for the observed behavior is that DNA carries a negative charge while the molecules being analyzed have a positive charge under experimental conditions. The biosensor is incubated with Lf in HBS-EP pH 7.4, whereas Lf's isoelectric point is 8.7. The previous SPR experiments on the development of DNA biorecognition elements for Lf [65] and other studies on DNA-Lf binding [221,225] support these findings. Similar charge transfer effects on impedimetric

spectra have been observed for the interaction of specific DNA sequences and the NF-κB factor [196], as well as *Mycobacterium tuberculosis* secreted immunogenic protein MPT64 [258].
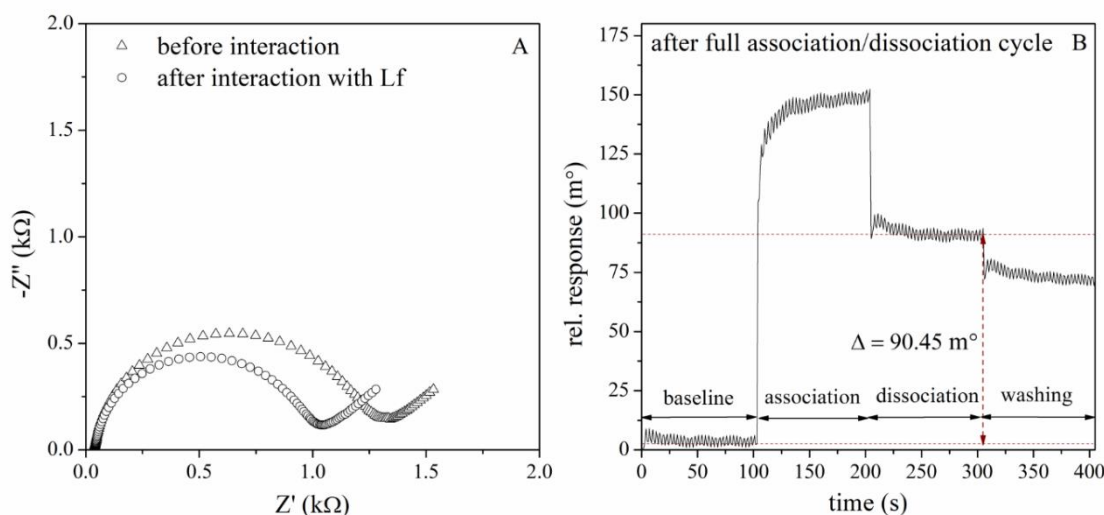
Fig. 30. The Nyquist plot obtained for the biosensor before and after interaction of immobilized *ds*DNA oligonucleotide bioreceptor with Lf using (A) EIS method in the faradaic model and (B) SPR. Incubation conditions: fixed concentration of Lf – 50 mg·L^{-1}, time – 2 minutes. Results of own research [257].

8.5. Quantitative analysis of lactoferrin concentration in laboratory samples

A concentration-dependent analysis of EIS spectra was conducted using a specific 72 bp DNA and a 23 bp strand to compare results in terms of metrological parameters. Calibration curves were presented in Fig. 31A-B to show the relationship between the normalized R_{3f} calculated for the faradaic process for 2 mM [Fe(CN)$_6$]$^{3-/4-}$ for both DNA oligonucleotides and Lf concentration. The normalized resistance R_{3f} was established as the ratio of R_{3f} value obtained for biosensors before and after binding with the analyte at various concentrations. Both characteristics exhibited linearity with correlation coefficients $R^2 = 0.99$, although the linear Lf concentration ranges differed. For the longer 72 bp sequence, the linear range was from 2.5 nM (LOQ) up to 625 nM, while for the shorter DNA strand, it was shifted towards higher concentration from 125 nM (LOQ) up to 2.5 μM. It is important to note that the sensitivity, expressed as the slope of the calibration curve, was higher for the dedicated 72 bp sequence. Similarly, the repeatability was higher for 72 bp oligonucleotide compared to 23 bp DNA, with higher SD bars for the latter. The limits of detection clearly demonstrate

the advantage of using a dedicated sequence over a shorter one. For the 72 bp DNA, the limit of detection was 1.25 nM (with LOQ of 2.5 nM), whereas for the 23 bp DNA, it was 60 nM (with LOQ of 125 nM) – almost 50 times higher. The calibration was conducted using the SPR method along with a specific 72 bp DNA oligonucleotide immobilized via a linear linker, which provided reference data for optical label-free Lf detection. Fig. 31C shows the SPR calibration curve for Lf, where the SPR biosensor response was nonlinear within the range of Lf concentration, similar to that of the impedimetric biosensor. Linearization can be obtained using the logarithmic scale of Lf concentration, indicating that the possible accuracy of measurements in the case of the SPR biosensors is lower than that of the 72 bp DNA-based impedimetric biosensor. Notably, the data utilized for concentration analysis was the relative (blank-subtracted) normalized signal after the full association/dissociation cycle. The correlation coefficient for the SPR biosensor is the same as that for electrochemical detection (0.99). Although the SD bars for respective concentration values were higher, the repeatability of SPR measurements was less satisfactory. The best repeatability was observed in impedimetric measurements using the developed biosensor with a 72 bp DNA oligonucleotide bioreceptor, as indicated by the lower SD bars for the respective concentration values. Moreover, the calculated LOD for SPR was established to be 0.75 nM, which is comparable to the LOD obtained for the corresponding impedimetric results of the same bioreceptor. It's important to note that the LOD and LOQ were estimated according to the standard method using the formulas $3SD_{blank}/S$ and $6SD_{blank}/S$, respectively, where SD_{blank} is the standard deviation of n replicates of blank (result obtained for the background buffer solution), and S is the biosensor sensitivity (slope of linear regression curve). The advantages of using DNA as a biorecognition element over Lf immunosensors proposed in the literature are evident from the data provided with the use of the proposed impedimetric DNA-based biosensors. The metrological parameters, particularly LOD, are more favorable for DNA-based systems [169,170,173,174,256]. For instance, the LOD for an SPR immunosensor working in batch mode is 280 nM, for an SPR immunosensor working in flow mode is 50 nM, and for an amperometric immunosensor is 25 nM, whereas the proposed DNA-based impedimetric biosensor has a LOD of just 1.25 nM.
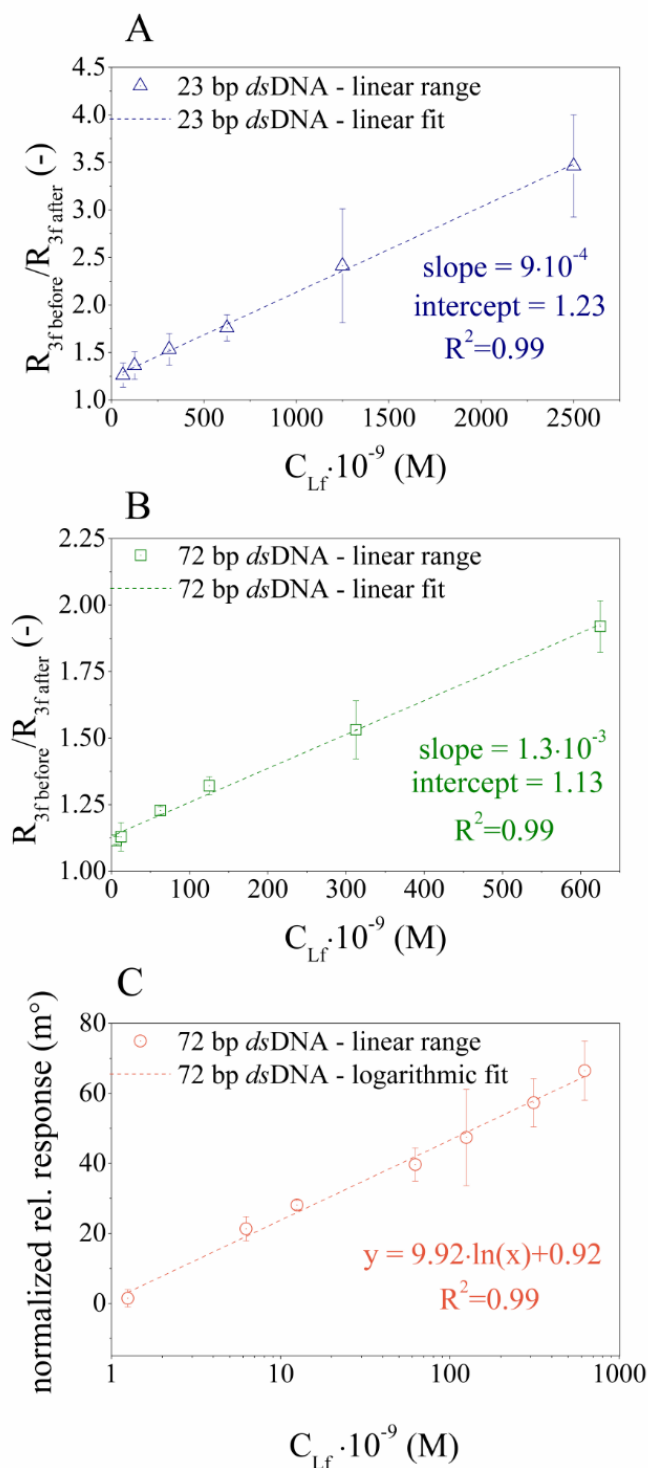
Fig. 31. Calibration curves obtained for Lf laboratory samples using (A) EIS method with 23 bp DNA-modified biosensors, (B) EIS method with 72 bp DNA-modified biosensors, (C) SPR method with 72 bp DNA-modified biosensors. The calibration characteristics were obtained for $n \geq 3$. All impedimetric measurements were performed for the faradaic process. All SPR measurements were carried out using HBS-PE pH 7.4 as a running/washing buffer and 10 mM HCl as a regeneration medium. Results of own research [257].

The proposed method for detecting Lf in this study is label-free, direct, and simple, providing ample opportunities for future improvements, including miniaturization. Aptamer-based electrochemical biosensors reported in the literature exhibited similar or inferior metrological parameters compared to the presented system. For example, a fluorescent aptasensor demonstrated 3 nM [156,157,179], whereas this work achieved 1.25 nM. Furthermore, the fluorescent aptasensor method is more expensive and time-consuming since it requires development and isolation from combinatorial libraries using the SELEX protocol, supported by sequencing methods.

8.6. Estimation of biosensor shelf-life

The shelf-life of the biosensors that were developed was evaluated through weekly measurements under carefully adjusted conditions for fixed Lf concentration. The results of the analysis are depicted in Fig. 32.
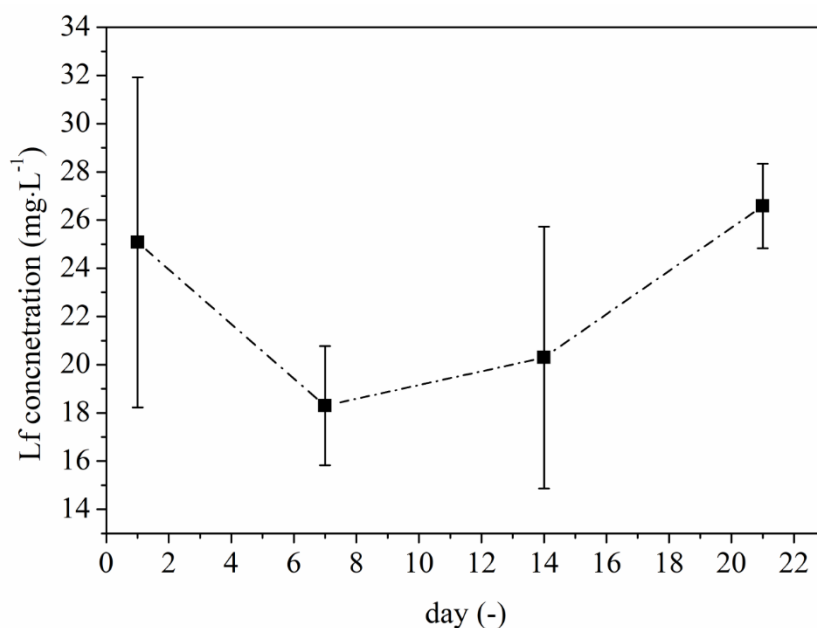
Fig. 32. The concentration of Lf was determined using the impedimetric biosensors on selected days of the sensors' storage period (1, 7, 14, and 21), n = 3. The concentration of Lf in the control sample of Lf was maintained at 25 mg·L^{-1}. Results of own research [257].

The biosensors were stored at 4°C between measurements. The values of Lf concentration were determined based on the calibration curve, considering the MW of Lf (80 kDa). The lowest estimation of Lf concentration was obtained on the seventh day of measurement (lower by ca. 34% with respect to the first day), and then it rose to the initial value. The stability of the biosensors was found to be relatively good. However, the repeatability was

114

observed to fluctuate, with the lowest on the first day and the highest after 3 weeks of storTo evaluate the shelf-life of the developed biosensors, weekly measurements were carried out under carefully adjusted conditions for fixed Lf concentration. The biosensors were stored at 4°C between measurements, and the values of Lf concentration were determined based on the calibration curve, taking into account the MW of Lf (80 kDa). It was observed that the stability of the biosensors was relatively good. However, the repeatability was found to fluctuate, with the lowest on the first day and the highest after 3 weeks of storage. This could be attributed to the fact that the biosensors were stored at a relatively low temperature and exposed to varying environmental conditions. Overall, the results suggest that the developed biosensors have good stability and can be reliably used for detecting Lf concentrations. However, it is recommended to repeat this experiment to obtain a more accurate estimation of shelf-life.

9. Determination of lactoferrin in human saliva samples

Developed DNA-based impedimetric biosensor vs. reference methods

The impedimetric biosensors were utilized for examining human saliva using three different approaches: DNA-based biosensing through EIS and SPR, as well as UV-Vis immunosensing employing a commercially available ELISA kit. The impedimetric measurements in human saliva functioned on the same principle as the Lf laboratory samples, as illustrated in Fig. 33A. In the case of EIS measurements, no dilution of saliva was necessary, thereby minimizing the sample preparation step. Conversely, during the SPR experiments, the data was fitted with the calibration curve after a 1:10 dilution, while the ELISA test required multiple repetitions to establish a sufficient 1:25,000 dilution for the collected saliva samples. The SPR sensorgrams recorded for detecting Lf in real samples are exemplified in Fig. 33B.
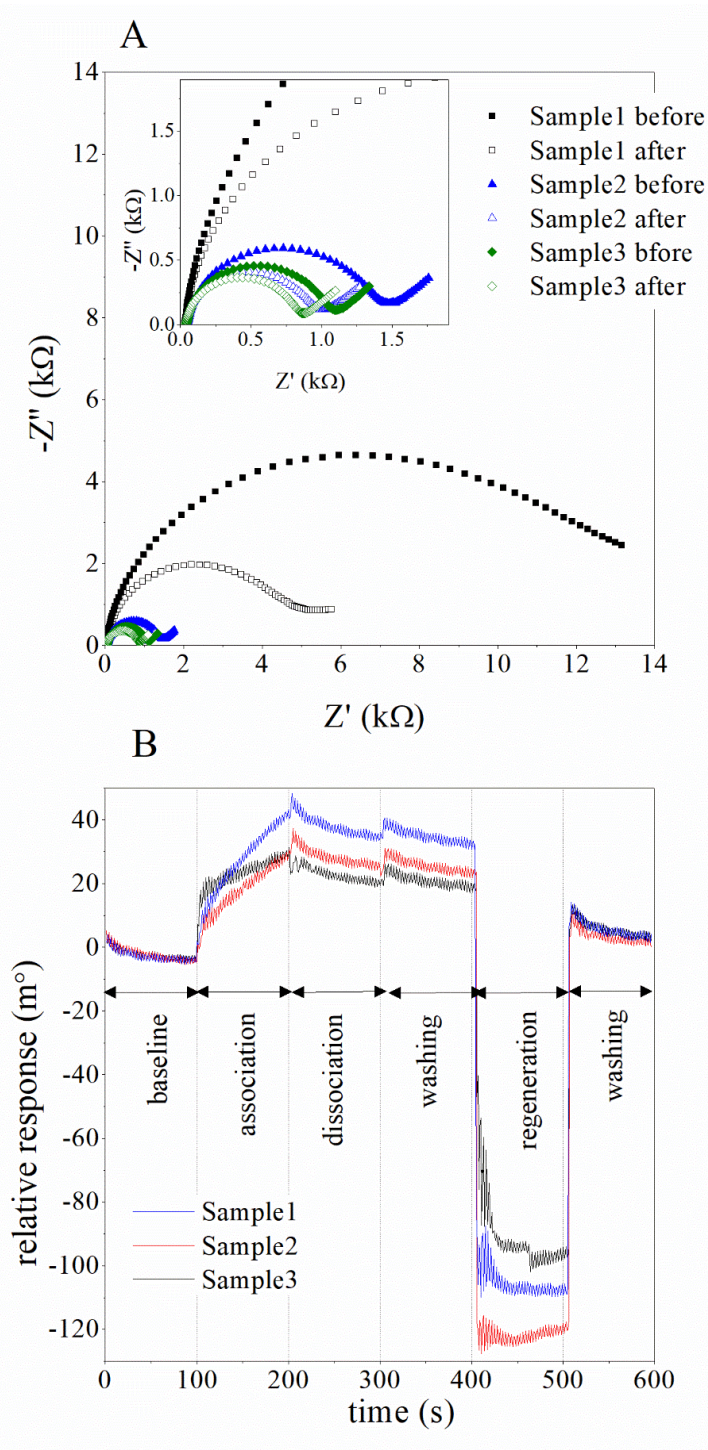
Fig. 33. (A) Nyquist plots for impedimetric measurements of human saliva samples, and (B) exemplary SPR sensorgrams obtained for human saliva samples. Impedimetric measurements were performed for the faradaic process. SPR measurements were carried out using HBS-PE pH 7.4 as a running/washing buffer and 10 mM HCl as a regeneration medium. Results of own research [257].

In the previous section, the calibration curves for both impedimetric and SPR biosensors were presented. These curves were then used for processing the results obtained from real sample measurements. The calibration curve for the ELISA method can be found in Fig. 34.
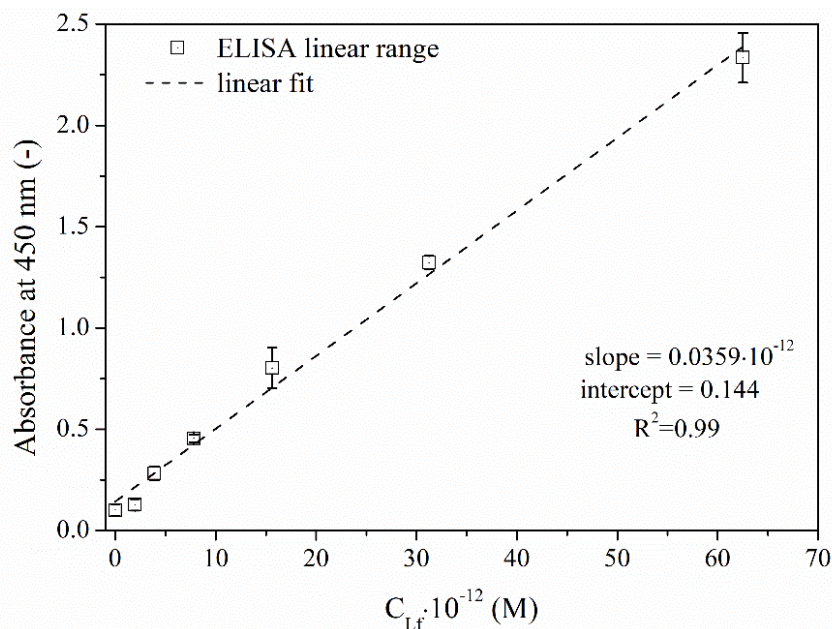
Fig. 34. Calibration curve obtained for ELISA kit, measurements performed according to the supplier's protocol, endpoint 450 nm, n = 3.

The sensitivity of this method was at the picomolar level, however, with a narrow linear concentration range from 1.95 to 62.5 pM of Lf. Compared to impedimetric DNA-based biosensor and SPR reference measurements with DNA-type specific receptor, LOD obtained for ELISA was 10.4 pM, which is two orders of magnitude lower, although other biosensors provided a significantly wider concentration range of lactoferrin. Table 13 summarizes the results of Lf determination in saliva samples, along with the relative errors for each sample. The relative error values were expressed as a percentage and calculated by finding the difference in mean Lf concentrations determined by the reference measurements (spectrophotometric ELISA tests and SPR) and by the impedimetric biosensors (EIS), divided by the mean value of the concentration determined by the reference measurements. The final results accounted for the declared dilutions of saliva samples. The ELISA tests had the lowest SD values, however, the impedimetric DNA-based biosensors achieved satisfactory repeatability, comparable to the one provided by ELISA. On the other hand, the SPR measurements had significantly poorer repeatability, plausibly due to the saliva sample

properties such as increased viscosity and density, which can significantly affect the analytical performance of the SPR method.

Table 13. Results of Lf determination in human saliva samples obtained with the use of developed impedimetric DNA-based biosensors, SPR readout, and ELISA kit. Each sample was aliquoted, and the mean and SD values were calculated for experimental data of at least 3 repetitions. The provided C_{Lf} values were calculated taking into account the dilutions used.

Saliva samples	EIS*		ELISA**		SPR***		Relative error (ELISA-EIS)/ ELISA	Relative error (SPR-EIS)/ SPR
	mean	SD	mean	SD	mean	SD	(%)	
			$C_{Lf} \cdot 10^{-9}$ (M)					
Sample 1	605.96	16.32	565.52	5.34	649.47	248.92	-7.2	6.7
Sample 2	326.44	123.48	291.88	12.31	268.55	47.78	-11.8	-21.6
Sample 3	236.05	22.81	192.33	3.90	236.80	54.69	-22.7	-0.3

* not diluted, ** diluted 25k times, *** diluted 10 times

The results presented in Table 13 reveal a significant, almost a 2-fold difference between Sample 1 and others. As shown before, the elevated levels of Lf can be associated with an existing inflammatory state within the organism. Sample 1 was donated by a volunteer who suffers from Leśniowski-Crohn disease, which might be related to the higher salivary Lf concentration. However, it is still at the physiological submicromolar level. In terms of comparing the concentration of Lf in the test samples using different methods, it is important to note that there may be slight variations in the values obtained for specific samples. However, overall results remain consistent, which is indicated by the relative errors. Based on this information, it can be concluded that the measurements obtained using the impedimetric biosensors tend to overestimate the concentration of Lf when compared to both reference measurements (ELISA and SPR). Although the salivary lactoferrin concentration can vary on a daily basis depending on factors such as age, physical activity, and medication intake, the developed biosensors are highly accurate and provide a wide range of analysis that covers the physiological micromolar level of lactoferrin found in healthy human saliva [14,237], which is a significant advantage in terms of its potential use for further clinical or research purposes.

10. Other investigated lactoferrin receptors

10.1.   Antibodies

Linear immobilization of antibodies

Polyclonal antibodies specific to human lactoferrin were immobilized on the surface of a gold sensor using a carboxylamine coupling method. This resulted in the formation of a biorecognition self-assembled monolayer. To prevent any unconjugated surface groups from interfering, they were blocked using a 1 M ethanolamine-HCl solution at pH 8.5. The loading density was determined to be 2.12 ng·mm^{-2}, using the conversion factor of 122 m°·mm^{2}·ng^{-1}. The protein was dissolved in 10 mM acetate buffer of pH 4.5, and the stock of pAb was diluted 100 times. The immobilization process involved the use of a linear linker, as illustrated in Fig. 35.
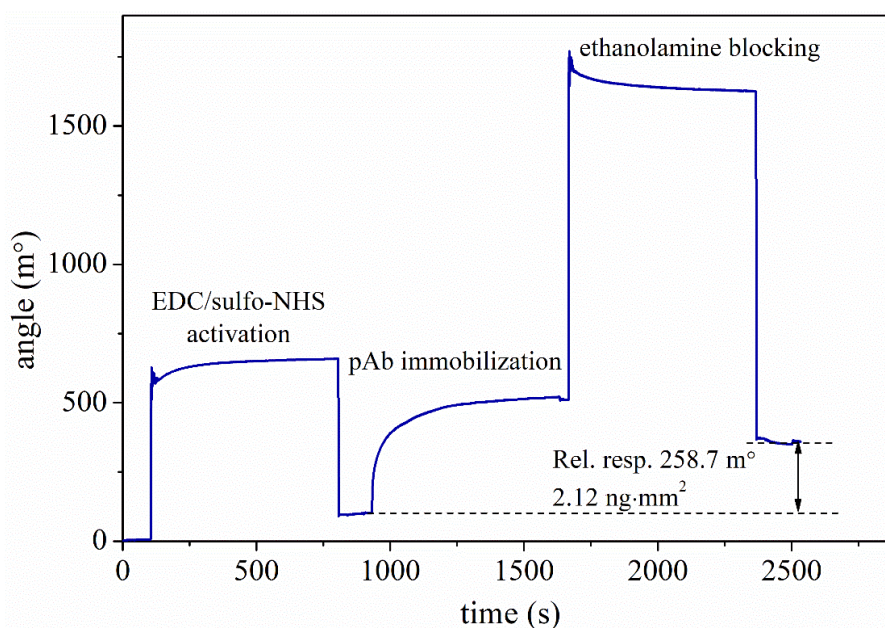
Fig. 35. Immobilization of 1:100 pAb in 10 mM acetic buffer at pH 4.5. The relative response was interpreted as a difference between the signal before pAb injection and after surface blocking with 1 M ethanolamine-HCl pH 8.5.

An immunosensor was utilized to determine the concentration of lactoferrin in the range of 0.0125 to 2.5 µM. Lactoferrin is a protein that carries a positive charge and undergoes structural changes in acidic environments, leading to a reduced ability to interact with antibodies. To avoid the negative effects of protein conformation on lactoferrin-antibody

interaction a near-physiological pH buffer was chosen for accurate quantitative measurements.
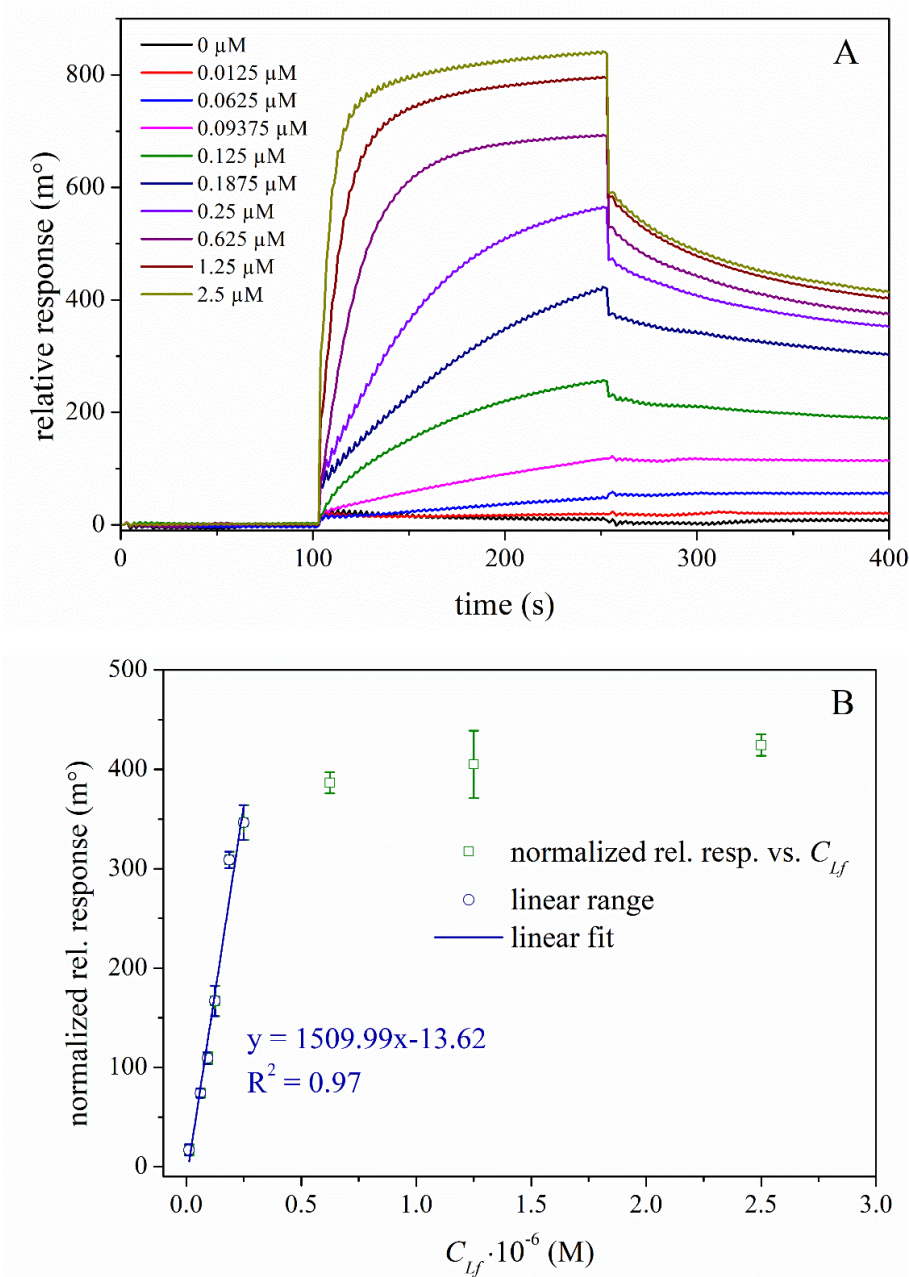
Fig. 36. (A) following sensorgrams with corrected baseline obtained for lactoferrin concentration in the range from 0.0125 to 2.5 µM in HBS-EP buffer at pH 7.4, (B) calibration curve for lactoferrin obtained using immunosensing layer with loading density of 2.12 ng·mm^{-2} pAb. Measurements (n = 3) were performed in HBS-EP buffer at pH 7.4.

Prior to use, the immunosensor was stabilized for an hour in 10 mM HBS-EP buffer at pH 7.4 to reduce the matrix effect that can negatively affect reproducibility and sensitivity. During SPR quantitative measurements, the association/dissociation phase was fixed for 2.5

minutes each. Following each lactoferrin injection, the immunosensor was regenerated with 5% (v/v) acetic acid solution, 10 mM HCl, 0.05% SDS, and 10 mM HCl to ensure proper analyte removal without losing ligand (antibodies) activity. The linear range for lactoferrin calibration was 12.5 to 250 nM, and the linear correlation coefficient R^2 was 0.97 (Fig. 36A-B). The response obtained was characterized by relatively good repeatability, as evident in standard deviation bars. The sensitivity of the immunosensor was calculated as a slope of the calibration curve and was determined to be 1.51 m°·nM^{-1}.

Immobilization of antibodies with the use of hyperbranched linkers

PAMAM dendrimers of two different generations, 2G and 4G, were used to modify MUA-functionalized gold SPR chips with the help of EDC/NHS cross-linkers. The dendrimers were used separately as a 1% (v/v) solution in supporting buffer or in a 1-2% (v/v) mixture.
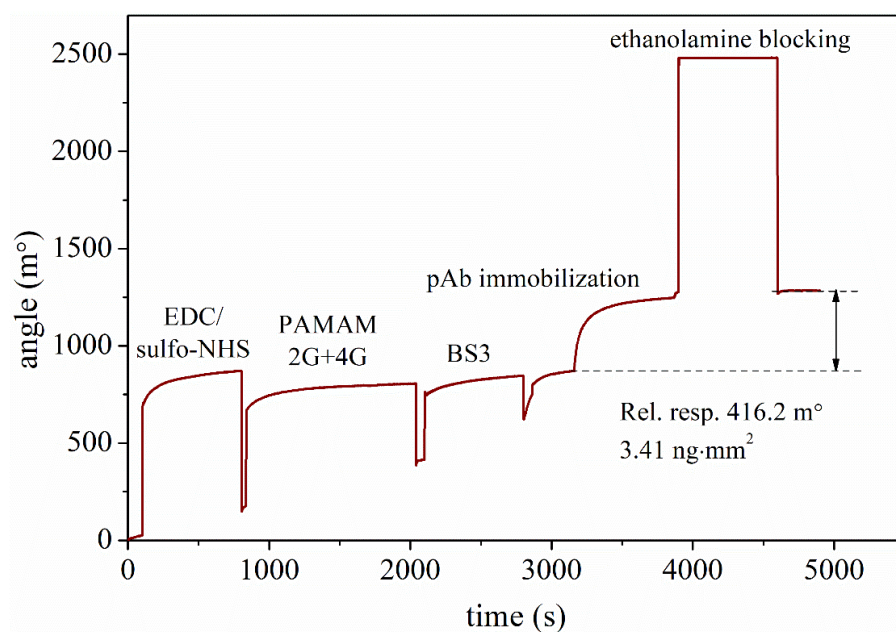
Fig. 37. Immobilization of 1:100 pAb in 10 mM HBS-EP buffer at pH 7.4. Relative response interpreted similarly as described previously.

It is important to note that each type of dendrimer was characterized by a specific number of peripheral functional groups (-NH$_2$), where 4G has double the number of functionalities as compared to 2G. An exemplary pAb immobilization procedure using a PAMAM 2G and 4G mixture is presented in Fig. 37. Due to the hyperbranched linker providing a multitude of functional groups, the ligand loading density obtained using both generations of PAMAM was higher than in the case of the linear linker. The relative response obtained in the

presented case, using a 1% mixture of PAMAM 4G and 2G, increased by more than 1.5 times. The dendrimer was attached to pAb using various types of linkers with different lengths. The linkers included amine groups (BS3, BS(PEG)9, GA) and carboxyl groups of antibodies via EDC/NHS activation. For amine-to-amine coupling, a 2.5 mM solution of the linker was used. The immobilization was done for different pAb dilution ratios (1:50, 1:100, 1:200, and 1:5000) to evaluate the loading density of the biosensor (Fig. 38B). Each variant of the biosensing layer was tested with 0.125 µM of lactoferrin solution in the supporting buffer. It is important to note that the dendrimer structure is sensitive to changes in pH. To investigate the effect of dendrimer structure state on further saturation with pAb, different supporting buffers with pH 4.5 and 7.4 were used. These buffers include 10 mM acetic buffer pH 4.5, 10 mM HBS-EP pH 7.4, and 10 mM PBS pH 7.4. These details are shown in Fig. 38D. To reduce the matrix effect, sensors were stabilized using a supporting buffer for an hour before immobilization. The impact of modification variables on ligand loading density was studied in relation to PAMAM generation and the ratio. It was found that the type of cross-linking chemistry between antibodies and the hyperbranched layer was preferential to amine groups from antibodies over carboxylic groups. This was evident in the significantly higher relative responses obtained for 1% GA, 2.5 mM BS3, and 2.5 mM BS(PEG)9 compared to the results obtained using EDC/NHS. The lower saturation for carboxyl-amine coupling could be attributed to cross-reaction between protein molecules, as the activation of -COOH groups was conducted in the lactoferrin solution, resulting in the blocking of protein binding sites. The study also investigated the effect of ligand (pAb) dilution and found that small differences occurred in the case of 1:100 and 1:200 ratios of dilution, while 1:5000 resulted in the lowest density of ligand at the sensors' surface. The 1:50 dilution ratio resulted in a slight increase in the response, suggesting that there is a threshold amount of ligand required for obtaining the necessary surface saturation. However, the amount and distribution of functional groups also play a significant role in the immobilization efficiency (Fig. 38A), as it determines the theoretical number of molecules that can be bound. This value depends on the size of the ligand, as using highly excessive ligand concentration can lead to steric hindrance, which can result in a loss of sensitivity. Additionally, too dense packing of the sensor's surface can decrease the bioreceptor activity, as the binding sites might be blocked. Therefore, the density of functional groups generated by the dendrimer is crucial for obtaining the appropriate ligand loading density for further measurements, which should be adjusted based on the size and molecular weight of the ligand and analyte.
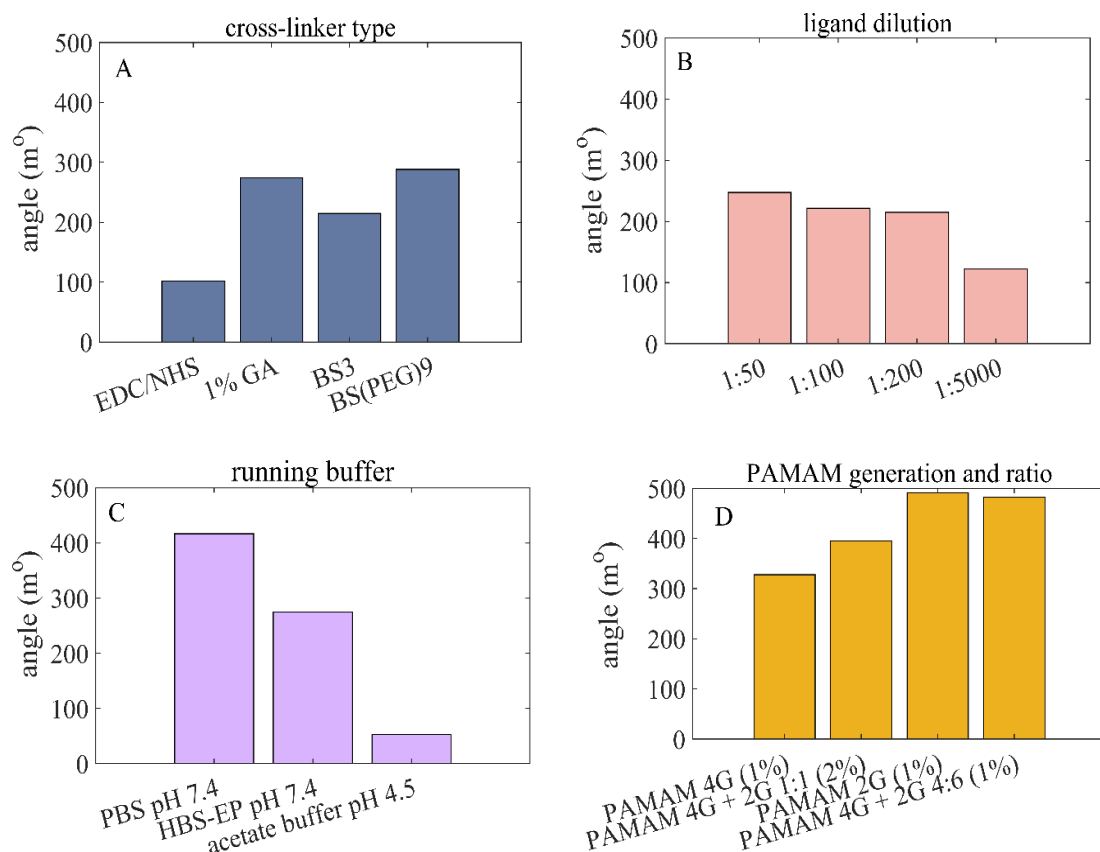
Fig. 38. Relative response vs. (A) type of cross-linker between dendrimer and pAb, ((B) ligand dilution, (C) type of supporting buffer, and (D) type of hyperbranched linkers used.

Dendrimers exhibit structural flexibility depending on the pH, which can affect the subsequent immobilization. The buffer solution composition and pH also impact the immobilization efficiency, with PBS buffer at pH 7.4 being the most preferable (Fig. 38C). Firstly, the performance of immunosensors was tested for a fixed value of lactoferrin – 0.125 µM, and the regeneration procedure was performed as previously described. Fig. 39A-B shows the exemplary results of the SPR measurements. Despite high ligand loading density on the PAMAM-modified immunosensor's surface, the response obtained for lactoferrin was lower than the results obtained for the same concentration using the MUA-modified biosensor. The measurements' repeatability varied depending on the dendrimer-antibody cross-linking chemistry and buffer used. Several conclusions can be identified from the results of lactoferrin-antibody interaction and obtained loading density using the MUA/PAMAM/pAb modified immunosensor.
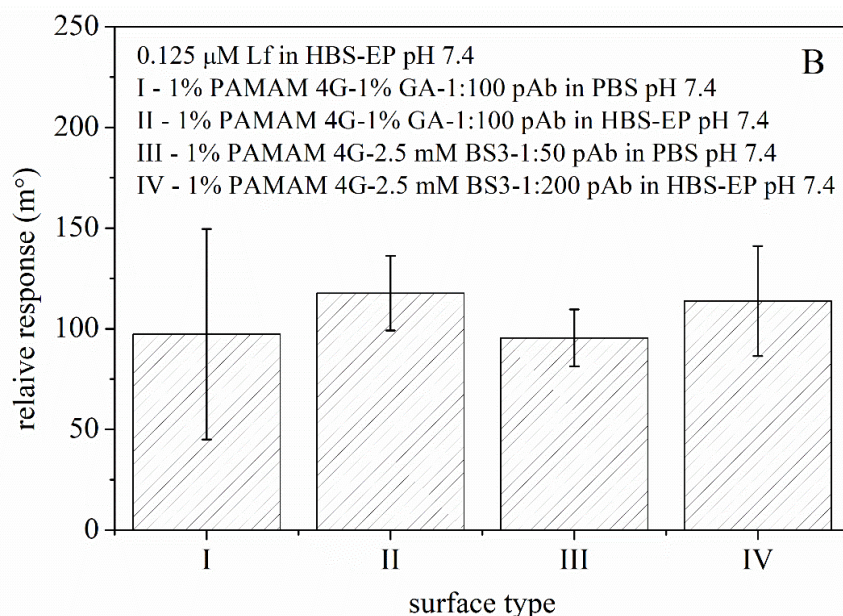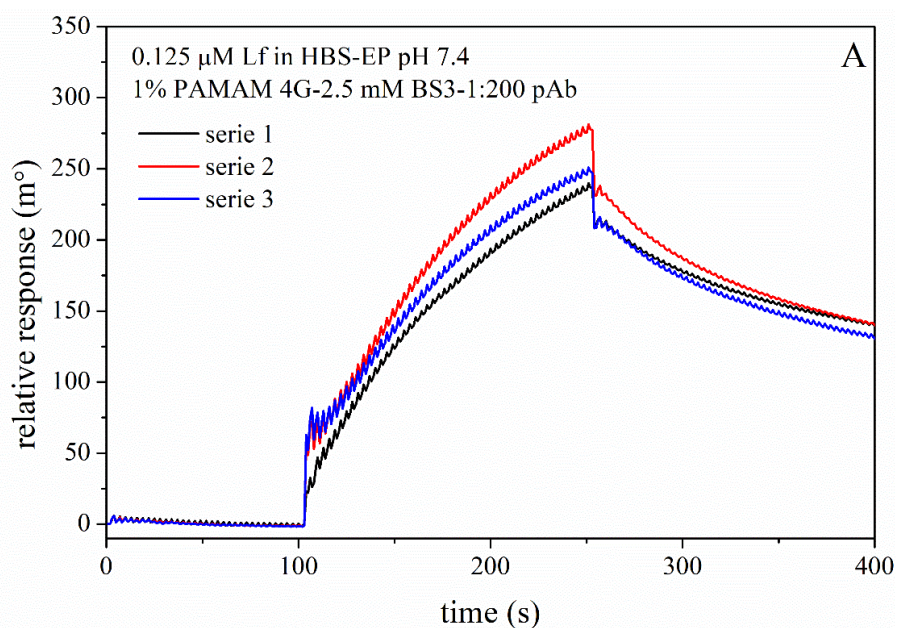
Fig. 39. (A) Sensorgrams obtained for 0.125 μM lactoferrin with the use of MUA/PAMAM/BS3/1:200 pAb-modified biosensor in HBS-EP buffer of pH 7.4, (B) comparison of signals obtained in HBS-EP pH 7.4 with the use of PAMAM-modified immunosensors prepared at different conditions.

Firstly, the size of the analyte plays a significant role in the efficiency of ligand-analyte binding, apart from the ligand loading density affected by its size and distribution of sensor surface functionalities. The distribution and spatial orientation of ligand molecules need to be tailored toward the parameters of the analyte, including its size, spatial structure, and location of binding sites. In the case of lactoferrin, which is a bulky asymmetric protein of high MW, the reason for the poor SPR response is most likely steric hindrance caused by

either too dense pAb packing on the surface or unfavorable spatial orientation of the ligand. As we already know from other experiments, the usage of a hyperbranched linker can be advisable for analytes of relatively low molecular weight [259]. Additionally, the aspects of immunosensor regeneration need to be considered. For the regeneration of the ligand layer, acidic solutions and anionic surfactant were used, which was a suitable procedure in the case of biosensors with the linear linker. However, in the context of PAMAM sensitivity to pH changes, such regeneration reagents could cause unfavorable changes in the spatial orientation of ligands due to dendrimer shrinking, in which distances between individual branches decrease.

10.2.   Molecularly imprinted polymers

Biomimetic layers – bulk imprinting approach

An initial attempt was made to develop a biomimetic sensing layer for the detection of lactoferrin. The molecular imprinting technique was used to create artificial cavities in polydopamine that were selective for lactoferrin. Polydopamine was chosen due to its biocompatibility (dopamine naturally occurs in the human body) and the ease of its preparation. A mixture of functional monomer and template (analyte) undergoes auto-polymerization in specific conditions, and the thickness of the layer can be controlled by adjusting the polymerization time. However, the results showed that there was non-specific binding of 1.5 µM lactoferrin to PDA, which led to relatively strong interactions (Fig. 40A-B). The response obtained for lactoferrin injected on the PDA layer was around 210 m°. Therefore, to decrease non-specific adsorption and provide selectivity, molecular imprints (MIs) need to be fabricated. As mentioned before, the analyte is characterised by a relatively big size, which makes the process of MI design more challenging.
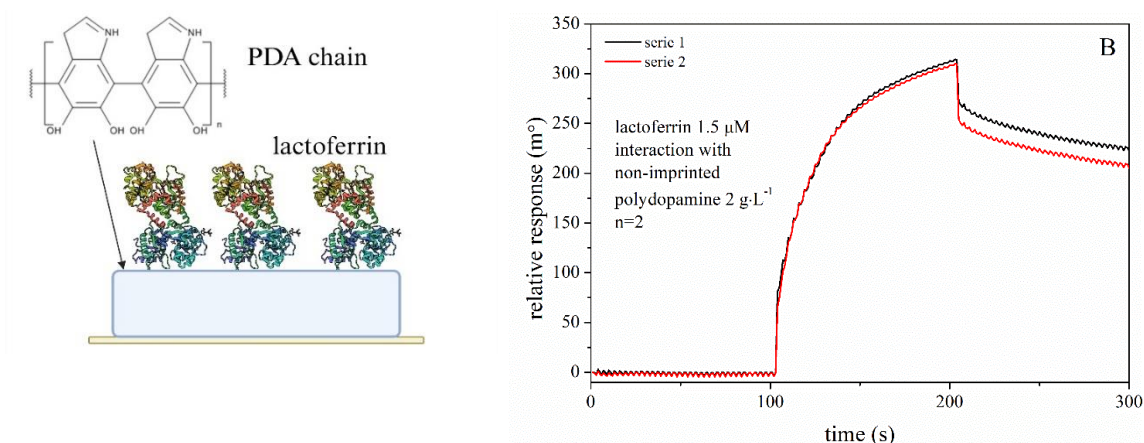
Fig. 40. (A) scheme of Lf non-specific adsorption on the polydopamine (PDA), (B) relative response obtained for lactoferrin injection onto PDA in HBS-EP buffer at pH 7.4.

Preliminary results have been received regarding the bulk imprinting strategy, which allowed the identification of major issues related to the preparation of molecularly imprinted materials. Additional research was conducted on removing lactoferrin molecules from the polymeric matrix using a UV-Vis spectrophotometer. The experiment is depicted in Fig. 41.
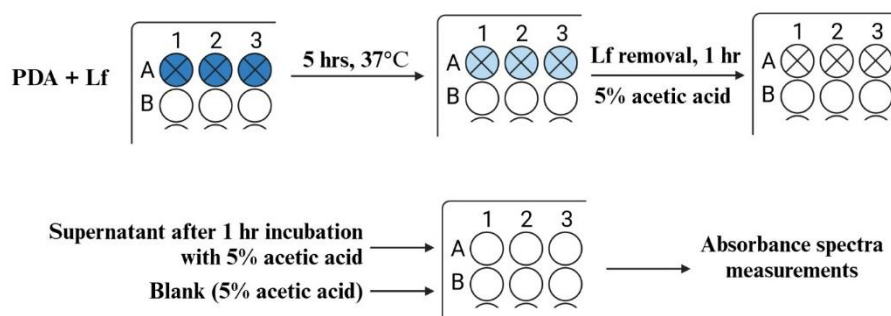
Fig. 41. Schematic representation of template removal experiments.

In brief, the polymerized layer was treated three times with a 5% acetic acid solution for an hour each time. The supernatant was then collected, and absorbance spectra were obtained to check for the presence of protein characteristic peaks. The exemplary absorbance spectra of the supernatant and blank (5% v/v acetic acid solution) are shown in Fig. 42. As can be seen, the height of the peak at 270 nm corresponding to the protein content is relatively small, indicating poor efficiency in removing the template (protein) from the PDA layer.

126
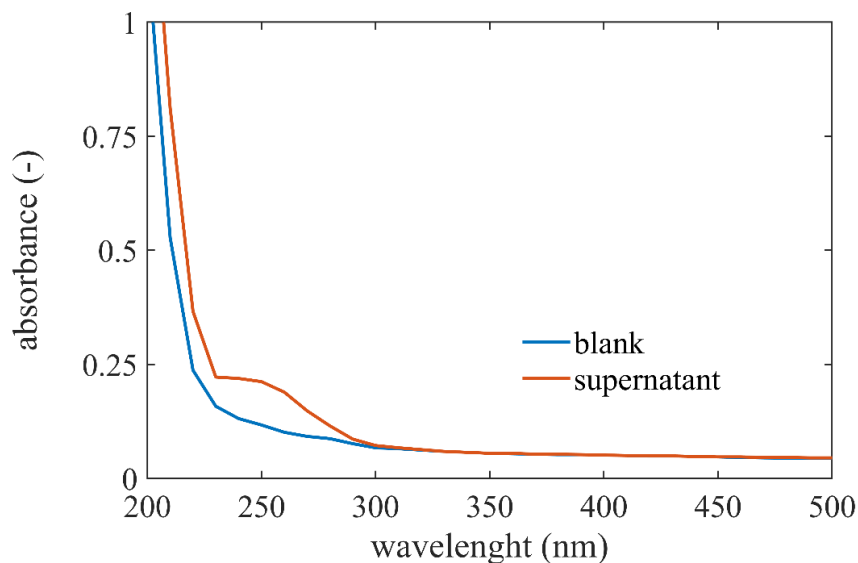
Fig. 42. Absorbance spectra of supernatant collected from template removal from PDA matrix after incubation with 5% acetic acid for 1 hr.

Different solutions for removing templates from molecularly imprinted polymers (MIPs) can be considered, such as using proteolytic enzymes. Additionally, efficient cavity formation requires the implementation of different procedures, such as epitope imprinting strategies. In this approach, a specific region of the molecule is selected to create selective molecular imprints and minimize the risk of clogging. It is important to note that difficulties in template removal may be caused by the thickness of the MIP layer, so further experiments are required to fine-tune the thickness for accurate template removal and selectivity. Another approach that could be used is the stamp-mold method, which involves using different functional monomers, such as norepinephrine or methacrylate.

11. Discussion

Lactoferrin is a versatile protein that has both direct and indirect effects on the immune system of mammals, including humans. Researchers believe this protein holds potential for many biotechnological and biomedical applications. It is considered as a factor that reduces the risk of infections in prosthetics and implantology. Additionally, it is hoped that the protein could be a component in developing new and more effective drug therapies. Lactoferrin is also thought to be a key ingredient in dietary supplements that can impact immunity, digestive systems, and human bacterial flora. Despite various studies that describe the effects of Lf on immune functions and inflammation regulation, there are still some

127

inconsistent results that require further investigation and deeper understanding. Many studies have suggested that lactoferrin could be a new biomarker for neurodegenerative diseases [5,6] and inflammatory autoimmune diseases [12,13]. However, diagnosing these diseases is challenging due to limited knowledge on their aetiology and the mechanisms of their development for individual patient's. Lactoferrin in saliva primarily exhibits antimicrobial function, however, intense studies are devoted to salivary lactoferrin in the diagnosis of Alzheimer's disease [5,260]. The dementia associated with this disease is placed by WHO reports in the top 10 causes of death among people over 65 years of age. Therefore, new methods for lactoferrin determination in real samples are highly necessary and ought to be included in routine tests to support the process of diagnosing the disease at an early stage of its occurrence, which will significantly contribute to speeding up the treatment process. By developing a new selective and stable bioreceptor for Lf, the gap in existing detection methods can be filled in by the application of such a bioreceptor to biosensing tools. The research presented in this dissertation attempts to address the need for a simple, cheap, and selective method for quantifying lactoferrin in human saliva. Our goal was achieved in two major steps: first, developing a new biorecognition element, and second – utilizing this element in biosensing by integrating a designed bioreceptor with a label-free electrochemical technique, thus confirming the validity of both theses T1 and T2 of the dissertation. The study related to bioreceptor development provided the adjusted conditions for the immobilization of DNA oligonucleotides using a capture molecule (streptavidin-biotin) strategy. The optimization of conditions addressing direct SPR measurements was established, which is not very typical for the molecular interaction-oriented studies presented in the literature. These activities resulted in the selection of a set of parameters that are very close to optimal for further analyses, such as kinetic, in which a variety of unwelcomed effects can emerge, e.g., mass transport limitations or strong impact of the bulk effect. Additionally, the possibility of using the same buffer solution for both immobilization and interaction allows to shorten the overall analysis time, because it eliminates the necessity of long stabilization prior to use. Although a lot of interaction studies, in general, are performed in a manner where both reactants are in a free state, e.g., using NMR as a readout method, to the best knowledge, this is the first time where particularly DNA is considered a biorecognition element for Lf and not reversed. The advantage of such an approach, firstly, is the fact that it enables the control of the surface orientation of ligand DNA molecules since their structure is linear, giving vast possibilities for terminal modification and

128

immobilization protocol choice. Secondly, the usage of flexible support such as 3D hydrogel for the systematic studies allows to initially estimate the conditions of analysis – obtaining desired ligand density is relatively easy due to real-time manner of SPR method. In the case of lactoferrin immobilization, as it was presented in other studies [134,204], simple amine coupling might result in a significant loss of activity of the biorecognition layer since the majority of proteins are unsymmetrical so that the binding sites can be insufficiently exposed for the analyte molecules. Moreover, for the non-spherical structures with high potency to aggregate, such as Lf, the issue of steric hindrance arises, often challenging the whole idea of investigation. Based on our experience, it can be expected that the usage of hyperbranched linkers for surface modification serving as an intermediate layer for the immobilization of bioreceptors can be beneficial for small molecular size analytes. The DNA oligonucleotide sequences that were proposed and scrutinized within this study were characterized with unique features in terms of, e.g., length and combination of nucleobases, specifically identified toward Lf. The screening analysis emerged the DNA oligonucleotide with the highest affinity for Lf out of the literature recognized sequences. The stronger affinity of Lf to double-stranded oligonucleotides over single-stranded ones was confirmed at the affinity screening step. The results also indicate the advantage of longer multiplied stands over short sequences that were used as building blocks for oligonucleotides > 50 base pairs, which results from the higher flexibility and potentially provides more than one binding cavity for lactoferrin. Nevertheless, the kinetic study resulted in the most simple one-to-one interaction between Lf and selected DNA, derived from the significant size difference and the fact that the smaller DNA ligand was immobilized, forming a relatively rigid and uniform layer. In our study, the kinetic parameters calculated form model based on SPR data were as follows: association rate constant $k_a = (2.49 \pm 0.03) \cdot 10^4$ M^{-1}·s^{-1}, dissociation rate constant $k_d = (1.89 \pm 0.02) \cdot 10^{-3}$ s^{-1}, and equilibrium constant $K_D = (7.61 \pm 0.18) \cdot 10^{-8}$ M, confirming strength and affinity of Lf intermolecular binding with proposed oligonucleotide sequence. On the other hand, the SPR-based kinetic parameters of human Lf interaction with nucleolin, which is a nuclear protein also acting as a cell surface receptor, were: $k_a = 6.89 \pm 0.46 \cdot 10^5$ M^{-1}·s^{-1}, $k_d = 0.164 \pm 0.001$ s^{-1}, and $K_D = (238 \pm 15) \cdot 10^{-9}$ M [207]. The study was dedicated to investigating lactoferrin interaction with cell surface proteins in order to get deeper insight into the biological function of such complexes and the overall Lf mechanism of action [207]. Although the equilibrium constant was at the nanomolar level, the interaction did not appear specific. Another study provided kinetic data on Lf binding with naringin, which is a

flavonoid found in citrus fruit, directed to explore Lf as a vehicle for bioactive molecules. The K_b was equal to $1.39 \cdot 10^5$ M^{-1}, which is not relevant for biosensing purposes [208]. Concerning the thermodynamic parameters of the proposed setup, analysis results presented here are in good agreement with the literature data [62,221], that obtained $\Delta G^o \sim$ -11.1 kcal·mol^{-1} (here $\sim$ -7.35 ÷ -9.16 kcal·mol^{-1}), confirming the high participation of electrostatic forces and hydrophobic binding in the complex formation process. The DNA-Lf binding appeared to be entropically driven and the binding constant K_b increases with temperature increment in the studied temperature range, reaching the thermodynamic equilibrium. It is worth noticing, that our study is one of the few results relating to kinetic and thermodynamic parameters for Lf interaction with DNA. The next crucial analysis was the selectivity evaluation using various interfering substances that might appear in the real samples, such as milk, urine, or saliva. The approach presented in this work differs from the typical one for investigation of the selectivity of protein binding site since the one immobilized is DNA, which limits the degree of freedom for the DNA but not for the Lf. Therefore, in practice, this study does not check the possible inhibition of the lactoferrin DNA-binding site but the interference of the DNA with another protein of distinct features present in various biological samples. The effects of the selectivity analysis showed that none of the utilized interferent BSA, GlutOx, GOx, urease, HRP, or LA interacted with the chosen DNA sequence with an efficiency > 3%, including low and high levels of injected samples. Notably, a lot of reports on lactoferrin detection do not provide a selectivity investigation (see Table 1) at all, while some aptamer-based methods did not neccesarily provide better selectivity [154,157].

The second track of the dissertation was solely based on the findings of lactoferrin interaction with selected DNA oligonucleotide that was identified as having the highest affinity among others during SPR studies. The methodology of surface modification with DNA was adapted to fabricate planar biosensing layers for impedimetric lactoferrin detection. The introduction of a linear linker and blocker mixture at the initial stage of modification allowed for control of the bioreceptor immobilization level toward forming a well-structured biosensing layer and obtaining the highest interaction response. The biosensors were examined under adjusted conditions using the EIS method coupled with a faradaic system, in which the electron transfer was supported by electroactive redox species and described by a Randles-based model. The ratio of resistance R_{3f} before and after the interaction was utilized as a lactoferrin concentration-dependent parameter. Metrological parameters of impedimetric 72 bp DNA-based biosensor were satisfactory, including high

sensitivity $1.3 \cdot 10^{-6}$ M^{-1} and low LOD of 1.25 nM concerning other data reported in the literature. Only a few reports on lactoferrin quantification presented similar or slightly better LOD (Table 2, [143,144,154,166,174,178,179,186]); however, some of them employed instrumental analysis [143,144] and other required utilization of labels involving immunotests and immunosensors [154,166,178,186]. Moreover, the majority of analytical methods for Lf detection are focused on bovine lactoferrin, which shares around 69% of amino acid sequence homology with the human form of this protein, thus differing in structure, stability, and biological functions [261]. The impedimetric biosensor with 72 bp DNA had a linear response range similar to the SPR biosensor with the same bioreceptor, ranging from the LOQ value of 2.5 nM to 625 nM. However, due to the logarithmic scale of Lf concentration for the SPR method, the resolution for concentration readot id lower, its accuracy of measurements was lower than that of the impedimetric biosensor (Fig. 31C). It was also showed that immobilized DNA bioreceptor can be easily regenerated in the SPR experiments using mild conditions. On the other hand, the impedimetric analyses require the biosensors to be used in a disposable mode.

For the first time, a non-aptamer biosensor based on DNA oligonucleotide was successfully applied for Lf detection in saliva samples. The results of quantitative measurements showed a significant difference in Lf level for one of the three tested samples. Interestingly, it could be associated with the fact that this particular sample was collected from a person suffering from autoimmune inflammatory disease. The impedimetric biosensor results were compared with two optical methods – SPR direct detection and spectrophotometric ELISA tests – indirect detection and were consistent with both but slightly overestimated. It is worth highlighting the operation simplicity of the impedimetric biosensor, minimalization of sample preparation steps, and label-free analysis of the proposed setup in comparison with ELISA. Furthermore, compared to SPR, the proposed biosensor has a potential for miniaturization, while there is still room for improvement, e.g., by introducing nanostructures as interlayers that enhance the electron transfer and, in consequence, sensitivity. Stability is another crucial feature of biosensing tools. In general, it results from several factors, primarily biosensor material and the biosensing layer, and often depends on their compatibility. The stability of the biosensor with the dedicated 72 bp DNA biorecognition element was justified by the standard deviations of the measurement points. On the other hand, the shelf stability of the biosensing layer was relatively poor, which might suggest the change of electrode material could be beneficial for the shelf-life improvement

of the developed biosensor. In terms of sensitivity, the experiments that were focused on using antibodies as biorecognition elements, with additional hyperbranched interlayer enhancing the loading density of the ligand, did not facilitate improved antibody-antigen interaction results compared to planarly immobilized antibody layers performed with EDC/NHS cross-linking chemistry. The higher ligand density did not provide higher sensitivity due to the steric hindrance phenomenon that occurred for the oversaturated surface subjected to the bulky character of both antibody and lactoferrin. Operational parameters such as buffer content and pH, cross-linking chemistry, generation of dendrimer, and ligand stock dilution were tested, indicating their significant effect on the antibody immobilization efficiency and further detection success. The immunosensor, fabricated using linear linker MUA and examined with the SPR method, resulted in a narrower linear concentration range (12.5-250 nM) characterized by a slightly lower correlation coefficient ($R^2 = 0.97$) compared to impedimetric DNA-based biosensor (2.5-625 nM and $R^2 = 0.99$). The SPR calibration obtained using a dedicated 72 bp DNA sequence was also characterized by a wider Lf concentration range from 12.5 to 625 nM. Eventually, the preliminary experiments on the development of a biomimetic sensing layer for Lf detection were conducted utilizing dopamine (DA) as a functional monomer along with a bulk imprinting strategy. It turned out that lactoferrin exhibited strong non-specific binding to PDA and limited ability to be washed off from the polymer matrix, which eliminated such an approach from potential application in biosensing. Therefore, more complex methods of imprint fabrication, such as epitope imprinting in which the specific region of the protein has to be selected for the templating, could be the direction of further studies on biomimetic Lf sensing. The poor selectivity that is a typical issue of biomimetic layers could also be addressed by changing the functional monomer and decreasing non-specific binding. This work proposes a global approach that takes into account the challenges of existing methods of lactoferrin detection, providing a feasible, cheap, and selective biosensing layer made of novel, specifically designed 72 bp *ds*DNA. The developed bioreceptor is characterized by high selectivity towards lactoferrin in relation to interferents, whereas applied to the label-free impedimetric method, it exhibits high operational stability, sensitivity, and repeatability, and the bioreceptor activity is not affected by the readout technique. As proven by the application to quantification of salivary lactoferrin, the established biosensor could serve as a proof of concept for pre-clinical screening in patients with suspected inflammation. Furthermore, the methodology developed for establishing a new Lf-selective DNA-type

bioreceptor can be approximated and adjusted to the studies devoted to other large molecules interacting with DNA, being clinically significant, especially proteins.

Conclusions and prospects

The described research falls under the field of biomedical engineering, showing the simple and efficient approach for the development of a selective DNA-based bioreceptor and its utilization in biosensing applications. The first part of the research was dedicated to the development of a DNA-based affinity-type bioreceptor for lactoferrin using optical and electrochemical investigations that included two label-free complementary methods: surface plasmon resonance and electrochemical impedance spectroscopy. For the designing and fabrication of biosensing layers, native DNA oligonucleotides were scrutinized and the best one was used in kinetic and thermodynamic analyses to get a better understanding of interaction mechanisms at the supramolecular level. Since advantageous parameters of the developed DNA-type bioreceptor 5'[TAGAGGATCAAAAAA]$_4$TAGAGGATCAAA3'] and its usefulness in label-free biosensors, both SPR and impedimetric, have been demonstrated, then thesis 1 regarding "DNA molecule of defined sequence exhibits high affinity towards endogenous immunomodulator lactoferrin and can serve as a selective bioreceptor for label-free biosensors" was proofed. Furthermore, the affinity screening of the designed DNA type bioreceptors performed using surface plasmon resonance enabled the identification of the designed DNA oligonucleotide selectively interacting with the target protein, confirming thesis 2. The oligonucleotide of choice, designed as the variation of literature-acknowledged oligonucleotide sequence interacting with Lf, exhibited satisfying selectivity toward target protein over interfering proteins, confirming the premise of DNA being a suitable biorecognition element for lactoferrin since the signal values obtained for interferents stayed below 3% of reference Lf signal. On the other hand, some aptamer-based methods presented less satisfying selectivity [154,157]. The prepared hydrogel-based DNA-modified SPR sensors were verified using FTIR analysis, confirming the steps of modification and subsequent interaction with the analyte. Kinetic and thermodynamic data suggest high strength of Lf-DNA binding based on electrostatic and hydrophobic forces between the N-terminal region of the protein and specific DNA oligonucleotide sequence.

The development of a specific DNA-based biorecognition element for lactoferrin was naturally followed by the second track of the research, which focused on the development of a sensitive label-free impedimetric biosensor for lactoferrin determination in human

saliva. The methods of surface modification with Lf-selective DNA sequence were adapted to the electrochemical analysis, and the immobilization was confirmed by FTIR measurements. The faradaic setup with a redox probe was proposed as an effective approach for EIS analysis using biological molecules as biorecognition elements. A correlation between lactoferrin concentration and EIS response was obtained. The established impedimetric DNA-based biosensor was characterized by satisfactory metrological parameters, including broad linear concentration range (2.5-625 nM), low LOD (1.25 nM), and LOQ (2.5 nM), as well as repeatability, that allowed for salivary lactoferrin quantitative measurements. This proves thesis 3 regarding the possible application of the developed DNA-type bioreceptor in impedimetric detection of lactoferrin in biological samples, e.g., saliva samples under physiological pH conditions. The results presented by new impedimetric biosensor were cross-examined with reference methods (ELISA and SPR), showing good agreement. On the other hand, the additional investigation on the immunosensing approach toward Lf sensing revealed the major issue with steric hindrance, especially when hyperbranched linkers aimed to enhance sensitivity were employed.

The biomimetic sensing of Lf was attempted by utilizing dopamine as a functional monomer along with the bulk imprinting method. The fabricated layers were binding Lf non-specifically, while the imprinting process itself was challenging due to difficulties with Lf removal from the polymer matrix. By carrying out a systematic SPR study, the potential bioreceptor emerged, being further used to fabricate a lactoferrin-selective biosensing tool of high potential to be commercialized. So far, DNA has not been considered a putative lactoferrin bioreceptor, as the majority of research on DNA-lactoferrin binding concerns the biological significance of such a complex. This work, by introducing a new approach to searching selective and stable biorecognition element for endogenous immunomodulator, can open possibilities to continue studies on new DNA-type biorecognition layers for other clinically important molecules that are capable of interacting with DNA.

Additionally, the vast perspectives of further improvement remain open, especially toward increased sensitivity, e.g. by introducing nanostructures enhancing electron transfer processes through the impedimetric biosensor interfaces.

List of Figures

List of Tables

References

[1]   A. Bar-Gil Shitrit, B. Koslowsky, D.M. Livovsky, et al., A prospective study of fecal calprotectin and lactoferrin as predictors of small bowel Crohn's disease in patients undergoing capsule endoscopy, Scand. J. Gastroenterol. 52 (2017) 328–333. https://doi.org/10.1080/00365521.2016.1253769.

[2]   Ã.R. Thomas Walker, M.L. Land, ô Alex Kartashov, et al., Fecal Lactoferrin Is a Sensitive and Specific Marker of Disease Activity in Children and Young Adults With Inflammatory Bowel Disease, 2007.

[3] A. Cutone, G. Ianiro, M.S. Lepanto, et al., Lactoferrin in the prevention and treatment of intestinal inflammatory pathologies associated with colorectal cancer development, Cancers (Basel). 12 (2020) 1–32. https://doi.org/10.3390/cancers12123806.

[4] R. Farah, H. Haraty, Z. Salame, et al., Salivary biomarkers for the diagnosis and monitoring of neurological diseases, Biomed. J. 41 (2018). https://doi.org/10.1016/j.bj.2018.03.004.

[5] E. Carro, F. Bartolomé, F. Bermejo-Pareja, et al., Early diagnosis of mild cognitive impairment and Alzheimer's disease based on salivary lactoferrin, Alzheimer's Dement. Diagnosis, Assess. Dis. Monit. 8 (2017) 131–138. https://doi.org/10.1016/j.dadm.2017.04.002.

[6] M. González-Sánchez, F. Bartolome, D. Antequera, et al., Decreased salivary lactoferrin levels are specific to Alzheimer's disease, J. Clean. Prod. (2020). https://doi.org/10.1016/j.ebiom.2020.102834.

[7] E.N. Baker, H.M. Baker, Molecular structure, binding properties and dynamics of lactoferrin, Cell. Mol. Life Sci. 62 (2005) 2531–2539. https://doi.org/10.1007/s00018-005-5368-9.

[8] C. Sill, R. Biehl, B. Hoffmann, et al., Structure and domain dynamics of human lactoferrin in solution and the influence of Fe(III)-ion ligand binding, BMC Biophys. 9 (2016) 1–13. https://doi.org/10.1186/s13628-016-0032-3.

[9] B. Wang, Y.P. Timilsena, E. Blanch, et al., Lactoferrin: Structure, function, denaturation and digestion, Crit. Rev. Food Sci. Nutr. 59 (2019) 580–596. https://doi.org/10.1080/10408398.2017.1381583.

[10] D. Legrand, Overview of Lactoferrin as a Natural Immune Modulator, J. Pediatr. 173 (2016) S10–S15. https://doi.org/10.1016/j.jpeds.2016.02.071.

[11] X. Cao, Y. Ren, Q. Lu, et al., Lactoferrin: A glycoprotein that plays an active role in human health, Front. Nutr. 9 (2023) 1–13. https://doi.org/10.3389/fnut.2022.1018336.

[12] N. Liu, G. Feng, X. Zhang, et al., The Functional Role of Lactoferrin in Intestine Mucosal Immune System and Inflammatory Bowel Disease, Front. Nutr. 8 (2021) 1–13. https://doi.org/10.3389/fnut.2021.759507.

[13] A.S.C. Louis Sam Titus, K. Vanarsa, S. Soomro, et al., Resistin, Elastase, and Lactoferrin as Potential Plasma Biomarkers of Pediatric Inflammatory Bowel Disease Based on Comprehensive Proteomic Screens, Mol. Cell. Proteomics 22 (2023) 100487. https://doi.org/10.1016/j.mcpro.2022.100487.

[14] L. Reseco, M. Atienza, M. Fernandez-Alvarez, et al., Salivary lactoferrin is associated with cortical amyloid-beta load, cortical integrity, and memory in aging, Alzheimer's Res. Ther. 13 (2021) 1–12. https://doi.org/10.1186/s13195-021-00891-8.

[15] C. Municio, E. Carro, Implication of salivary lactoferrin and periodontal-mediated infections in Alzheimer ' s disease, Neural Regen. Res. 18 (2023) 2691–2692.

[16] C. Zürcher, C. Humpel, Saliva: a challenging human fluid to diagnose brain disorders with a focus on Alzheimer's disease, Neural Regen. Res. 18 (2023) 2606–2610. https://doi.org/10.4103/1673-5374.373675.

[17] L. Huo, K. Zhang, J. Ling, et al., Antimicrobial and DNA-binding activities of the peptide fragments of human lactoferrin and histatin 5 against Streptococcus mutans, Arch. Oral Biol. 56 (2011) 869–876. https://doi.org/10.1016/j.archoralbio.2011.02.004.

[18] F. Shafqat, S.U. Rehman, K. Niaz, Lactoferrin Can Attenuate SARS-CoV-2: An Analysis of Evidential Relations, Biomed. Res. Ther. 9 (2022) 4901–4919. https://doi.org/10.15419/bmrat.v9i2.727.

[19] M. Miotto, L. Di Rienzo, L. Bò, et al., Molecular Mechanisms Behind Anti SARS-

CoV-2 Action of Lactoferrin, Front. Mol. Biosci. 8 (2021). https://doi.org/10.3389/fmolb.2021.607443.

[20] I. Bukowska-Ośko, D. Sulejczak, K. Kaczyńska, et al., Lactoferrin as a Human Genome "Guardian"—An Overall Point of View, Int. J. Mol. Sci. 23 (2022) 5248. https://doi.org/10.3390/ijms23095248.

[21] F. Carmona, A. González, M. Sánchez, et al., Varying iron release from transferrin and lactoferrin proteins. A laboratory experiment, Biochem. Mol. Biol. Educ. 45 (2017) 521–527. https://doi.org/10.1002/bmb.21075.

[22] A. Rogowska, O. Pryshchepa, N.N. Som, et al., Study on the zinc ions binding to human lactoferrin, J. Mol. Struct. 1282 (2023). https://doi.org/10.1016/j.molstruc.2023.135149.

[23] A. Albar, H. Almehdar, V. Uversky, et al., Structural Heterogeneity and Multifunctionality of Lactoferrin, Curr. Protein Pept. Sci. 15 (2014) 778–797. https://doi.org/10.2174/1389203715666140919124530.

[24] J.R. Kanwar, K. Roy, Y. Patel, et al., Multifunctional iron bound lactoferrin and nanomedicinal approaches to enhance its bioactive functions, Molecules 20 (2015) 9703–9731. https://doi.org/10.3390/molecules20069703.

[25] M. Sienkiewicz, A. Jaśkiewicz, A. Tarasiuk, et al., Lactoferrin: an overview of its main functions, immunomodulatory and antimicrobial role, and clinical significance, Crit. Rev. Food Sci. Nutr. 62 (2022) 6016–6033. https://doi.org/10.1080/10408398.2021.1895063.

[26] I.A. García-Montoya, T.S. Cendón, S. Arévalo-Gallegos, et al., Lactoferrin a multiple bioactive protein: An overview, Biochim. Biophys. Acta - Gen. Subj. 1820 (2012) 226–236. https://doi.org/10.1016/j.bbagen.2011.06.018.

[27] M.L. Kruzel, M. Zimecki, J.K. Actor, Lactoferrin in a context of inflammation-induced pathology, Front. Immunol. 8 (2017). https://doi.org/10.3389/fimmu.2017.01438.

[28] A. Jańczuk, A. Brodziak, T. Czernecki, et al., Lactoferrin—The Health-Promoting Properties and Contemporary Application with Genetic Aspects, Foods 12 (2023). https://doi.org/10.3390/foods12010070.

[29] K. Kaczyńska, M. Jampolska, P. Wojciechowski, et al., Potential of Lactoferrin in the Treatment of Lung Diseases, Pharmaceuticals 16 (2023). https://doi.org/10.3390/ph16020192.

[30] D.B. Kell, E.L. Heyden, E. Pretorius, The Biology of Lactoferrin, an Iron-Binding Protein That Can Help Defend Against Viruses and Bacteria, Front. Immunol. 11 (2020). https://doi.org/10.3389/fimmu.2020.01221.

[31] B. Li, B. Zhang, X. Liu, et al., The effect of lactoferrin in aging: Role and potential, Food Funct. 13 (2022). https://doi.org/10.1039/d1fo02750f.

[32] G.H. Schirmbeck, S. Sizonenko, E.F. Sanches, Neuroprotective Role of Lactoferrin during Early Brain Development and Injury through Lifespan, Nutrients 14 (2022). https://doi.org/10.3390/nu14142923.

[33] P. Ministro, D. Martins, Fecal biomarkers in inflammatory bowel disease: how, when and why?, Expert Rev. Gastroenterol. Hepatol. 11 (2017) 317–328. https://doi.org/10.1080/17474124.2017.1292128.

[34] G. Weinbaum, P.C. Atkins, C.V.O.N. Allmen, et al., Release of lactoferrin and elastase in human allergic skin reactions . Information about subscribing to The Journal of Immunology is online at : RELEASE OF LACTOFERRIN AND ELASTASE IN, (2019).

[35] S. Telang, Lactoferrin: A critical player in neonatal host defense, Nutrients 10 (2018) 1–16. https://doi.org/10.3390/nu10091228.

[36] M.S. Lepanto, L. Rosa, R. Paesano, et al., Lactoferrin in aseptic and septic inflammation, Molecules 24 (2019) 1–27. https://doi.org/10.3390/molecules24071323.

[37] A. Nakamura, F. Kimura, S. Tsuji, et al., Bovine lactoferrin suppresses inflammatory cytokine expression in endometrial stromal cells in chronic endometritis, J. Reprod. Immunol. 154 (2022). https://doi.org/10.1016/j.jri.2022.103761.

[38] J.N. Yong, B.H. Sang, S.K. Jong, et al., Lactoferrin works as a new LPS-binding protein in inflammatory activation of macrophages, Int. Immunopharmacol. 4 (2004) 1187–1199. https://doi.org/10.1016/j.intimp.2004.05.009.

[39] L. Wisgrill, I. Wessely, A. Spittler, et al., Human lactoferrin attenuates the proinflammatory response of neonatal monocyte-derived macrophages, Clin. Exp. Immunol. 192 (2018) 315–324. https://doi.org/10.1111/cei.13108.

[40] D. Latorre, P. Puddu, P. Valenti, et al., Reciprocal interactions between lactoferrin and bacterial endotoxins and their role in the regulation of the immune response, Toxins (Basel). 2 (2010) 54–68. https://doi.org/10.3390/toxins2010054.

[41] K. Sakamoto, Y. Ito, T. Mori, et al., Interaction of human lactoferrin with cell adhesion molecules through RGD motif elucidated by lactoferrin-binding epitopes, J. Biol. Chem. 281 (2006) 24472–24478. https://doi.org/10.1074/jbc.M604974200.

[42] H. Shau, A. Kim, S.H. Golub, Modulation of natural killer and lymphokine-activated killer cell cytotoxicity by lactoferrin, J. Leukoc. Biol. 51 (1992) 343–349. https://doi.org/10.1002/jlb.51.4.343.

[43] H.A. Alhadrami, G.A.R.Y. Suaifan, M.M. Zourob, A Portable Nanoprobe for Rapid and Sensitive Detection of SARS-CoV-2 S1 Protein, Biosensors 12 (2022). https://doi.org/10.3390/bios12040232.

[44] E. Campione, C. Lanna, T. Cosio, et al., Lactoferrin Against SARS-CoV-2: In Vitro and In Silico Evidences, Front. Pharmacol. 12 (2021). https://doi.org/10.3389/fphar.2021.666600.

[45] L. Rosa, A. Cutone, M.P. Conte, et al., An overview on in vitro and in vivo antiviral activity of lactoferrin: its efficacy against SARS-CoV-2 infection, BioMetals 36 (2023). https://doi.org/10.1007/s10534-022-00427-z.

[46] G.A. Nevinsky, How enzymes, proteins and antibodies recognize extended dnas; general regularities, Int. J. Mol. Sci. 22 (2021) 1–35. https://doi.org/10.3390/ijms22031369.

[47] S.E. Soboleva, O.D. Zakharova, S.E. Sedykh, et al., DNase and RNase activities of fresh cow milk lactoferrin, J. Mol. Recognit. 32 (2019) e2777. https://doi.org/10.1002/jmr.2777.

[48] D. V. Semenov, T.G. Kanyshkova, V.N. Buneva, et al., Human milk lactoferrin binds ATP and dissociates into monomers, Biochem. Mol. Biol. Int. 47 (1999). https://doi.org/10.1080/15216549900201183.

[49] S. Buderus, J.H. Boone, M.J. Lentze, Fecal Lactoferrin: Reliable Biomarker for Intestinal Inflammation in Pediatric IBD, Gastroenterol. Res. Pract. 2015 (2015). https://doi.org/10.1155/2015/578527.

[50] E.K. Wright, M.A. Kamm, P. De Cruz, et al., Comparison of fecal inflammatory markers in Crohn's disease, Inflamm. Bowel Dis. 22 (2016) 1086–1094. https://doi.org/10.1097/MIB.0000000000000671.

[51] M.G. Rubio, K. Amo-Mensah, J.M. Gray, et al., Fecal lactoferrin accurately reflects mucosal inflammation in inflammatory bowel disease, World J. Gastrointest. Pathophysiol. 10 (2019) 54–63. https://doi.org/10.4291/wjgp.v10.i5.54.

[52] T. Sipponen, E. Savilahti, P. Kärkkäinen, et al., Fecal calprotectin, lactoferrin, and endoscopic disease activity in monitoring anti-TNF-alpha therapy for Crohn's

disease, Inflamm. Bowel Dis. 14 (2008) 1392–1398. https://doi.org/10.1002/ibd.20490.

[53]   C.A. Lamb, J.C. Mansfield, Measurement of faecal calprotectin and lactoferrin in inflammatory bowel disease, Frontline Gastroenterol. 2 (2011) 13–18. https://doi.org/10.1136/fg.2010.001362.

[54]   L. Fernández-Delgado, A. Vega-Rioja, I. Ventura, et al., Allergens induce the release of lactoferrin by neutrophils from asthmatic patients, PLoS One 10 (2015) 1–13. https://doi.org/10.1371/journal.pone.0141278.

[55]   C. Chea, M. Miyauchi, T. Inubushi, et al., Molecular Mechanisms of Inhibitory Effects of Bovine Lactoferrin on Invasion of Oral Squamous Cell Carcinoma, Pharmaceutics 15 (2023). https://doi.org/10.3390/pharmaceutics15020562.

[56]   K.K. Darmawan, T.C. Karagiannis, J.G. Hughes, et al., Molecular insights into the interaction of apo-lactoferrin with the receptor binding domain of the SARS-CoV-2 spike protein: a molecular dynamics simulation study, J. Biomol. Struct. Dyn. 41 (2023). https://doi.org/10.1080/07391102.2022.2121759.

[57]   R.M. Bennett, J. Davis, Lactoferrin interacts with deoxyribonucleic acid: a preferential reactivity with double-stranded DNA and dissociation of DNA-anti-DNA complexes, J. Lab. Clin. Med. 99 (1982) 127–138. https://doi.org/https://doi.org/10.5555/uri:pii:0022214382900373.

[58]   P. Furmanski, J. He, L. Ying, Functional Significance of the Binding of Lactoferrin to DNA, in: T.W. Hutchens, B. Lonnerdal (Eds.), Lact. Interact. Biol. Funct., Humana Press Inc., NJ, 1995: pp. 313–332.

[59]   Y. Takayama, R. Aoki, Roles of lactoferrin on skin wound healing, Biochem. Cell Biol. 90 (2012) 497–503. https://doi.org/10.1139/o11-054.

[60]   J. Engelmayer, P. Blezinger, A. Varadhachary, Talactoferrin Stimulates Wound Healing With Modulation of Inflammation, J. Surg. Res. 149 (2008) 278–286. https://doi.org/10.1016/j.jss.2007.12.754.

[61]   J. He, P. Furmanski, Sequence specificity and transcriptional activation in the binding of lactoferrin to DNA, Nature 373 (1995) 721–724. https://doi.org/10.1038/373721a0.

[62]   T.G. Kanyshkova, D. V. Semenov, V.N. Buneva, et al., Human milk lactoferrin binds two DNA molecules with different affinities, FEBS Lett. 451 (1999) 235–237. https://doi.org/10.1016/S0014-5793(99)00579-7.

[63]   C.L. Day, B.F. Anderson, J.W. Tweedie, et al., Structure of the recombinant N-terminal lobe of human lactoferrin at 2.0 Å resolution, J. Mol. Biol. 232 (1993). https://doi.org/10.1006/jmbi.1993.1462.

[64]   E.N. Baker, B.F. Anderson, H.M. Baker, et al., Three-dimensional structure of lactoferrin in various functional states, Adv. Exp. Med. Biol. 357 (1994) 1–12. https://doi.org/10.1007/978-1-4615-2548-6_1.

[65]   A. Paziewska-Nowak, M. Urbanowicz, K. Sadowska, et al., DNA-based molecular recognition system for lactoferrin biosensing, Int. J. Biol. Macromol. 253 (2023) 126747. https://doi.org/10.1016/j.ijbiomac.2023.126747.

[66]   W.R. Seitz, C.J. Grenier, J.R. Csoros, et al., Molecular Recognition: Perspective and a New Approach, Sensors (Basel). 21 (2021) 1–9. https://doi.org/10.3390/s21082757.

[67]   H. Liu, J. Ge, E. Ma, et al., Advanced biomaterials for biosensor and theranostics, in: L. Yang, S.B. Bhaduri, T.J. Webster (Eds.), Biomater. Transl. Med. A Biomater. Approach, Academic Press, 2018: pp. 213–255. https://doi.org/10.1016/B978-0-12-813477-1.00010-4.

[68]   S. Sharma, H. Byrne, R.J. O'Kennedy, Antibodies and antibody-derived analytical biosensors, Essays Biochem. 60 (2016) 9–18. https://doi.org/10.1042/EBC20150002.

[69] Y. Saylan, Ö. Erdem, F. Inci, et al., Advances in biomimetic systems for molecular recognition and biosensing, Biomimetics 5 (2020). https://doi.org/10.3390/BIOMIMETICS5020020.

[70] Y. Du, S. Dong, Nucleic acid biosensors: Recent advances and perspectives, Anal. Chem. 89 (2017) 189–215. https://doi.org/10.1021/acs.analchem.6b04190.

[71] S.M. Shaban, D.H. Kim, Recent advances in aptamer sensors, Sensors (Switzerland) 21 (2021) 1–31. https://doi.org/10.3390/s21030979.

[72] N. Xia, F. Feng, C. Liu, et al., The detection of mercury ion using DNA as sensors based on fluorescence resonance energy transfer, Talanta 192 (2019) 500–507. https://doi.org/10.1016/j.talanta.2018.08.086.

[73] H. Abu-Ali, A. Nabok, T.J. Smith, Development of novel and highly specific ssDNA-aptamer-based electrochemical biosensor for rapid detection of mercury (II) and lead (II) ions in water, Chemosensors 7 (2019) 1–14. https://doi.org/10.3390/chemosensors7020027.

[74] M.R. Saidur, A.R.A. Aziz, W.J. Basirun, Recent advances in DNA-based electrochemical biosensors for heavy metal ion detection: A review, Biosens. Bioelectron. 90 (2017) 125–139. https://doi.org/10.1016/j.bios.2016.11.039.

[75] Z. Yu, J. Spiegel, L. Melidis, et al., Chem-map profiles drug binding to chromatin in cells, Nat. Biotechnol. (2023). https://doi.org/10.1038/s41587-022-01636-0.

[76] K.T. McQuaid, A. Pipier, C.J. Cardin, et al., Critical Reviews and Perspectives Interactions of small molecules with DNA junctions, Nucleic Acids Res. 50 (2022) 12636–12656. https://doi.org/10.1093/nar/gkac1043.

[77] A. Paziewska-Nowak, J. Jankowska-Śliwińska, M. Dawgul, et al., Selective Electrochemical Detection of Pirarubicin by Means of DNA-modified Graphite Biosensor, Electroanalysis 29 (2017) 1810–1819. https://doi.org/10.1002/elan.201700067.

[78] K. Lozano Untiveros, E.G. da Silva, F.C. de Abreu, et al., An electrochemical biosensor based on Hairpin-DNA modified gold electrode for detection of DNA damage by a hybrid cancer drug intercalation, Biosens. Bioelectron. 133 (2019) 160–168. https://doi.org/10.1016/j.bios.2019.02.071.

[79] W.B.S. Machini, I.P.G. Fernandes, A.M. Oliveira-Brett, Antidiabetic Drug Metformin Oxidation and in situ Interaction with dsDNA Using a dsDNA-electrochemical Biosensor, Electroanalysis 31 (2019) 1977–1987. https://doi.org/10.1002/elan.201900162.

[80] A. Erdem, H. Karadeniz, G. Mayer, et al., Electrochemical sensing of aptamer-protein interactions using a magnetic particle assay and single-use sensor technology, Electroanalysis 21 (2009) 1278–1284. https://doi.org/10.1002/elan.200804557.

[81] J. Bhardwaj, N. Chaudhary, H. Kim, et al., Subtyping of influenza A H1N1 virus using a label-free electrochemical biosensor based on the DNA aptamer targeting the stem region of HA protein, Anal. Chim. Acta 1064 (2019) 94–103. https://doi.org/10.1016/j.aca.2019.03.005.

[82] S. Herrera-Velarde, J.R. Villanueva-Valencia, P. Mendoza-Espinosa, et al., Stability and structural evolution of double-stranded DNA molecules under high pressures: A molecular dynamics study, Front. Phys. 11 (2023) 1–9. https://doi.org/10.3389/fphy.2023.1076787.

[83] R.A.C. Ferraz, A.L.G. Lopes, J.A.F. da Silva, et al., DNA–protein interaction studies: a historical and comparative analysis, Plant Methods 17 (2021) 1–21. https://doi.org/10.1186/s13007-021-00780-z.

[84] S.K. Singh, R. Singh, Surface Plasmon Resonance, a Novel Technique for Sensing Cancer Biomarker: Folate Receptor and Nanoparticles Interface, Methods Mol. Biol.

2413 (2022) 211–228. https://doi.org/10.1007/978-1-0716-1896-7_21.

[85] R. Peltomaa, B. Glahn-Martínez, E. Benito-Peña, et al., Optical Biosensors for Label-Free Detection of Small Molecules, Sensors (Basel). 18 (2018). https://doi.org/10.3390/s18124126.

[86] K. Pervushin, R. Riek, G. Wider, et al., Attenuated T2 relaxation by mutual cancellation of dipole–dipole coupling and chemical shift anisotropy, Proc. Natl. Acad. Sci. U. S. A. 94 (1997) 12366–12371.

[87] M. Salzmann, K. Pervushin, G. Wider, et al., Trosy in triple-resonance experiments: New perspectives for sequential NMR assignment of large proteins, Proc. Natl. Acad. Sci. U. S. A. 95 (1998) 13585–13590. https://doi.org/10.1073/pnas.95.23.13585.

[88] S. Campagne, V. Gervais, A. Milon, Nuclear magnetic resonance analysis of protein-DNA interactions, J. R. Soc. Interface 8 (2011) 1065–1078. https://doi.org/10.1098/rsif.2010.0543.

[89] M. Soler, C.S. Huertas, L.M. Lechuga, Label-free plasmonic biosensors for point-of-care diagnostics: a review, Expert Rev. Mol. Diagn. 19 (2019) 71–81. https://doi.org/10.1080/14737159.2019.1554435.

[90] H. Kurt, A.E. Eyüpoğlu, T. Sütlü, et al., Plasmonic Selection of ssDNA Aptamers against Fibroblast Growth Factor Receptor, ACS Comb. Sci. 21 (2019) 578–587. https://doi.org/10.1021/acscombsci.9b00059.

[91] A. Tadimety, Y. Zhang, K.M. Kready, et al., Design of peptide nucleic acid probes on plasmonic gold nanorods for detection of circulating tumor DNA point mutations, Biosens. Bioelectron. 130 (2019) 236–244. https://doi.org/10.1016/j.bios.2019.01.045.

[92] W. Jia, H. Li, T. Wilkop, et al., Silver decahedral nanoparticles empowered SPR imaging-SELEX for high throughput screening of aptamers with real-time assessment, Biosens. Bioelectron. 109 (2018). https://doi.org/10.1016/j.bios.2018.02.029.

[93] H.H. Nguyen, J. Park, S. Kang, et al., Surface plasmon resonance: A versatile technique for biosensor applications, Sensors (Switzerland) 15 (2015) 10481–10510. https://doi.org/10.3390/s150510481.

[94] M. Ritzefeld, N. Sewald, Real-Time Analysis of Specific Protein-DNA Interactions with Surface Plasmon Resonance, J. Amino Acids 2012 (2012) 816032. https://doi.org/10.1155/2012/816032.

[95] G. Ertürk Bergdahl, T. Andersson, M. Allhorn, et al., In Vivo Detection and Absolute Quantification of a Secreted Bacterial Factor from Skin Using Molecularly Imprinted Polymers in a Surface Plasmon Resonance Biosensor for Improved Diagnostic Abilities, ACS Sensors 4 (2019) 717–725. https://doi.org/10.1021/acssensors.8b01642.

[96] P.B. Tiwari, C. Bencheqroun, M. Lemus, et al., SPRD: a surface plasmon resonance database of common factors for better experimental planning, BMC Mol. Cell Biol. 22:17 (2021) 1–8. https://doi.org/10.1186/s12860-021-00354-w.

[97] B. Byrne, E. Stack, N. Gilmartin, et al., Antibody-based sensors: Principles, problems and potential for detection of pathogens and associated toxins, Sensors (Switzerland) 9 (2009). https://doi.org/10.3390/s90604407.

[98] K.M. Koczula, A. Gallotta, Lateral flow assays, Essays Biochem. 60 (2016) 111–120. https://doi.org/10.1042/EBC20150012.

[99] A. Nyamsi Hendji, P. Bataillard, N. Jaffrezic-Renault, Covalent immobilization of glucose oxidase on silanized platinum microelectrode for the monitoring of glucose, Sensors Actuators B. Chem. 15 (1993) 127–134. https://doi.org/10.1016/0925-4005(93)85038-C.

[100] A. Sassolas, L.J. Blum, B.D. Leca-Bouvier, Immobilization strategies to develop enzymatic biosensors, Biotechnol. Adv. 30 (2012) 489–511. https://doi.org/10.1016/j.biotechadv.2011.09.003.

[101] A.B. Hashkavayi, J.B. Raoof, Nucleic acid-based electrochemical biosensors, Elsevier Inc., 2019. https://doi.org/10.1016/B978-0-12-816491-4.00009-7.

[102] R. Zhang, Y. Wang, X. Qu, et al., Exonuclease III-powered DNA Walking Machine for Label-free and Ultrasensitive Electrochemical Sensing of Antibiotic, Sensors Actuators, B Chem. 297 (2019) 126771. https://doi.org/10.1016/j.snb.2019.126771.

[103] K.-K. Hamed, R. Vahideh, E. Ali, et al., DNA Biosensors Techniques and Their Applications in Food Safety, Environmental Protection and Biomedical Research: A mini-review, J. Cell Dev. Biol. 3 (2020) 28–35. https://doi.org/10.36959/596/446.

[104] H. Zhang, X. Xu, W. Jiang, An interparticle relatively motional DNA walker and its sensing application, Chem. Sci. 11 (2020) 7415–7423. https://doi.org/10.1039/d0sc00109k.

[105] J. Xu, P.X. Medina-Rangel, K. Haupt, et al., Guide to the Preparation of Molecularly Imprinted Polymer Nanoparticles for Protein Recognition by Solid-Phase Synthesis, 1st ed., Elsevier Inc., 2017. https://doi.org/10.1016/bs.mie.2017.02.004.

[106] H.J. Schneider, Binding mechanisms in supramolecular complexes, Angew. Chemie - Int. Ed. 48 (2009) 3924–3977. https://doi.org/10.1002/anie.200802947.

[107] S. Abdullah, M. Uddin, Introduction to Immunosensors, Immunosensors (2019) 1–20. https://doi.org/10.1039/9781788014373-00001.

[108] R. Jain, S. Miri, V.L. Pachapur, et al., Advances in antibody-based biosensors in environmental monitoring, in: Tools, Tech. Protoc. Monit. Environ. Contam., 2019. https://doi.org/10.1016/B978-0-12-814679-8.00014-5.

[109] D.S. Dkhar, R. Kumari, S. Mahapatra, et al., Antibody-receptor bioengineering and its implications in designing bioelectronic devices, Int. J. Biol. Macromol. 218 (2022). https://doi.org/10.1016/j.ijbiomac.2022.07.109.

[110] S.B. Nimse, K. Song, M.D. Sonawane, et al., Immobilization techniques for microarray: Challenges and applications, Sensors (Switzerland) 14 (2014) 22208–22229. https://doi.org/10.3390/s141222208.

[111] P. Bettotti, V. Visone, L. Lunelli, et al., Structure and Properties of DNA Molecules over the Full Range of Biologically Relevant Supercoiling States, Sci. Rep. 8 (2018) 1–14. https://doi.org/10.1038/s41598-018-24499-5.

[112] K.A. Wilson, J.L. Kellie, S.D. Wetmore, DNA-protein π-interactions in nature: Abundance, structure, composition and strength of contacts between aromatic amino acids and DNA nucleobases or deoxyribose sugar, Nucleic Acids Res. 42 (2014) 6726–6741. https://doi.org/10.1093/nar/gku269.

[113] K. V, DNA Biosensors-A Review, J. Bioeng. Biomed. Sci. 07 (2017). https://doi.org/10.4172/2155-9538.1000222.

[114] Y. Xu, J. McSally, I. Andricioaei, et al., Modulation of Hoogsteen dynamics on DNA recognition, Nat. Commun. 9 (2018) 1–10. https://doi.org/10.1038/s41467-018-03516-1.

[115] S. Lei, Z. Liu, L. Xu, et al., A "signal-on" electrochemical biosensor based on DNAzyme-driven bipedal DNA walkers and TdT-mediated cascade signal amplification strategy, Elsevier B.V., 2020. https://doi.org/10.1016/j.aca.2019.12.008.

[116] W.R. Browne, B.L. Feringa, Making molecular machines work, Nat. Nanotechnol. 1 (2006) 25–35. https://doi.org/10.1142/9789814287005_0009.

[117] J. Sauvage, V. Duplan, F. Niess, Contractile and Extensile Molecular Systems, in: R.M. Izatt (Ed.), Macrocycl. Supramol. Chem. How Izatt-Christensen Award

Winners Shaped F., 1st ed., John Wiley and Sons Ltd., 2016: pp. 444–464. https://doi.org/10.1002/9781119053859.ch22.

[118] J.F. Stoddart, The master of chemical topology, Chem. Soc. Rev. 38 (2009) 1521–1529. https://doi.org/10.1039/b819336n.

[119] Y. Li, H. Liu, H. Huang, et al., A sensitive electrochemical strategy via multiple amplification reactions for the detection of E. coli O157: H7, Biosens. Bioelectron. 147 (2020) 111752. https://doi.org/10.1016/j.bios.2019.111752.

[120] L. Song, Y. Zhuge, X. Zuo, et al., DNA Walkers for Biosensing Development, Adv. Sci. 9 (2022) 1–21. https://doi.org/10.1002/advs.202200327.

[121] M. Yu, T. He, Q. Wang, et al., Unraveling the Possibilities: Recent Progress in DNA Biosensing, Biosensors 13 (2023). https://doi.org/10.3390/bios13090889.

[122] M. Hasanzadeh, N. Shadjou, M. de la Guardia, Aptamer-based assay of biomolecules: Recent advances in electro-analytical approach, TrAC - Trends Anal. Chem. 89 (2017) 119–132. https://doi.org/10.1016/j.trac.2017.02.003.

[123] S. Weaver, M.H. Mohammadi, N. Nakatsuka, Aptamer-functionalized capacitive biosensors, Biosens. Bioelectron. 224 (2023) 115014. https://doi.org/10.1016/j.bios.2022.115014.

[124] S. Arshavsky-Graham, C. Heuer, X. Jiang, et al., Aptasensors versus immunosensors—Which will prevail?, Eng. Life Sci. 22 (2022) 319–333. https://doi.org/10.1002/elsc.202100148.

[125] G. Ertürk, B. Mattiasson, Molecular imprinting techniques used for the preparation of biosensors, Sensors (Switzerland) 17 (2017) 1–17. https://doi.org/10.3390/s17020288.

[126] B. Regan, F. Boyle, R. O'Kennedy, et al., Evaluation of molecularly imprinted polymers for point-of-care testing for cardiovascular disease, Sensors (Switzerland) 19 (2019). https://doi.org/10.3390/s19163485.

[127] M. Hussain, J. Wackerlig, P.A. Lieberzeit, Biomimetic strategies for sensing biological species, Biosensors 3 (2013) 89–107. https://doi.org/10.3390/bios3010089.

[128] S. Di Masi, M. Costa, F. Canfarotta, et al., An impedimetric sensor based on molecularly imprinted nanoparticles for the determination of trypsin in artificial matrices - towards point-of-care diagnostics, Anal. Methods 16 (2023) 742–750. https://doi.org/10.1039/d3ay01762a.

[129] K.G. Shevchenko, I.S. Garkushina, F. Canfarotta, et al., Nano-molecularly imprinted polymers (nanoMIPs) as a novel approach to targeted drug delivery in nanomedicine, RSC Adv. 12 (2022) 3957–3968. https://doi.org/10.1039/d1ra08385f.

[130] H. Yu, H. Li, X. Sun, et al., Biomimetic Flexible Sensors and Their Applications in Human Health Detection, Biomimetics 8 (2023). https://doi.org/10.3390/biomimetics8030293.

[131] Y. Xiao, T. Zhang, H. Zhang, Recent advances in the peptide-based biosensor designs, Colloids Surfaces B Biointerfaces 231 (2023) 113559. https://doi.org/10.1016/j.colsurfb.2023.113559.

[132] Z. Pirkhezranian, M. Tahmoorespur, H. Monhemi, et al., Computational Peptide Engineering Approach for Selection the Best Engendered Camel Lactoferrin-Derive Peptide with Potency to Interact with DNA, Int. J. Pept. Res. Ther. 26 (2020). https://doi.org/10.1007/s10989-019-10012-7.

[133] Y. Shi, Y. Zhang, Y. Hu, et al., Smartphone-based fluorescent sensing platforms for point-of-care ocular lactoferrin detection, Sensors Actuators B Chem. 378 (2023). https://doi.org/10.1016/j.snb.2022.133128.

[134] N.M. Nunes, H.M.C. de Paula, Y.L. Coelho, et al., Surface plasmon resonance study of interaction between lactoferrin and naringin, Food Chem. 297 (2019) 125022.

https://doi.org/10.1016/j.foodchem.2019.125022.

[135] L.H. Hansen, S.J. Sørensen, The use of whole-cell biosensors to detect and quantify compounds or conditions affecting biological systems, Microb. Ecol. 42 (2001) 483–494. https://doi.org/10.1007/s00248-001-0025-9.

[136] Y. Zhang, F. Lou, W. Wu, et al., Determination of bovine lactoferrin in food by HPLC with a heparin affinity column for sample preparation, J. AOAC Int. 100 (2017) 133–138. https://doi.org/10.5740/jaoacint.16-0259.

[137] E. Tsakali, A. Chatzilazarou, D. Houhoula, et al., A rapid HPLC method for the determination of lactoferrin in milk of various species, J. Dairy Res. 86 (2019) 238–241. https://doi.org/10.1017/S0022029919000189.

[138] J. Oberčkal, H. Liaqat, B.B. Matijašić, et al., Quantification of lactoferrin in human milk using monolithic cation exchange HPLC, J. Chromatogr. B Anal. Technol. Biomed. Life Sci. 1214 (2023). https://doi.org/10.1016/j.jchromb.2022.123548.

[139] F. Ostertag, C.M. Schmidt, S. Berensmeier, et al., Development and validation of an RP-HPLC DAD method for the simultaneous quantification of minor and major whey proteins, Food Chem. 342 (2021). https://doi.org/10.1016/j.foodchem.2020.128176.

[140] A.M. Williams, Y. Zhou, N. Luo, et al., Determination of native lactoferrin and other whey proteins at different pH conditions after UHT using reverse phase HPLC, Int. Dairy J. 141 (2023). https://doi.org/10.1016/j.idairyj.2023.105621.

[141] K. Mao, H. Du, L. Bai, et al., Poly (2-methyl-2-oxazoline) coating by thermally induced immobilization for determination of bovine lactoferrin in infant formula with capillary electrophoresis, Talanta 168 (2017) 230–239. https://doi.org/10.1016/j.talanta.2017.03.051.

[142] T. Zimina, N. Sitkov, V. Karasev, et al., Design of Peptide Ligand for Lactoferrin and Study of Its Binding Specificity, Chemosensors 11 (2023). https://doi.org/10.3390/chemosensors11030162.

[143] C. Zhu, L. Li, G. Yang, et al., High-efficiency selection of aptamers for bovine lactoferrin by capillary electrophoresis and its aptasensor application in milk powder, Talanta 205 (2019) 120088. https://doi.org/10.1016/j.talanta.2019.06.088.

[144] M. Yuan, C. Feng, S. Wang, et al., Selection of possible signature peptides for the detection of bovine lactoferrin in infant formulas by LC-MS/MS, PLoS One 12 (2017) 1–11. https://doi.org/10.1371/journal.pone.0184152.

[145] J. Zhang, S. Lai, Z. Cai, et al., Determination of bovine lactoferrin in dairy products by ultra-high performance liquid chromatography-tandem mass spectrometry based on tryptic signature peptides employing an isotope-labeled winged peptide as internal standard, Anal. Chim. Acta 829 (2014) 33–39. https://doi.org/10.1016/j.aca.2014.04.025.

[146] X. Li, Z. Li, E. Xu, et al., Determination of lactoferrin in camel milk by ultrahigh-performance liquid chromatography-tandem mass spectrometry using an isotope-labeled winged peptide as internal standard, Molecules 24 (2019). https://doi.org/10.3390/molecules24224199.

[147] M. Chen, F. Wen, Y. Zhang, et al., Determination of native lactoferrin in milk by HPLC on HiTrapTM Heparin HP column, Food Anal. Methods 12 (2019) 2518–2526. https://doi.org/10.1007/s12161-019-01572-x.

[148] F. Peysselon, S. Ricard-Blum, Heparin-protein interactions: From affinity and kinetics to biological roles. Application to an interaction network regulating angiogenesis, Matrix Biol. 35 (2014) 73–81. https://doi.org/10.1016/j.matbio.2013.11.001.

[149] J. Pang, Q. Xiao, H. Yan, et al., Bovine Lactoferrin Quantification in Dairy Products by a Simple Immunoaffinity Magnetic Purification Method Coupled with High-

Performance Liquid Chromatography with Fluorescence Detection, J. Agric. Food Chem. 68 (2020) 892–898. https://doi.org/10.1021/acs.jafc.9b06043.

[150] J. Jiménez-Guzmán, I. Méndez-Palacios, A. López-Luna, et al., Development of a molecularly imprinted polymer for the recovery of lactoferrin, Food Bioprod. Process. 92 (2014) 226–232. https://doi.org/10.1016/j.fbp.2014.02.001.

[151] A.Y. Alhalwani, J.E. Repine, M.K. Knowles, et al., Development of a sandwich ELISA with potential for selective quantification of human lactoferrin protein nitrated through disease or environmental exposure, Anal. Bioanal. Chem. 410 (2018). https://doi.org/10.1007/s00216-017-0779-7.

[152] B. Gao, Z. He, B. He, et al., Wearable eye health monitoring sensors based on peacock tail-inspired inverse opal carbon, Sensors Actuators, B Chem. 288 (2019). https://doi.org/10.1016/j.snb.2019.03.029.

[153] L.I. Mukhametova, S.A. Eremin, D.A. Arutyunyan, et al., Fluorescence Polarization Immunoassay of Human Lactoferrin in Milk Using Small Single-Domain Antibodies, Biochem. 87 (2022). https://doi.org/10.1134/S0006297922120227.

[154] Z. Chen, H. Li, W. Jia, et al., Bivalent Aptasensor Based on Silver-Enhanced Fluorescence Polarization for Rapid Detection of Lactoferrin in Milk, Anal. Chem. 89 (2017) 5900–5908. https://doi.org/10.1021/acs.analchem.7b00261.

[155] Y. Zhang, P. Yan, H. Tang, et al., Rapid detection of tear lactoferrin for diagnosis of dry eyes by using fluorescence polarization-based aptasensor, Sci. Rep. 13 (2023). https://doi.org/10.1038/s41598-023-42484-5.

[156] J. Liu, T. Li, H. Qin, et al., Self-assembly and label-free fluorescent aptasensor based on deoxyribonucleic acid intercalated dyes for detecting lactoferrin in milk powder, Front. Nutr. 9 (2022) 992188. https://doi.org/10.3389/fnut.2022.992188.

[157] Y. Zhang, J. Zhang, Fluorescence Resonance Energy Transfer-Based Aptasensor Made of Carbon-Based Nanomaterials for Detecting Lactoferrin at Low Concentrations, ACS Omega 7 (2022) 37964–37970. https://doi.org/10.1021/acsomega.2c05129.

[158] F. Ostertag, D. Sommer, S. Berensmeier, et al., Development and validation of an enzyme-linked immunosorbent assay for the determination of bovine lactoferrin in various milk products, Int. Dairy J. 125 (2022). https://doi.org/10.1016/j.idairyj.2021.105246.

[159] G.G. Kaiser, N.C. Mucci, V. González, et al., Detection of recombinant human lactoferrin and lysozyme produced in a bitransgenic cow, J. Dairy Sci. 100 (2017) 1605–1617. https://doi.org/10.3168/jds.2016-11173.

[160] F. Zhang, H. Du, L. Li, et al., Enzyme-Linked Aptamer Kits for Rapid, Visual, and Sensitive Determination of Lactoferrin in Dairy Products, Foods 11 (2022). https://doi.org/10.3390/foods11233763.

[161] M.A. Goicolea, A. Gómez-Caballero, M. Saumell-Esnaola, et al., A linear-polymer-based lactoferrin-selective recognition element for an ELISA mimic: A proof of concept, Anal. Chim. Acta 1191 (2022). https://doi.org/10.1016/j.aca.2021.339309.

[162] H. Kudo, K. Maejima, Y. Hiruta, et al., Microfluidic Paper-Based Analytical Devices for Colorimetric Detection of Lactoferrin, SLAS Technol. 25 (2020) 47–57. https://doi.org/10.1177/2472630319884031.

[163] R. Wang, J. Wang, H. Liu, et al., Sensitive immunoassays based on specific monoclonal IgG for determination of bovine lactoferrin in cow milk samples, Food Chem. 338 (2021) 127820. https://doi.org/10.1016/j.foodchem.2020.127820.

[164] Z. Li, F. Wen, Z. Li, et al., Simultaneous detection of α-Lactoalbumin, β-Lactoglobulin and Lactoferrin in milk by Visualized Microarray, BMC Biotechnol. 17 (2017) 1–9. https://doi.org/10.1186/s12896-017-0387-9.

[165] S. Zhang, J. Echegoyen, Point of care diagnosis of dry eye disease with a sensitive immunoassay for dual biomarker detection, Biochem. Biophys. Reports 32 (2022). https://doi.org/10.1016/j.bbrep.2022.101396.

[166] K. Zhu, H. Zou, J. Chen, et al., Rapid and sensitive determination of lactoferrin in milk powder by boronate affinity amplified dynamic light scattering immunosensor, Food Chem. 405 (2023). https://doi.org/10.1016/j.foodchem.2022.134983.

[167] Y. Xu, C. Hu, J. Liu, et al., Detection of synovial fluid LTF and S100A8 by chemiluminescence immunoassay for the diagnosis of periprosthetic joint infection, Clin. Chim. Acta 545 (2023). https://doi.org/10.1016/j.cca.2023.117369.

[168] Y. Lu, H. Ke, Y. Wang, et al., A ratiometric electrochemiluminescence resonance energy transfer platform based on novel dye BODIPY derivatives for sensitive detection of lactoferrin, Biosens. Bioelectron. 170 (2020) 112664. https://doi.org/10.1016/j.bios.2020.112664.

[169] M. Tomassetti, E. Martini, L. Campanella, et al., Lactoferrin determination using flow or batch immunosensor surface plasmon resonance: Comparison with amperometric and screen-printed immunosensor methods, Sensors Actuators, B Chem. 179 (2013) 215–225. https://doi.org/10.1016/j.snb.2012.09.096.

[170] J.M. Billakanti, C.J. Fee, F.R. Lane, et al., Simultaneous, quantitative detection of five whey proteins in multiple samples by surface plasmon resonance, Int. Dairy J. 20 (2010) 96–105. https://doi.org/10.1016/j.idairyj.2009.08.008.

[171] W. Jia, Z. Wang, Z. Lu, et al., The discovery of lactoferrin dual aptamers through surface plasmon resonance imaging combined with a bioinformation analysis, Analyst 145 (2020) 6298–6306. https://doi.org/10.1039/d0an01513j.

[172] H.R. Culver, M.E. Wechsler, N.A. Peppas, Label-Free Detection of Tear Biomarkers Using Hydrogel-Coated Gold Nanoshells in a Localized Surface Plasmon Resonance-Based Biosensor, ACS Nano 12 (2018) 9342–9354. https://doi.org/10.1021/acsnano.8b04348.

[173] L. Campanella, E. Martini, M. Pintore, et al., Determination of lactoferrin and immunoglobulin G in animal milks by new immunosensors, Sensors 9 (2009) 2202–2221. https://doi.org/10.3390/s90302202.

[174] J. Huang, Z. He, J. Cao, et al., Electrochemical immunosensor detection for lactoferrin in milk powder, Int. J. Electrochem. Sci. 13 (2018) 7816–7826. https://doi.org/10.20964/2018.08.47.

[175] Y. Pan, G.A. Sonn, M.L.Y. Sin, et al., Electrochemical immunosensor detection of urinary lactoferrin in clinical samples for urinary tract infection diagnosis, Biosens. Bioelectron. 26 (2010) 649–654. https://doi.org/10.1016/j.bios.2010.07.002.

[176] O. Zitka, S. Krizkova, S. Skalickova, et al., Microfluidic tool coupled with electrochemical assay for detection of lactoferrin isolated by antibody-modified paramagnetic beads, Electrophoresis 34 (2013) 2120–2128. https://doi.org/10.1002/elps.201200631.

[177] V. Adam, O. Zitka, P. Dolezal, et al., Lactoferrin isolation using monolithic column coupled with spectrometric or micro-amperometric detector, Sensors 8 (2008) 464–487. https://doi.org/10.3390/s8010464.

[178] A. Sun, A.G. Venkatesh, D.A. Hall, A Multi-Technique Reconfigurable Electrochemical Biosensor: Enabling Personal Health Monitoring in Mobile Devices, IEEE Trans. Biomed. Circuits Syst. 10 (2016) 945–954. https://doi.org/10.1109/TBCAS.2016.2586504.

[179] M. Naseri, A. Halder, M. Mohammadniaei, et al., A multivalent aptamer-based electrochemical biosensor for biomarker detection in urinary tract infection, Electrochim. Acta 389 (2021) 138644.

https://doi.org/10.1016/j.electacta.2021.138644.

[180] K.S. Shalini Devi, V.T. Mahalakshmi, A.R. Ghosh, et al., Unexpected co-immobilization of lactoferrin and methylene blue from milk solution on a Nafion/MWCNT modified electrode and application to hydrogen peroxide and lactoferrin biosensing, Electrochim. Acta 244 (2017) 26–37. https://doi.org/10.1016/j.electacta.2017.05.077.

[181] F. Ebrahimi, H.S. Amoli, S.A. Mozaffari, Impedimetric and single-frequency capacitance spectroscopy strategy in label-free rapid screening of lactoferrin, Sensors Actuators B Chem. 354 (2022) 131107. https://doi.org/10.1016/j.snb.2021.131107.

[182] B.G. Andryukov, N.N. Besednova, R. V. Romashko, et al., Label-free biosensors for laboratory-based diagnostics of infections: Current achievements and new trends, Biosensors 10 (2020) 1–22. https://doi.org/10.3390/bios10020011.

[183] S. Sang, Y. Wang, Q. Feng, et al., Progress of new label-free techniques for biosensors: A review, Crit. Rev. Biotechnol. 36 (2016) 465–481. https://doi.org/10.3109/07388551.2014.991270.

[184] M. Bolognesi, M. Prosa, M. Toerker, et al., A Fully Integrated Miniaturized Optical Biosensor for Fast and Multiplexing Plasmonic Detection of High- and Low-Molecular-Weight Analytes, Adv. Mater. 35 (2023). https://doi.org/10.1002/adma.202208719.

[185] I.R. Suhito, K.M. Koo, T.H. Kim, Recent advances in electrochemical sensors for the detection of biomolecules and whole cells, Biomedicines 9 (2021) 1–20. https://doi.org/10.3390/biomedicines9010015.

[186] L. Huang, H. Huang, Z. Zhang, et al., Contractile Hairpin DNA-Mediated Dual-Mode Strategy for Simultaneous Quantification of Lactoferrin and Iron Ion by Surface-Enhanced Raman Scattering and Fluorescence Analysis, Anal. Chem. 95 (2023). https://doi.org/10.1021/acs.analchem.2c05473.

[187] A.C. Lazanas, M.I. Prodromidis, Electrochemical Impedance Spectroscopy—A Tutorial, ACS Meas. Sci. Au 3 (2023) 162–193. https://doi.org/10.1021/acsmeasuresciau.2c00070.

[188] Z. Wang, A. Murphy, A. O'riordan, et al., Equivalent impedance models for electrochemical nanosensor-based integrated system design, Sensors 21 (2021) 3259. https://doi.org/10.3390/s21093259.

[189] E.B. Bahadir, M.K. Sezgintürk, A review on impedimetric biosensors, Artif. Cells, Nanomedicine Biotechnol. 44 (2016) 248–262. https://doi.org/10.3109/21691401.2014.942456.

[190] V. Pinkova Gajdosova, L. Lorencova, A. Blsakova, et al., Challenges for impedimetric affinity sensors targeting protein detection, Curr. Opin. Electrochem. 28 (2021) 100717. https://doi.org/10.1016/j.coelec.2021.100717.

[191] F. Malvano, R. Pilloton, D. Albanese, Label-free impedimetric biosensors for the control of food safety–a review, Int. J. Environ. Anal. Chem. 100 (2020) 468–491. https://doi.org/10.1080/03067319.2019.1667096.

[192] S. Gürsoy, N. Dükar, Y.T. Yaman, et al., Electroactive polyglycine coatings for nanobiosensing applications: Label-free DNA hybridization, DNA-Antitumor agent interaction and antitumor agent determination, Anal. Chim. Acta 1072 (2019) 15–24. https://doi.org/10.1016/j.aca.2019.04.044.

[193] J. Leva-Bueno, I. Meuskens, D. Linke, et al., A novel, proof-of-concept electrochemical impedimetric biosensor based on extracellular matrix protein-adhesin interaction, Sensors and Diagnostics 1 (2022) 1003–1013. https://doi.org/10.1039/d2sd00075j.

[194] J.S. Park, H.J. Kim, J.H. Lee, et al., Amyloid beta detection by faradaic

electrochemical impedance spectroscopy using interdigitated microelectrodes, Sensors (Switzerland) 18 (2018) 426. https://doi.org/10.3390/s18020426.

[195] C. Witte, F. Lisdat, Direct Detection of DNA and DNA-Ligand Interaction by Impedance Spectroscopy, Electroanalysis 23 (2011) 339–346. https://doi.org/10.1002/elan.201000410.

[196] C. Tersch, F. Lisdat, Label-free detection of protein-DNA interactions using electrochemical impedance spectroscopy, Electrochim. Acta 56 (2011) 7673–7679. https://doi.org/10.1016/j.electacta.2011.06.063.

[197] D. Caballero, E. Martinez, J. Bausells, et al., Impedimetric immunosensor for human serum albumin detection on a direct aldehyde-functionalized silicon nitride surface, Anal. Chim. Acta 720 (2012) 43–48. https://doi.org/10.1016/j.aca.2012.01.031.

[198] D. Lima, A.C.M. Hacke, J. Inaba, et al., Electrochemical detection of specific interactions between apolipoprotein E isoforms and DNA sequences related to Alzheimer's disease, Bioelectrochemistry 133 (2020) 1–9. https://doi.org/10.1016/j.bioelechem.2019.107447.

[199] L.C.T. Shoute, G.N. Abdelrasoul, Y. Ma, et al., Label-free impedimetric immunosensor for point-of-care detection of COVID-19 antibodies, Microsystems Nanoeng. 9 (2023). https://doi.org/10.1038/s41378-022-00460-5.

[200] P. Kanyong, C. Catli, J.J. Davis, Ultrasensitive Impedimetric Immunosensor for the Detection of C-Reactive Protein in Blood at Surface-Initiated-Reversible Addition-Fragmentation Chain Transfer Generated Poly(2-hydroxyethyl methacrylate) Brushes, Anal. Chem. 92 (2020) 4707–4710. https://doi.org/10.1021/acs.analchem.9b05030.

[201] L. Rosa, A. Cutone, M.S. Lepanto, et al., Lactoferrin: A natural glycoprotein involved in iron and inflammatory homeostasis, Int. J. Mol. Sci. 18 (2017). https://doi.org/10.3390/ijms18091985.

[202] Y. Zhang, C. Lu, J. Zhang, Lactoferrin and its detection methods: A review, Nutrients 13 (2021) 2492. https://doi.org/10.3390/nu13082492.

[203] K. Sakamoto, Y. Ito, T. Mori, et al., Interaction of human lactoferrin with cell adhesion molecules through RGD motif elucidated by lactoferrin-binding epitopes, J. Biol. Chem. 281 (2006) 24472–24478. https://doi.org/10.1074/jbc.M604974200.

[204] Y.L. Coelho, H.M.C. de Paula, A.J.P. Agudelo, et al., Lactoferrin-phenothiazine dye interactions: Thermodynamic and kinetic approach, Int. J. Biol. Macromol. 136 (2019) 559–569. https://doi.org/10.1016/j.ijbiomac.2019.06.097.

[205] V.B. Vasilyev, A. V. Sokolov, V.A. Kostevich, et al., Binding of lactoferrin to the surface of low-density lipoproteins modified by myeloperoxidase prevents intracellular cholesterol accumulation by human blood monocytes, Biochem. Cell Biol. 99 (2021) 109–116. https://doi.org/10.1139/bcb-2020-0141.

[206] F. Berlutti, S. Schippa, C. Morea, et al., Lactoferrin downregulates pro-inflammatory cytokines upexpressed in intestinal epithelial cells infected with invasive or noninvasive Escherichia coli strains, in: Biochem. Cell Biol., 2006. https://doi.org/10.1139/O06-039.

[207] D. Legrand, K. Vigié, E.A. Said, et al., Surface nucleolin participates in both the binding and endocytosis of lactoferrin in target cells, Eur. J. Biochem. 271 (2004) 303–317. https://doi.org/10.1046/j.1432-1033.2003.03929.x.

[208] N.M. Nunes, H.M.C. de Paula, Y.L. Coelho, et al., Surface plasmon resonance study of interaction between lactoferrin and naringin, Food Chem. 297 (2019). https://doi.org/10.1016/j.foodchem.2019.125022.

[209] S. Zou, C.E. Magura, W.L. Hurley, Heparin-binding properties of lactoferrin and lysozyme, Comp. Biochem. Physiol. -- Part B Biochem. 103 (1992) 889–895.

https://doi.org/10.1016/0305-0491(92)90210-I.

[210] C. Garré, G. Bianchi-Scarrà, M. Sirito, et al., Lactoferrin binding sites and nuclear localization in K562(S) cells, J. Cell. Physiol. 153 (1992). https://doi.org/10.1002/jcp.1041530306.

[211] P. Mulligan, N.R.J. White, G. Monteleone, et al., Breast milk lactoferrin regulates gene expression by binding bacterial DNA CpG motifs but not genomic DNA promoters in model intestinal cells, Pediatr. Res. 59 (2006) 656–661. https://doi.org/10.1203/01.pdr.0000214958.80011.e1.

[212] I.G. Danilova, N.I. Sinogeeva, M.M. Shavlovskii, et al., The interaction of lactoferrin with plasmid DNA, as studied by laser correlation spectroscopy, Biofizika 46 (2001) 444.

[213] R.M. Bennett, M.M. Merritt, G. Gabor, Lactoferrin binds to neutrophilic membrane DNA, Br. J. Haematol. 63 (1986) 105–117. https://doi.org/10.1111/j.1365-2141.1986.tb07500.x.

[214] R.M. Bennett, J. Davis, S. Campbell, et al., Lactoferrin binds to cell membrane DNA. Association of surface DNA with an enriched population of B cells and monocytes, J. Clin. Invest. 71 (1983) 611–618. https://doi.org/10.1172/JCI110807.

[215] B.E. Britigan, T.S. Lewis, M. Waldschmidt, et al., Lactoferrin Binds CpG-Containing Oligonucleotides and Inhibits Their Immunostimulatory Effects on Human B Cells, J. Immunol. 167 (2001) 2921–2928. https://doi.org/10.4049/jimmunol.167.5.2921.

[216] T.W. Hutchens, J.S. Magnuson, T.T. Yip, Interaction of human lactoferrin with DNA: One-step purification by affinity chromatography on single-stranded DNA-agarose, Pediatr. Res. 26 (1989) 618–622. https://doi.org/10.1203/00006450-198912000-00021.

[217] A. Emamjomeh, D. Choobineh, B. Hajieghrari, et al., DNA–protein interaction: identification, prediction and data analysis, Mol. Biol. Rep. 46 (2019) 3571–3596. https://doi.org/10.1007/s11033-019-04763-1.

[218] M.M. Gromiha, C. Santhosh, S. Ahmad, Structural analysis of cation-π interactions in DNA binding proteins, Int. J. Biol. Macromol. 34 (2004) 203–211. https://doi.org/10.1016/j.ijbiomac.2004.04.003.

[219] F. Cozzolino, I. Iacobucci, V. Monaco, et al., Protein-DNA/RNA Interactions: An Overview of Investigation Methods in the -Omics Era, J. Proteome Res. 20 (2021) 3018–3030. https://doi.org/10.1021/acs.jproteome.1c00074.

[220] Y. Pan, S. Zhou, J. Guan, Computationally identifying hot spots in protein-DNA binding interfaces using an ensemble approach, BMC Bioinformatics 21 (2020). https://doi.org/10.1186/s12859-020-03675-3.

[221] T.A. Guschina, S.E. Soboleva, G.A. Nevinsky, Recognition of specific and nonspecific DNA by human lactoferrin, J. Mol. Recognit. 26 (2013) 136–148. https://doi.org/10.1002/jmr.2257.

[222] A.Y. Solovyev, S.I. Tarnovskaya, I.A. Chernova, et al., The interaction of amino acids, peptides, and proteins with DNA, Int. J. Biol. Macromol. 78 (2015) 39–45. https://doi.org/10.1016/j.ijbiomac.2015.03.054.

[223] A.B. Kolomeisky, Mechanisms of protein binding to DNA: Statistical interactions are important, Biophys. J. 104 (2013) 966–967. https://doi.org/10.1016/j.bpj.2013.01.039.

[224] G.D. Stormo, Y. Zhao, Determining the specificity of protein-DNA interactions, Nat. Rev. Genet. 11 (2010) 751–760. https://doi.org/10.1038/nrg2845.

[225] Z. Pirkhezranian, M. Tahmoorespur, X. Daura, et al., Interaction of camel Lactoferrin derived peptides with DNA: A molecular dynamics study, BMC Genomics 21:60 (2020) 1–14. https://doi.org/10.1186/s12864-020-6458-7.

[226] D.C. Carter, J.X. Ho, Structure of serum albumin, Adv. Protein Chem. 45 (1994) 153–176. https://doi.org/10.1016/S0065-3233(08)60640-3.

[227] J.I.A. Rashid, N.A. Yusof, The strategies of DNA immobilization and hybridization detection mechanism in the construction of electrochemical DNA sensor: A review, Sens. Bio-Sensing Res. 16 (2017) 19–31. https://doi.org/10.1016/j.sbsr.2017.09.001.

[228] N. Sandhyarani, Surface modification methods for electrochemical biosensors, Elsevier Inc., 2019. https://doi.org/10.1016/B978-0-12-816491-4.00003-6.

[229] Y.S.N. Day, C.L. Baird, R.L. Rich, et al., Direct comparison of binding equilibrium, thermodynamic, and rate constants determined by surface- and solution-based biophysical methods, Protein Sci. 11 (2002) 1017–1025. https://doi.org/10.1110/ps.4330102.

[230] G.K. Krishnamoorthy, P. Alluvada, S. Hameed Mohammed Sherieff, et al., Isothermal titration calorimetry and surface plasmon resonance analysis using the dynamic approach, Biochem. Biophys. Reports 21 (2020) 100712. https://doi.org/10.1016/j.bbrep.2019.100712.

[231] J.K. Barrows, M.W. Van Dyke, Biolayer interferometry for DNA-protein interactions, PLoS One 17 (2022). https://doi.org/10.1371/journal.pone.0263322.

[232] M.-V.K. and M.M. Friese C, Yang J, Analytical methods for kinetic studies of obiological interactions: a review, Physiol. Behav. 46 (2019) 248–256. https://doi.org/10.1016/j.jpba.2015.01.042.ANALYTICAL.

[233] D.A. Edwards, Steric hindrance effects on surface reactions: Applications to BIAcore, J. Math. Biol. 55 (2007) 517–539. https://doi.org/10.1007/s00285-007-0093-7.

[234] Y. Wang, A. Partridge, Y. Wu, Improving nanoparticle-enhanced surface plasmon resonance detection of small molecules by reducing steric hindrance via molecular linkers, Talanta 198 (2019) 350–357. https://doi.org/10.1016/j.talanta.2019.02.035.

[235] Q. Gong, Y. Wang, H. Yang, A sensitive impedimetric DNA biosensor for the determination of the HIV gene based on graphene-Nafion composite film, Biosens. Bioelectron. 89 (2017) 565–569. https://doi.org/10.1016/j.bios.2016.02.045.

[236] M. Birla, S. Yogi, K. Chaudhary, et al., Saliva: A Non-Invasive and Multifaceted Tool in the Sphere of Diagnostics, J. Pharm. Sci. Res. 14 (2022) 713–720.

[237] F. Bartolome, G. Orive, E. Carro, Standardizing salivary lactoferrin measurements to obtain a robust diagnostic biomarker for alzheimer's disease, Alzheimer's Dement. Diagnosis, Assess. Dis. Monit. 13 (2021) 1–7. https://doi.org/10.1002/dad2.12173.

[238] L. Rosa, M.S. Lepanto, A. Cutone, et al., Lactoferrin and oral pathologies: A therapeutic treatment, Biochem. Cell Biol. 99 (2021). https://doi.org/10.1139/bcb-2020-0052.

[239] J. Satija, V.V.R. Sai, S. Mukherji, Dendrimers in biosensors: Concept and applications, J. Mater. Chem. 21 (2011) 14367–14386. https://doi.org/10.1039/c1jm10527b.

[240] G. Congur, A. Erdem, PAMAM dendrimer modified screen printed electrodes for impedimetric detection of miRNA-34a, Microchem. J. 148 (2019) 748–758. https://doi.org/10.1016/j.microc.2019.05.040.

[241] E.E. Ferapontova, Hybridization Biosensors Relying on Electrical Properties of Nucleic Acids, Electroanalysis 29 (2017) 6–13. https://doi.org/10.1002/elan.201600593.

[242] J. Zhang, H.P. Lang, G. Yoshikawa, et al., Optimization of DNA hybridization efficiency by pH-driven nanomechanical bending, Langmuir 28 (2012) 6494–6501. https://doi.org/10.1021/la205066h.

[243] H.F. Teh, W.Y.X. Peh, X. Su, et al., Characterization of protein-DNA interactions using surface plasmon resonance spectroscopy with various assay schemes,

Biochemistry 46 (2007) 2127–2135. https://doi.org/10.1021/bi061903t.

[244] A.A. Elshanawany, A.M. Ramadan, R.A. Salem, Synthesis, spectrophotometric and stoichiometric studies of metal complexes of four antipsychotic drugs in bulk, spiked human plasma and pharmaceutical dosage forms, Der Pharma Chem. 8 (2016) 143–157.

[245] Z. Li, B. Li, Z. Zhao, et al., Rapid Identification and Quantitative Analysis of Polycarboxylate Superplasticizers Using ATR-FTIR Spectroscopy Combined with Chemometric Methods, Math. Probl. Eng. 2021 (2021) 6613382. https://doi.org/10.1155/2021/6613382.

[246] K. V. Abrosimova, O. V. Shulenina, S. V. Paston, FTIR study of secondary structure of bovine serum albumin and ovalbumin, J. Phys. Conf. Ser. 769 (2016) 012016. https://doi.org/10.1088/1742-6596/769/1/012016.

[247] M. Banyay, M. Sarkar, A. Gräslund, A library of IR bands of nucleic acids in solution, Biophys. Chem. 104 (2003) 477–488. https://doi.org/10.1016/S0301-4622(03)00035-8.

[248] R.S. Spolar, M.T. Record, Coupling of local folding to site-specific binding of proteins to DNA, Science (80-.). 263 (1994) 777–784. https://doi.org/10.1126/science.8303294.

[249] J.H. Nuijens, P.H.C. Van Berkel, M.E.J. Geerts, et al., Characterization of recombinant human lactoferrin secreted in milk of transgenic mice, J. Biol. Chem. 272 (1997) 8802–8807. https://doi.org/10.1074/jbc.272.13.8802.

[250] H. Fukada, K. Takahashi, Enthalpy and heat capacity changes for the proton dissociation of various buffer components in 0.1 M potassium chloride, Proteins Struct. Funct. Genet. 33 (1998) 159–166. https://doi.org/10.1002/(SICI)1097-0134(19981101)33:2<159::AID-PROT2>3.0.CO;2-E.

[251] J.H. Ha, R.S. Spolar, M.T. Record, Role of the hydrophobic effect in stability of site-specific protein-DNA complexes, J. Mol. Biol. 209 (1989) 801–816. https://doi.org/10.1016/0022-2836(89)90608-6.

[252] B.M. Baker, K.P. Murphy, Prediction of binding energetics from structure using empirical parameterization, Methods Enzymol. 295 (1998) 294–315. https://doi.org/10.1016/S0076-6879(98)95045-5.

[253] R.N. Roy, L.N. Roy, S. Ashkenazi, et al., Buffer standards for pH measurement of N-(2-hydroxyethyl)piperazine-N'-2- ethanesulfonic acid (HEPES) for I=0.16 mol kg-1 from 5 to 55 °c, J. Solution Chem. 38 (2009) 449–458. https://doi.org/10.1007/s10953-009-9378-3.

[254] L. Samuelsen, R. Holm, A. Lathuile, et al., Buffer solutions in drug formulation and processing: How pK a values depend on temperature, pressure and ionic strength, Int. J. Pharm. 560 (2019) 357–364. https://doi.org/10.1016/j.ijpharm.2019.02.019.

[255] R.N. Goldberg, N. Kishore, R.M. Lennen, Thermodynamic quantities for the ionization reactions of buffers, J. Phys. Chem. Ref. Data 31 (2002) 231–370. https://doi.org/10.1063/1.1416902.

[256] H.E. Indyk, E.L. Filonzi, Determination of lactoferrin in bovine milk, colostrum and infant formulas by optical biosensor analysis, Int. Dairy J. 15 (2005) 429–438. https://doi.org/10.1016/j.idairyj.2004.09.003.

[257] A. Paziewska-Nowak, M. Urbanowicz, D.G. Pijanowska, Label-free impedimetric biosensor based on a novel DNA-type receptor for selective determination of lactoferrin in human saliva, Sensors Actuators B Chem. 405 (2024) 135377. https://doi.org/10.1016/j.snb.2024.135377.

[258] M. Sypabekova, K. Dukenbayev, A. Tsepke, et al., An aptasensor for the detection of Mycobacterium tuberculosis secreted immunogenic protein MPT64 in clinical

samples towards tuberculosis detection, Sci. Rep. 9 (2019) 16273. https://doi.org/10.1038/s41598-019-52685-6.

[259] M. Urbanowicz, K. Sadowska, B. Lemieszek, et al., Effect of dendrimer-based interlayers for enzyme immobilization on a model electrochemical sensing system for glutamate, Bioelectrochemistry 152 (2023). https://doi.org/10.1016/j.bioelechem.2023.108407.

[260] K. Nijakowski, W. Owecki, J. Jankowski, et al., Salivary Biomarkers for Alzheimer's Disease: A Systematic Review with Meta-Analysis, Int. J. Mol. Sci. 25 (2024). https://doi.org/10.3390/ijms25021168.

[261] A. Pierce, D. Colavizza, M. Benaissa, et al., Molecular cloning and sequence analysis of bovine lactotransferrin, Eur. J. Biochem. 196 (1991) 177–184. https://doi.org/10.1111/j.1432-1033.1991.tb15801.x.

List of publications

Included in PhD dissertation

P1 – **Agnieszka Paziewska-Nowak**, Marcin Urbanowicz, Kamila Sadowska, Dorota G. Pijanowska. DNA-based molecular recognition system for lactoferrin biosensing. *Inter J Biol Macromol* 2023, 253, 126747 DOI: https://doi.org/10.1016/j.ijbiomac.2023.126747 (IF=8.025; CS=14.5; MEiN points=100)

P2 – **Agnieszka Paziewska-Nowak**, Marcin Urbanowicz, Dorota G. Pijanowska. Selective determination of lactoferrin in human saliva with label-free impedimetric DNA-based biosensor. *Sens Actuators B Chem* 2024, 405, 135377 DOI: https://doi.org/10.1016/j.snb.2024.135377 (IF=8.4; CS=14.6; MEiN points=200)

Publication in PhD dissertation summary IF=16.425; CS=29.1; MEiN points=300

PhD candidate contribution

P1 – First author. Corresponding author. Conceptualization, Investigation, Methodology, Results analysis, Visualization, Writing – original draft, Manuscript editing, Funding acquisition, Data curation.

P2 – First author. Corresponding author. Investigation, Methodology, Results analysis, Visualization, Writing – original draft, Manuscript editing, Funding acquisition, Data curation.

Other publications

1. Marcin Urbanowicz, Magdalena Urbanowicz, Kornelia Bobrowska, Kamila Sadowska, **Agnieszka Paziewska-Nowak**, Dorota G. Pijanowska. A novel dsDNA decamer-based electrochemical biosensor for selective determination of irinotecan active metabolite – SN38. *Sens Actuators B Chem* 2023, 397, 134701 DOI: https://doi.org/10.1016/j.snb.2023.134701 (IF=8.4; CS=14.6; MEiN points=200)

2. Marcin Urbanowicz, Kamila Sadowska, Bartłomiej Lemieszek, **Agnieszka Paziewska-Nowak**, Anna Sołdatowska, Marek Dawgul, Dorota G. Pijanowska. Effect of dendrimer-based interlayer for enzyme immobilization on a model electrochemical sensing system for glutamate. *Bioelectrochemistry* 2023, 152, 108407 DOI: 10.1016/j.bioelechem.2023.108407 (IF=5.76; CS=9; MEiN points=100)

3. Marcin Urbanowicz, Kamila Sadowska, **Agnieszka Paziewska-Nowak**, Anna Sołdatowska, Dorota G. Pijanowska. Biosensor based on coupled enzyme reactions for determination of arginase activity. *Bioelectrochemistry* 2022, 146, 108137 DOI: https://doi.org/10.3390/membranes11110898 (IF=5.76; CS=9; MEiN points=100)

4. Marcin Urbanowicz, Kamila Sadowska, **Agnieszka Paziewska-Nowak**, Anna Sołdatowska, Dorota G. Pijanowska. Highly stable potentiometric (bio)sensor for urea and urease activity determination. *Membranes* 2021, 11, 898 DOI: 10.3390/membranes11110898 (IF=4.106; CS=4.4; MEiN points=100)

5. Tomasz Raczyński, Daniel Janczak, Joanna Jankowska-Śliwińska, Marek Dawgul, **Agnieszka Paziewska-Nowak**, Dorota G. Pijanowska, Marcin Zych, Małgorzata Jakubowska. Screen printed graphene electrodes for voltammetric dopamine determination. *Proc. SPIE* 11176, Photonics Applications in Astronomy, Communications, Industry, and High-Energy Physics Experiments 2019, 111764L, 6.11.2019 DOI: 10.1117/12.2535784 (IF=0; CS=0; MEiN points=0)

6. **Agnieszka Paziewska-Nowak**, Marek Dawgul, Dorota G. Pijanowska. Comparative study on voltammetric and spectrofluorimetric methods for fluorescein detection. *Inter J Electrochem Sci* 2019, 14, 3764-3776 DOI: 10.20964/2019.04.07 (IF=1.541; CS=2.7; MEiN points=40)

7. **Agnieszka Paziewska-Nowak**, Tomasz Raczyński, Dorota G. Pijanowska, Daniel Janczak, Małgorzata Jakubowska. Evaluation of Fluorescein as a Label in Electrochemical and Optical Measurements. 2018 XV International Scientific Conference on Optoelectronic and Electronic Sensors (COE), IEEE *Xplore* Digital Library, Warszawa, 2018, 1-4 DOI: 10.1109/coe.2018.8435165 (IF=0; CS=0; MEiN points=0)

8. **Agnieszka Paziewska-Nowak**, Joanna Jankowska-Śliwińska, Marek Dawgul, Dorota G. Pijanowska. Selective electrochemical detection of pirarubicin by means of DNA-modified graphite biosensor. *Electroanalysis* 2017, 29(7), 1810-1819 DOI: 10.1002/elan.201700067 (IF=3.077; CS=5; MEiN points=70)

9. Jakub M. Gac, **Agnieszka Paziewska**. Badanie porywania kropel zdeponowanych na włókninowych wkładach filtracyjnych. *Inż. Ap. Chem.* 2015, 54(3), 082-084 DOI: (IF=0; CS=0; MEiN points=5)

Other publications summary IF=20.244; CS=30.1; ministerial points=415

All publications summary IF=40.814; CS=65.2; ministerial points=715

List of presentations

1. Marcin Urbanowicz, Bartłomiej Lemieszek, Kamila Sadowska, Anna Sołdatowska, **Agnieszka Paziewska-Nowak**, Marek Dawgul, Dorota G. Pijanowska. A new low-range biosensor for glutamate based on hyperbranched linkers. XII Polish Conference on Biocybernetics and Biomedical Engineering, 19-21 May 2021, on-line, book of abstracts, 1 page, poster presentation by Marcin Urbanowicz

2. Anna Sołdatowska, Marcin Urbanowicz, **Agnieszka Paziewska-Nowak**, Kamila Sadowska, Dorota G. Pijanowska. Bioplatform development for DNA-azathioprine interaction studies. XII Polish Conference on Biocybernetics and Biomedical Engineering, 19-21 May 2021, on-line, book of abstracts, 1 page, poster presentation by Anna Sołdatowska

3. **Agnieszka Paziewska-Nowak**, Marcin Urbanowicz, Anna Sołdatowska, Kamila Sadowska, Dorota G. Pijanowska. A multimodal, optical and electrochemical, approach towards detection of endogenous immunomodulators. XII Polish Conference on Biocybernetics and Biomedical Engineering, 19-21 May 2021, on-line, book of abstracts, 1 page, oral presentation by Agnieszka Paziewska-Nowak

4. Marcin Urbanowicz, **Agnieszka Paziewska-Nowak**, Anna Marczak, Dorota G. Pijanowska. A novel solid state potentiometric biosensor for determination of arginase activity. Matrafured' 19 International Conference on Electrochemical Sensors, 16-21 June 2019, Visegrad, book of abstracts, 1 page, poster presentation by Agnieszka Paziewska-Nowak

5. Anna Marczak, **Agnieszka Paziewska-Nowak**, Marcin Urbanowicz, Marek Dawgul, Dorota G. Pijanowska. Towards a novel voltammetric azathioprine biosensor based on interaction with DNA. Matrafured' 19 International Conference on Electrochemical Sensors, 16-21 June 2019, Visegrad, book of abstracts, 1 page, poster presentation by Anna Marczak (Sołdatowska)

6. Anna Marczak, **Agnieszka Paziewska-Nowak**, Marcin Urbanowicz, Marek Dawgul, Dorota G. Pijanowska. Preliminary electrochemical study of azathioprine interaction with DNA. 8th Intercollegiate Biotechnology Symposium, 17-18 May 2019, Warsaw University of Technology, Poland, book of abstracts ISBN: 978-83942342-9-4, 1 page, poster presentation by Anna Marczak (Sołdatowska)

7. **Agnieszka Paziewska-Nowak**, Tomasz Raczyński, Dorota G. Pijanowska, Daniel Janczak, Małgorzata Jakubowska. Evaluation of Fluorescein as a Label in Electrochemical and Optical Measurements. 2018 XV International Scientific Conference on Optoelectronic and Electronic Sensors (COE), IEEE *Xplore* Digital Library, DOI: 10.1109/COE.2018.8435165, Warsaw, 2018, 1-4, poster presentation by Agnieszka Paziewska-Nowak

8. Joanna Jankowska-Śliwińska, **Agnieszka Paziewska-Nowak**, Marek Dawgul, Władysław Torbicz, Dorota G. Pijanowska. Drugs determination based on electrochemical DNA biosensors. 155th International Center of Biocybernetics Seminar, 14th Polish-Japanese Seminar on Biomedical Engineering, Warsaw, 9-12.06.2017, book of abstracts, 1 page, oral presentation by Dorota G. Pijanowska

9. **Agnieszka Paziewska-Nowak**, Joanna Jankowska-Śliwińska, Marek Dawgul, Dorota G. Pijanowska. Electrochemical detection of pirarubicin by means of DNA biosensor. 150th International Center of Biocybernetics Seminar, Warsaw, 12-14.10.2016, book of abstracts, 1 page, poster presentation by Agnieszka Paziewska-Nowak

10. Joanna Jankowska-Śliwińska, **Agnieszka Paziewska-Nowak**, Marek Dawgul, Dorota G. Pijanowska. Intercalation based electrochemical DNA biosensors. 150th International Center of Biocybernetics Seminar, Warsaw, 12-14.10.2016, book of abstracts, 1 page, oral presentation by Joanna Jankowska-Śliwińska

11. Aleksandra Kutkowska, **Agnieszka Paziewska**, Marcin Grzeczkowicz, Andrzej Chwojnowski, Dorota Lewińska. Selection of synthetic polymer solutions for the production of partially biodegradable microcapsules. 43rd European Society for Artificial Organs Congress, Warsaw, 14-17.09.2016, book of abstracts, 1 page, poster presentation by Aleksandra Kutkowska

12. Joanna Jankowska-Śliwińska, **Agnieszka Paziewska**, Marek Dawgul, Dorota G. Pijanowska. Electrochemical determination of pirarubicin by means of modified and unmodified electrodes. 14th Conference on Optical and Electronic Sensors (COE), Gdańsk, 19-22.07.2016, book of abstracts, 1 page, poster presentation by Joanna Jankowska-Śliwińska

Nalecz Institute of Biocybernetics and Biomedical Engineering Annual Seminars:

1. A multimodal, optical and electrochemical, determination of immune response biomarkers. 11.03.2021 – presented by Agnieszka Paziewska-Nowak

2. DNA oligonucleotides as potential bioreceptor for lactoferrin detection. 29.03.2022 – presented by Agnieszka Paziewska-Nowak

3. Study of DNA-lactoferrin interaction using surface plasmon resonance. 08.03.2023 – presented by Agnieszka Paziewska-Nowak

POWER OCh!DOK programme Summer Schools' poster presentations:

1. If lactoferrin – an immunomodulator, may serve as a local inflammatory marker? 12-14.06.2019
2. Development of optical method for determination of immune response markers with lactoferrin as a model immunomodulator. 16-18.09.2020
3. Immuno-optical detection of lactoferrin based on surface plasmon resonance technique. 27-29.09.2021

Summary: 2 full articles related to Ph.D. dissertation topic (first author), 8 full articles outside Ph.D. dissertation topic (in 3 – first author), 7 presentations related to Ph.D. dissertation topic (4 oral and 3 posters – as presenting author, including IBBE PAS Annual Seminars), 11 presentations outside Ph.D. dissertation topic (3 as presenting author).

Internship at Faculty of Chemistry "Ugo Schiff", University of Florence, Italy, internship within the frame of Erasmus+ Mobility Program under the supervision of Prof. Maria Minunni, 01.10-01.12.2019, entitled *Surface plasmon resonance for detection of selected biomolecules*, aimed at familiarizing with surface plasmon resonance and its applications.

List of projects

Projects that results were included in this dissertation:

FBW/1.2/22 Study of lactoferrin-DNA oligonucleotides interactions – towards new selective lactoferrin bioreceptor. 01.03.2022-28.02.2023

FBW/3.2/20 Polimery przewodzące z odciskiem molekularnym jako biomimetyczne warstwy czujnikowe do oznaczeń wybranego immunomodulatora metodą powierzchniowego rezonansu plazmonów. 01.10.2020-30.09.2021

POWR.03.02.00-00-I028/17-00, POWER OChDOK! Interdyscyplinarne, stacjonarne studia doktoranckie – Rozwój i wykorzystanie metod bioinżynieryjnych i informatycznych w prewencji, diagnostyce i terapii chorób cywilizacyjnych – kompleksowy rozwój kompetencji zawodowych młodej kadry naukowej Och!DOK, scholarship 02.2019-02.2023

Other projects:

DWM/POLTAJ9/2/2022 Polish-Taiwanese project, Multimodalne elektrochemiczno-optyczne układy czujnikowe z fotowzmocnieniem do oznaczeń β-amyloidu i α-synucleiny – wczesnych markerów chorób neurodegeneracyjnych (ModSens-4NDs), Principle Investigator: Dorota G. Pijanowska, Ph.D. D.Sc. Eng. Prof., 15.04.2022-14.04.2025

Other achievements

1. 1st Award of Director of Nalecz Institute of Biocybernetics and Biomedical Engineering PAS for young researchers scientific achievements in 2019
2. 1st Award for the best poster on COE2018 conference in Warsaw 2018
3. 2nd Award of Director of Nalecz Institute of Biocybernetics and Biomedical Engineering PAS for young researchers scientific achievements in 2017
4. Winner of the 1st place in Competition of Ministry of Treasury in 2015 "Budujemy wartość polskiej gospodarki. Pracuj dla nas!" – awarded with internship in Zakłady Azotowe Puławy.